

**A Magnetostrictive Transducer Analysis for the Investigation
of Potential System Enhancements**

*A Thesis Submitted to Cardiff University
in Candidature for the Degree of*

Doctor of Philosophy

by

Paul Andrew Bartlett

B.Sc. (Hons) (Brighton Polytechnic)
M.Sc. (The University of Hull)

Cardiff School of Engineering, Cardiff University

April, 2009

UMI Number: U585236

All rights reserved

INFORMATION TO ALL USERS

The quality of this reproduction is dependent upon the quality of the copy submitted.

In the unlikely event that the author did not send a complete manuscript and there are missing pages, these will be noted. Also, if material had to be removed, a note will indicate the deletion.



UMI U585236

Published by ProQuest LLC 2013. Copyright in the Dissertation held by the Author.
Microform Edition © ProQuest LLC.


All rights reserved. This work is protected against
unauthorized copying under Title 17, United States Code.



ProQuest LLC
789 East Eisenhower Parkway
P.O. Box 1346
Ann Arbor, MI 48106-1346

DECLARATION

This work has not previously been accepted in substance for any degree and is not being concurrently submitted in candidature for any degree.

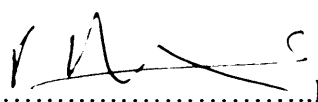
Signed..........Paul Andrew BARTLETT

Date: 30 April 2009

STATEMENT 1

This thesis is the result of my own investigations, except where otherwise stated.

Information from other sources is acknowledged by reference numbers giving explicit references in ascending order, appended to the end of each chapter.

Signed..........Paul Andrew BARTLETT

Date: 30 April 2009

STATEMENT 2

I hereby give consent for my thesis, if accepted, to be available for photocopying and for inter-library loan, and for the title and summary available to outside organisations.

Signed..........Paul Andrew BARTLETT

Date: 30 April 2009

ACKNOWLEDGEMENTS

The work was carried out at the Wolfson Centre for Magnetism, Cardiff School of Engineering, Cardiff University. I would like to thank Prof. A.J. Moses for giving me the opportunity to undertake this course of study whilst a member of staff. In addition, I would like to thank Dr. P.I. Williams, Dr. P. Anderson and Dr. S. Zurek for technical advice and for the use of University equipment.

I must acknowledge the extensive help and assistance from the University of Birmingham. This includes Prof. A.D Walmsley, Dr. S.C. Lea and Dr. G. Landini from the School of Dentistry and Prof. R. Harris of the Department of Metallurgy and Metals who initially came up with the idea for this programme of work.

In addition, I acknowledge the mentoring and assistance that I have received over the years from Dr. A. R. Piercy and Dr. S. Busbridge of the University of Brighton, Dr. R.D. Greenough of the University of Hull, Dr. M.G. Maylin of QinetiQ Ltd, Prof. N. Skipper of UCL and Dr. N. Galloway of Motorola Ltd.

I would also like to thank Miss Paula Chivers for supporting me throughout my career as a Physicist.

DEDICATION

I would like to dedicate this work to the memory of Dr. A.G. Jenner of the University of Hull whose untimely death was a great loss to magnetics research in the UK.

SUMMARY

Magnetostrictive transducers have been used for many years by dentists for the removal of deposits on teeth that contribute to tooth decay.

A study of current commercial magnetostrictive scalers has been undertaken so that potentially beneficial modifications to the present designs could be identified and investigated. This has resulted in suggestions for upgrades to the drive coil design and changes to the frequency of the applied dynamic magnetic field (which produces magnetostriction) that could improve system performance. In addition, a 'capacitance compensation system' has been produced and tested that significantly reduces the power requirements for current and future dental scalers by compensating for dynamic losses in a resonant transducer.

Magnetostrictive materials are identified as replacement for those currently used in dental scalers. It is demonstrated that although they possess some of the qualities that could offer advantages for new types of dental scalers, they are unable to produce satisfactory results when compared to extant nickel-based systems if based on current device geometries.

Finite element modelling has been used to investigate the mode-shapes associated with resonant magnetostrictive dental scaler components. The modelling indicates that flexural modes can be generated and the resultant flexing of 'tips' are equivalent to those measured in real devices. In addition, it is shown that coupled longitudinal-flexural resonant modes must be stimulated to produce the required tip vibrations for dental scaling.

Suggestions are also made for future work that includes the development of more advanced finite element models, improved dental scaler designs and new transducer measurement techniques.

NOMENCLATURE

A	Ampere; Cross sectional area
B	Flux density
B_r	Remanent magnetic induction
B_s	Saturation magnetic induction
B_{max}	Maximum magnetic induction
C	Capacitance
D	Diameter
d_{33}	Magnetostriction constant
E	Young's modulus
f	Frequency
F	Force
G	Strain gauge factor
H	Magnetic field strength
H_c	Coercivity
H_D	Demagnetising field
H_{int}	Internal field
H_K	Anisotropy field
I	Current
ID	Inner diameter
J	Magnetic polarisation
k	Magnetomechanical coupling factor
K	Anisotropy constant
K_u	Induced anisotropy constant
K_s	Shape anisotropy constant
L	Length, inductance
l	Length
m	Mass
M	Magnetisation
M_s	Saturation magnetisation
N	Number of turns
n	Number of turns per metre
OD	Outer diameter
ppm	Parts per million
r	Radius
R	Resistance
s^H	Mechanical compliance at fixed field strength
S	Longitudinal strain
t	Time
T	Temperature; period, stress
T_c	Curie temperature
T_{em}	Transduction co-efficient (electrical from mechanical)
T_{me}	Transduction co-efficient (mechanical from electrical)
u	Displacement
V	Voltage
v	velocity
w	Width
x	Distance; measureand
y	Output

Z	Impedance
Z_c	Blocked electrical impedance
Z_{ec}	Electrical impedance of whole transducer system
z_m	Mechanical impedance
Z_{mot}	Impedance due to motional effects
z_l	Mechanical impedance of load

Greek letters

χ	Susceptibility, eddy current factor
δ	Derivative
Δ	Change in
ε	Strain
η	Magnetomotive force
Φ	Easy axis angle, flux
λ	Magnetostriction
λ_s	Saturation magnetostriction
μ	Permeability
μ_0	Permeability of free space
μ_r	Relative permeability
ξ	Damping factor
θ	Angle
ρ	Resistivity, density
σ	Stress, conductivity
τ	Time constant
ω	Angular frequency

1	Introduction.....	10
1.1	Aims and objectives	10
1.2	History of magnetism and magnetostriction	11
1.3	Magnetostrictive transducers	12
	References for Chapter 1	13
2	MAGNETIC PROPERTIES	14
2.1	Introduction	14
2.2	Basic ferromagnetic principles.....	14
	References for Chapter 2	24
3	MAGNETOSTRICTION.....	25
3.1	Introduction	25
3.2	Magnetostriction in isotropic and anisotropic materials	25
	References for Chapter 3	31
4	MAGNETOSTRICTIVE TRANSDUCERS	32
4.1	Introduction	32
4.2	Basic magnetostrictive transduction concepts	33
4.3	Mechanical resonance	39
4.4	Magnetomechanical coupling	40
4.5	The electrical impedance of magnetostrictive dental scalers.....	44
	References for Chapter 4	56
5	MAGNETOSTRICTIVE DENTAL SCALERS	58
5.1	Introduction	58
5.2	Dental scaler system components	58
5.3	Dental scaler system.....	61
5.4	Dental scaler component analysis	64
5.5	Densply Dental Scaler Systems	68
5.6	Initial dental scaler analysis	70
5.7	Initial resonance measurements	74
5.8	Dynamic displacement measurements of dental scaler tips as a result of the application of dynamic magnetic fields	81
	References for chapter 5	97
6	MEASUREMENTS OF QUASI-STATIC MAGNETOSTRICTION OF ALTERNATIVE SCALER STACK MATERIALS	98
6.1	Introduction	98
6.2	Results	109
6.3	Summary of material suitability for new scaler inserts.....	122
	References for chapter 6	123
7	MEASUREMENT OF THE DYNAMIC MAGNOSTRICTION OF DENTAL SCALER STACK MATERIALS	124
7.1	Introduction	124
7.2	Single strip measurements.....	124
7.3	Results	129
	References for chapter 7	134
8	THE MANUFACTURE AND TESTING OF INSERTS BASED ON CANDIDATE REPLACEMENT MAGNETOSTRICTIVE MATERIALS.....	135
8.1	Introduction	135
8.2	Stack inserts	136
8.3	Production of Stacks	136
8.4	Stack manufacture: Electrical Insulation	137
8.5	Stack manufacture: Insert binding and soldering.....	138

8.6	Stack manufacture: Impedance measurement and compensation	142
	References for Chapter 8	151
9	THE MODELLING OF MAGNETOSTRICTIVE INSERTS TO IDENTIFY THEIR RESONANCES AND VIBRATION MODES.....	152
9.1	Introduction	152
9.2	FEMLAB 3.1	153
9.3	FEMLAB 3.1 modelling basics.....	153
9.4	3d Structural Mechanics Module Finite Element Models.....	160
9.5	3D Finite Element Modelling.....	160
9.6	Simple 3d stack models.....	162
	Extended mesh	163
	Base mesh	163
9.7	3d FEM analysis of multi-strip inserts	169
9.8	3d Finite element model of Inserts with different solid core materials.....	172
9.9	3d scaler inserts modelled with different solid-stack materials	180
9.10	Suggested Future Coupled Models.....	189
	References for chapter 9	191
10	RESONANCE MEASUREMENTS OF NEW AND COMMERCIAL INSERTS 192	
10.1	Introduction	192
10.2	Use of a new laser vibrometer	192
10.3	Use of a MXF 900 Power Amplifier	194
10.4	Use of the capacitance compensation system and MXF 900 power supply with non-nickel based inserts.....	199
10.5	Suggested Future Transducers.....	200
10.6	Conclusions	201
	References for Chapter 10	202
11	CONCLUSIONS	203
12	FUTURE WORK.....	207
	Appendix A: Error Analysis	210
	Appendix B: Rayleigh damping	212
	Appendix C: Publications and presentations	213

1 Introduction

For many years, magnetostrictive materials have been utilised in numerous transducer applications [1.1]. These have ranged from high-power sonar projectors to functional components in anti-vibration systems [1.2, 1.3].

Commercial magnetostrictive devices have been available for many years but in some cases there has been a tendency to utilise familiar magnetic transducer materials and designs rather than investigate the introduction of alternatives [1.4].

1.1 Aims and objectives

The objective of this study was to investigate new ultrasonic dental scaler inserts that could provide advantages over current systems [1.5]. New magnetostrictive material drive-elements and any associated power supplies would be identified and produced prior to characterisation.

The aims of the project were to:

- 1 Increase the understanding of how current magnetostrictive dental scalers function and develop new concepts for future devices.
- 2 Identify new magnetostrictive materials which may be used to drive ultrasonic scalers
- 3 Produce a new range of prototype scalar inserts having characteristics that could offer potential advantages over present models.

1.2 History of magnetism and magnetostriction

Magnetism is one of the oldest branches of solid-state physics. The ancient Greeks were amongst the first to study the properties of magnetite, a mineral composed of FeO and Fe_3O_4 . The initial studies into such materials resulted in the use of lodestone for ships' compasses but it was not until the sixteenth century that Sir William Gilbert formalised the investigation of magnetism. Considerable advances in the study of electricity and magnetism were made at the end of the eighteenth century and throughout the nineteenth century. However, with the development of Maxwell's equations for electromagnetism and quantum mechanics, a greater understanding of magnetic materials has been achieved [1.6].

The existence of magnetostriction was first discovered by Joule [1.7] but it was not until the production of early sonar devices that magnetostrictive nickel, nickel-iron or cobalt-iron alloys were widely utilised. Although these materials could achieve strains of ~ 150 ppm with optimum magnetomechanical coupling coefficients in the range of 0.3-0.4 (where unity indicates 100% transduction efficiency) they were quickly superseded by advanced ceramic piezoelectric materials [1.9]. Indeed, magnetostrictive materials have often struggled to find a niche in device applications as a result of competition with piezoelectric equivalents [1.9]. It was not until the development of so-called 'giant' magnetostrictive materials such as Terfenol-D [1.10] (with strains of ~ 2000 ppm) that magnetostrictive materials were considered to be a viable alternative to piezoelectrics as a result of comparable strain outputs and transduction efficiencies [1.9].

Despite the dominance of piezoelectric materials in many common transducer applications, a number of research and commercial transducers have been developed using magnetostrictive materials. These include the Feonic 'SoundBug' and 'Whispering Windows' speaker systems [1.12], Blue Wave ultrasonic baths [1.13], high power anti-vibration systems [1.14] and Dentsply dental scaler units [1.15].

1.3 Magnetostrictive transducers

Although it is possible to identify magnetostrictive transducers that have been produced to be 'maid of all work' devices [1.13], it is more common to find that a sensor or actuator has been designed to meet a specific specification. Each potential application has its own requirements that the transducer designer must take into account, if the device is to be successful [1.15]. System considerations can include the nature of the load to be actuated, the length of the desired stroke, the frequency response and the physical size and power requirements of the transducer. Consequently, once the requirements for a transducer have been specified, the designer must select a magnetostrictive material that can achieve the application needs. Once this has been done, it is possible to address the magnetic, electrical, mechanical and physical properties that will need to be optimised so that it can be incorporated into a system that will supply power and control for a given application [1.15, 1.16].

References for Chapter 1

- [1.1] Claeysen.F., et al “Actuators, transducers and motors based on giant magnetostrictive materials”, Journal of Alloys and Compounds, Volume 258, Number 0, 1 August 1997 , pp. 61-73(13).
- [1.2] Kawamori. A., et al “A low-frequency projector using giant magnetostrictive rods”, Journal of the Acoustical Society of America, Volume 96, Issue 5, November 1994, p. 3318
- [1.3] Bartlett. P.A., et al “High-power, low frequency magnetostrictive actuation for anti-vibration applications”, Sensors and Actuators A: Physical, Volume 91, Number 1, June 2001 , pp. 133-136(4).
- [1.4] Burman. Å., et al, “On the influence of functional materials on engineering design”, Research in Engineering Design, Volume 12, Number 1, July 2000, p. 39-47.
- [1.5] Lea. S. C., “Assessing the vibrations of dental ultrasonic scalers”, Journal of Sound and Vibration, Volume 271, Issues 3-5, April 2004, Pages 1113-1120.
- [1.6] Burns. G, “Solid state physics”, Academic Press, 1985, p. 565.
- [1.7] Jiles. D., “Introduction to magnetism and magnetic materials”, 2nd Ed, Chapman and Hall, London, 1991, p.121.
- [1.8] Bartlett. P.A., “Properties and applications of magnetostrictive materials”, MSc Thesis, University of Hull, 1997.
- [1.9] Greenough. R.D., et al, “The properties and applications of magnetostrictive rare earth compounds”, J. of Mag. & Mag. Mat. 101 (1991) 75-80.
- [1.10] Clark. A.E, “Introduction to highly magnetostrictive rare earth materials”, US J of Underwater Acoustics. Vol 27, No.1, Jan 1977, p.109.
- [1.11] Feonic PLC, <http://www.feonic.com/>
- [1.12] Bluewave Inc. <http://www.bluewaveinc.com/>
- [1.13] Etrema Products Inc. <http://www.etrema-usa.com/>
- [1.14] Dentsply Ltd. <http://www.dentsply.co.uk/products/preventive/cavitronplus.html>
- [1.15] Engdahl. G., “Handbook of giant magnetostrictive materials”, Academic Press, 1999.
- [1.16] Bright. C., Bright Engineering Inc. (Private Communication), 1998.

2 MAGNETIC PROPERTIES

2.1 Introduction

There are a number of basic parameters and concepts that are commonly used in any discussion on the properties of ferromagnetic materials [2.1]. These are outlined in the following sections.

2.2 Basic ferromagnetic principles

Magnetic field intensity: A conductor that is carrying an electric current will generate a magnetic field around itself. It is possible to produce a uniform magnetic field by winding a long, thin solenoid from such a conductor. If a current i flows in the windings of a solenoid with n turns per metre, the magnetic field intensity H produced and solenoid length L is given by (2.1) [2.2].

$$H = n.i/L \quad (\text{A/m}) \quad (2.1)$$

Permeability: The permeability, μ , is the factor that determines the flux density that will be induced within a ferromagnetic material as a result of the application of a magnetic field (see (2.3)) [2.3]. The permeability can be expressed as

$$\mu = \mu_o \mu_r \quad (\text{H/m}) \quad (2.2)$$

Where μ_o is the permeability of free space ($\mu_o = 4\pi \times 10^{-7}$ H/m) and μ_r is the relative permeability of a magnetic material with respect to μ_o .

As magnetic materials can possess non-linear properties, μ_r may not be constant. Consequently, an understanding of the full magnetic properties of a material is important for

many engineering applications [2.4]. However, for some ferromagnetic materials, the relative permeability can remain relatively constant over much of the characteristic B vs. H range [2.5].

Magnetic flux density (induction): A material that can be magnetised when exposed to a magnetic field is said to have a magnetisation \mathbf{M} (A/m) and a magnetic flux density \mathbf{B} (T) [2.6].

$$\mathbf{B} = \mu(\mathbf{H} + \mathbf{M}) = \mu_0 \mu_r (\mathbf{H} + \mathbf{M}) \quad (\text{T}) \quad (2.3)$$

Also, the magnetic polarisation, \mathbf{J} is defined as

$$\mathbf{J} = \mu \mathbf{M} \quad (\text{T}) \quad (2.4)$$

It must be noted that for free space, where no magnetic material is present, \mathbf{B} is given by

$$\mathbf{B} = \mu_0 \mathbf{H} \quad (\text{T}) \quad (2.5)$$

Susceptibility: A relationship between a material's magnetisation \mathbf{M} and an applied field \mathbf{H} is [2.7]

$$\mathbf{M} = \chi \mathbf{H} \quad (\text{A/m}) \quad (2.6)$$

where dimensionless χ is a measure of the ease by which a given magnetic field will establish a particular magnetisation. However, it must be borne in mind that magnetisation and magnetostriction of ferromagnetic materials also exhibit hysteresis.

The relative permeability is related to the susceptibility where:

$$\mu_r = \chi + 1 \quad (2.7)$$

Hysteresis and the hysteresis loop: The most common way to represent the bulk magnetic properties of a ferromagnetic material is by plotting magnetic induction B against H [2.8]. Such a plot is known as a BH loop. This BH loop shows the relationship between the

induced magnetic flux density B and the magnetising force H . It is also possible to plot M against H but as a result of (2.3) no additional information would be displayed in such a graph. The BH loop can offer the engineer considerable insight into the properties of a magnetic material. Figure 2-1 shows the general form of a typical BH loop [2.9].

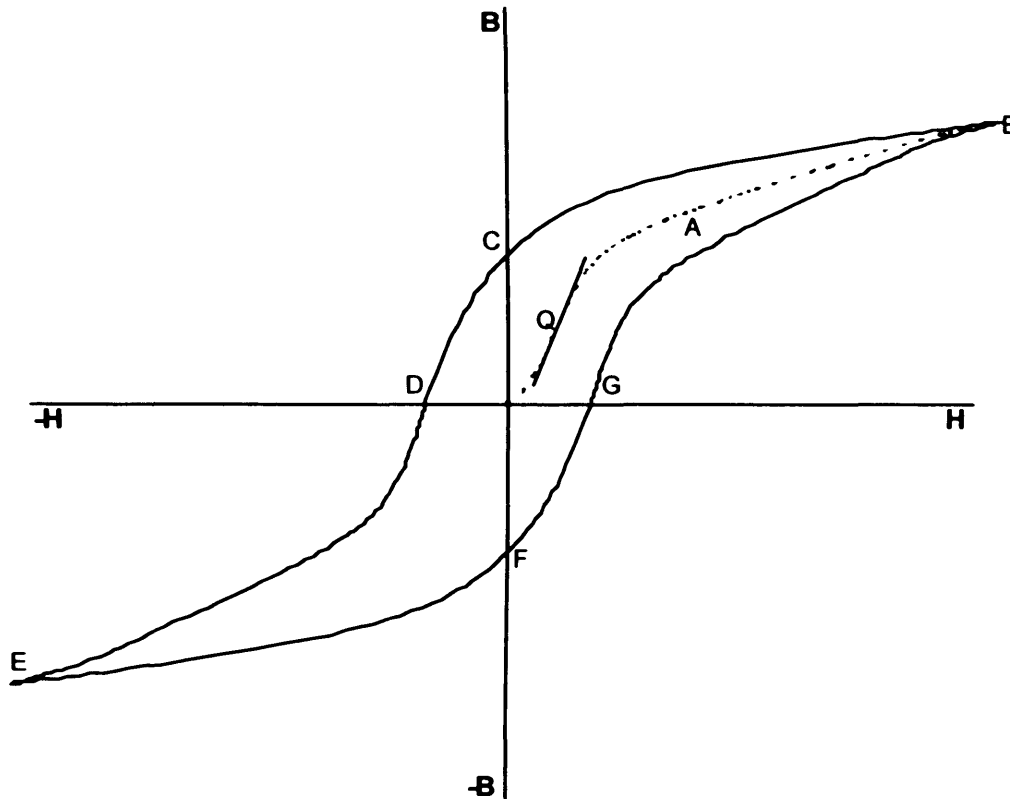


Figure 2-1 Typical BH curve for a ferromagnetic material showing the resultant induced B -field as a result of an applied H -field.

The loop is generated by measuring the magnetic flux density of a ferromagnetic material while the magnetising field is changed [2.8]. A ferromagnetic material that has never been previously magnetised or has been thoroughly demagnetized will follow the dashed line (indicated by “A”) as H is increased (see figure 2-1). Increasing the magnitude of the applied H -field, then increases the B -field that is induced in the material. At point “B” almost all of the magnetic domains are aligned, where the material approaches what is called saturation induction, B_s .

When H is reduced to zero, the curve will follow a path from point “B” to point “C”. At this point, it can be seen that some magnetic flux remains in the material even though the applied H -field is zero. This is referred to as the point of retentivity on the graph and indicates the remanence B_r or level of residual induction in the material. (Some of the magnetic domains remain aligned but some have lost their alignment.) As the magnetizing force is reversed, the curve moves to point “D”, where the flux has been reduced to zero. This is called the coercivity (H_c). The material (in this situation, the reversed magnetising H -field has rotated the magnetic domains so that the net induced B -field within the material is zero). The H -field required to remove this residual magnetism from the material is called the ‘coercive force’ ($-H_c$).

As the applied H -field continues to be increased in the opposite sense, the material will again become magnetically saturated but in the opposite direction (point “E”). Reducing the applied H -field to zero brings the curve to point “F”. It will have a magnitude of residual magnetism equal to that achieved at point C but in the opposite direction. Increasing the applied H -field further will return the induced B -field to zero. Notice that the curve does not return to the origin of the graph as an applied H -field is required to remove the residual magnetism. The curve will take a different path from point “G” back to the saturation point where it will complete the loop.

The line indicated by point “Q” is a tangent to the initial magnetisation curve whose maximum gradient yields the maximum incremental permeability for the material.

As can be seen, the plot is non-linear and possesses hysteresis. Hysteresis is the lag between making a change, such as increasing or decreasing applied field, and the response or

effect of that change. These BH loops can vary considerably from material to material. Indeed, such BH curves can also be dependent on the 'magnetic history' of the material; the 'stress history' and the past and present thermal states of the sample in question [2.10]. In addition, the BH characteristics can be influenced by the nature of the any dynamic H-fields that are applied to it.

A material is considered to be magnetically 'hard' if it has a high value of H_c and 'soft' if H_c is low (see table 2-1 for examples) [2.11].

	Initial	Maximum		
	μ_r	μ_r	H_c (A/m)	B_{sat} (T)
Soft				
3% Si-Fe	1.5×10^3	4.0×10^4	8.0	2.0
Mn-Zn Ferrite	1.0×10^3	1.5×10^3	0.8	0.2
Mumetal	2.0×10^4	1.0×10^5	4.0	0.6
Supermalloy	1.0×10^5	1.0×10^6	0.2	0.8
Hard				
		$(BH)_{max}$ (J/m ³)	H_c (A/m)	B_r (T)
5% Chromium Steel		2.4×10^3	5×10^3	0.94
Alnico (high remanence)		1.8×10^4	8×10^4	0.62
Cobalt-samarium, Co ₅ Sm		1.5×10^5	1×10^6	1.50

Table 2-1 Properties of some representative ferromagnetic materials [2.11]

By applying a cyclic H-field to a ferromagnetic material, the resultant induction will follow a BH-loop which possesses hysteresis [2.12]. The hysteresis associated with the magnetisation curve is related to the existence of magnetic domains in the material. Once the magnetic domains are reoriented by an applied H-field, it takes energy to turn them back again. Consequently, energy is lost as work is done in the material as its domains align with an applied H-field. The work done in this case (W_h) is directly related to the area bounded by the hysteresis loop and is given by:

$$W_h = \oint H \cdot dB \text{ (per cycle)} \quad (\text{Jm}^{-3}) \quad (2.8)$$

Easy axes (easy directions): The easy axis refers to the energetically favourable direction of the spontaneous magnetization in a ferromagnetic material. These axes are determined by factors such as the mechanical stress, magnetocrystalline anisotropy and shape anisotropy [2.13].

Domains: Ferromagnetic materials exhibit a long-range ordering phenomenon at the atomic level which causes the unpaired electron spins to line up parallel (the magnetic moments align) with each other in a region called a domain. Within the domain, the magnetic field is intense, but in a bulk sample the material will usually be unmagnetised because the many domains will themselves be randomly oriented with respect to one another [2.14, 2.15, 2.16].

Although each domain will be spontaneously magnetised to saturation in a definite crystalline direction, adjacent domains will have different directions. These domains (see figure 2-2) are separated by domain walls in which the direction of the spins is changing from the direction of one domain to that of its neighbour. Domains are formed to minimise the energy within the material but although smaller domains mean less energy [2.16] their wall area increases and the process ceases when the decrease in energy due to a splitting into smaller domains equals the increase due to the resultant increase of wall area.

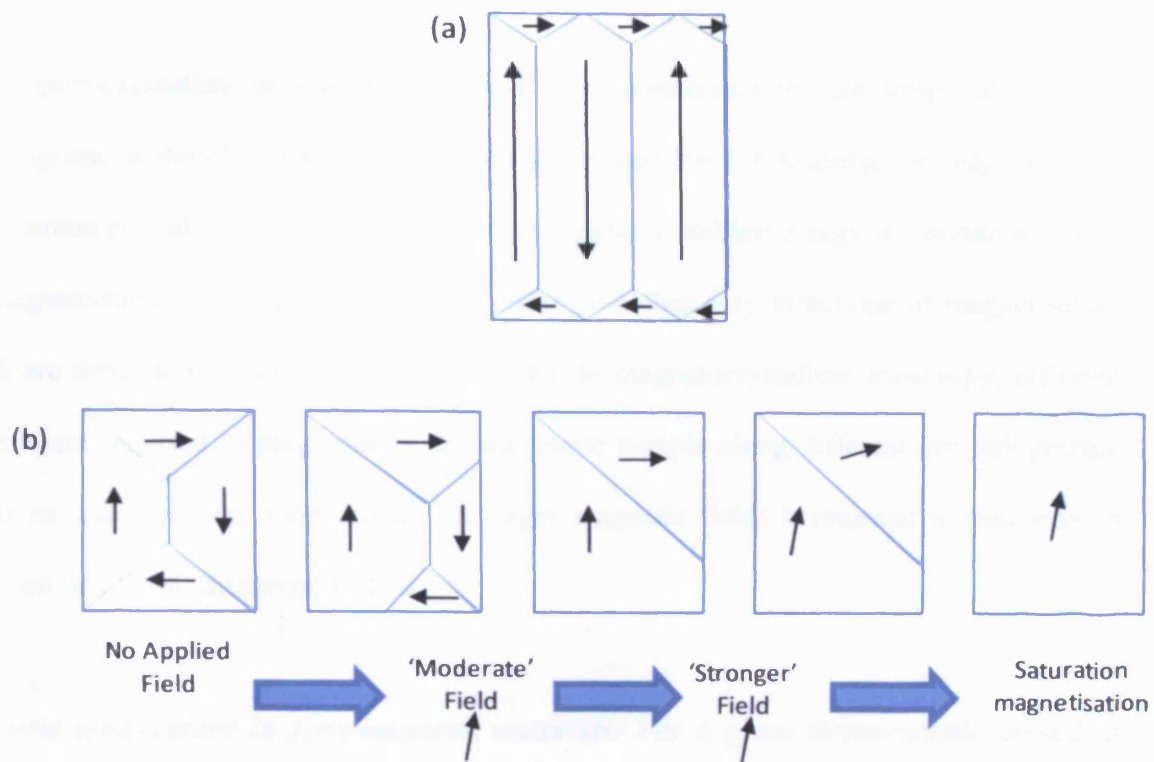


Figure 2-2 Ferromagnetic domains: (a) showing typical closure pattern; (b) showing effect of applying an external magnetic field [2.13]

The application of an increasing magnetic field causes [2.16] (see fig. 2-2) (i) initially, reversible wall movements allowing domains that are 'more favourably' magnetised to grow at the expense of those that are not, (ii) for 'moderate' fields, irreversible wall movements of the same types but hindered by impurities or defects in the crystal structure, and (iii) for 'stronger' fields, rotation of magnetisation from easy directions towards that of the applied field. Each of these stages accounts for part of the hysteresis loop and the irreversible step (ii) can be detected audibly by electromotances induced in loudspeaker coils wound on a ferromagnetic specimen as a wall 'jumps' irreversibly across a defect (known as the Barkhausen effect). The pattern of domains on the surfaces of materials can be made visible under the microscope by the application of fine ferromagnetic powders or colloidal suspensions (such as ferrofluid). Consequently, domain wall movements can be observed as a varying magnetic field is applied [2.16].

Magnetocrystalline anisotropy energy: The magnetocrystalline anisotropy energy in a ferromagnetic material is the energy which is responsible for aligning the magnetisation along certain crystallographic directions. The magnetocrystalline energy is a minimum when the magnetisation is aligned along one of these so-called easy directions of magnetisation which are dependent on crystal symmetry. Due to magnetocrystalline anisotropy, different energies are required to magnetise a ferromagnetic sample along different crystallographic directions and therefore, more energy (a larger magnetic field) is required to magnetise a specimen in a 'hard' direction. [2.17].

Curie temperature in ferromagnetic materials: For a given ferromagnetic crystal at absolute zero, the spontaneous magnetisation is equal in magnitude to the saturation value and all of the magnetic moments are aligned in parallel. As the temperature is increased from absolute zero the thermal energy increases. This thermal agitation prevents the magnetic moments from aligning in parallel and causes more disorder as the temperature is increased. This has the effect of reducing the spontaneous magnetisation within a domain. At a critical temperature, the randomising effect of the thermal agitation overcomes the aligning effect of the interaction energy and the material become paramagnetic in nature. The temperature at which this transition takes place is referred to as the Curie temperature (T_c) [2.17].

Demagnetisation factor: Demagnetisation factors are used to correct data on particular magnetic samples to give results that are intrinsic to the magnetic material when of that geometry. The demagnetisation correction adjusts the applied field H_a by the demagnetising field H_d to yield the internal magnetic field strength [2.18]:

$$H = H_a + H_d \quad (2.9)$$

Magnetic susceptibility, permeability and the shape of the magnetisation curve, as a function of field, are all affected by the demagnetisation correction. The demagnetising field H_d is related to the magnetisation M of the sample by the geometric demagnetisation factor N [2.18]:

$$H_d = -NM \quad (2.10)$$

The demagnetising correction is important in materials with large magnetic susceptibilities (or permeabilities) or in samples whose relative dimension parallel to the applied field is small [2.18]. The demagnetisation factor is determined by the ratios of the sample axes. Hence if the magnetisation components and lengths of axes are known, the H inside the body can be found [2.19]. The determination of N can be complex except for the special cases of ellipsoids of revolution [2.19] where, it is possible to produce expressions that can produce values for N for cylinders and rectangular samples of magnetic materials [2.20]. For example; a rod of rectangular cross-section is shown in figure 2-3.

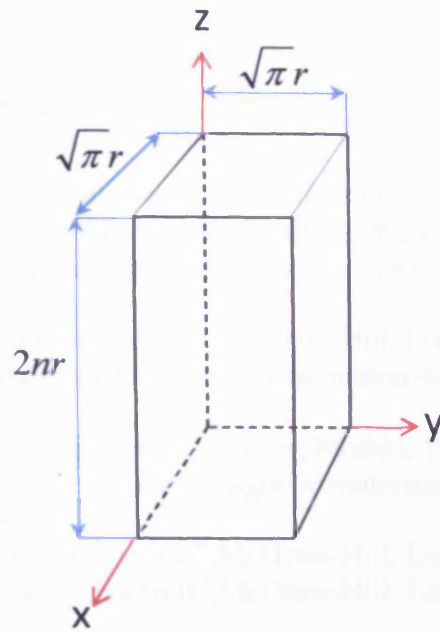


Figure 2-3 Rectangular rod of magnetic material with its dimensions specified so that the demagnetisation factors for it can be calculated using Eqs 2.11 and 2.12 [2.20]

By re-stating the lengths l_x , l_y and l_z as $\sqrt{\pi}r$, $\sqrt{\pi}r$ and $2nr$ respectively then the demagnetisation factors in the x , y and z directions can be approximately calculated using [2.20]:

$$N_x = N_y = \frac{2n/\sqrt{\pi}}{\left[2\left(\frac{2n}{\sqrt{\pi}}\right) + 1\right]} \quad (2.11) [2.20]$$

$$N_z = \frac{1}{\left[2\left(\frac{2n}{\sqrt{\pi}}\right) + 1\right]} \quad (2.12) [2.20]$$

References for Chapter 2

- [2.1] Oduncu H, "Development of amorphous magnetostrictive sensors with application to monitoring of fracture healing", Ph.D thesis, University of Wales, Cardiff, 1997.
- [2.2] Jiles D, "Introduction to magnetism and magnetic materials", Chapman and Hall, London, 2nd Ed, 1998, p.19.
- [2.3] Duffin W.J., "Electricity and magnetism", McGraw-Hill, London, 3rd Ed, 1980 p.339.
- [2.4] Jiles D, "Introduction to magnetism and magnetic materials", Chapman and Hall, London, 2nd Ed, 1998, p.92-94.
- [2.5] Chikazumi. S, "Physics of magnetism", Krieger, Florida, 1986, p.491.
- [2.6] Jiles D, "Introduction to magnetism and magnetic materials", Chapman and Hall, London, 2nd Ed, 1998, p.45-46.
- [2.7] Duffin W.J., "Electricity and magnetism", McGraw-Hill, London, 3rd Ed, 1980 p.338.
- [2.8] Duffin W.J., "Electricity and magnetism", McGraw-Hill, London, 3rd Ed, 1980 p.344-347.
- [2.9] Jiles D, "Introduction to magnetism and magnetic materials", Chapman and Hall, London, 2nd Ed, 1998, p.93-94.
- [2.10] Atherton, D.L, "Magnetization changes induced by stress under constant applied field in 2% Mn pipeline steel", IEEE Trans. Mag. Vol. 24, No.3, 1988, p2029.
- [2.11] Duffin W.J., "Electricity and magnetism", McGraw-Hill, London, 3rd Ed, 1980 p.346.
- [2.12] Duffin W.J., "Electricity and magnetism", McGraw-Hill, London, 3rd Ed, 1980 p.344-345.
- [2.13] Galloway N, "Optimisation of the magnetoelastic properties of Terfenol-D", Ph.D thesis, University of Hull, 1992, p28.
- [2.14] <http://hyperphysics.phy-astr.gsu.edu/Hbase/Solids/ferro.html>
- [2.15] Jiles D, "Introduction to magnetism and magnetic materials", Chapman and Hall, London, 2nd Ed, 1998, p.135-153.
- [2.16] Duffin W.J., "Electricity and magnetism", McGraw-Hill, London, 3rd Ed, 1980 p.358-359.
- [2.17] Galloway N, "Optimisation of the magnetoelastic properties of Terfenol-D", Ph.D thesis, University of Hull, 1992, p17.
- [2.18] Evettes J, "Concise encyclopedia of magnetic and superconducting materials", Pergamon, Oxford, 1st Ed, 1992, p.103-104.
- [2.19] Osborn J.A, "Demagnetizing Factors of the General Ellipsoid", Physical Review, V.67 No.s 11 and 12, 1945, p.351-357.
- [2.20] Sato M, Ishii Y, "Simple and approximate expressions of demagnetizing factors of uniformly magnetized rectangular rod and cylinder", J. Appl. Phys. 66(2), 1989, p.983-985.

3 MAGNETOSTRICTION

3.1 Introduction

The magnetisation of a ferromagnetic material is usually associated with a change in dimensions [3.1]. The resulting strain is known as magnetostriction λ where

$$\lambda = \delta l / l \quad (3.1)$$

and ' l ' is the length of the material in the direction in which the strain is measured.

There are two contributions to the overall magnetostriction. The first is the spontaneous magnetostriction due to the ordering of magnetic moments into domains at the Curie temperature and the second is due to the application of a magnetic field. It is this second contribution that is utilised in magnetostrictive transducers.

3.2 Magnetostriction in isotropic and anisotropic materials

When a ferromagnetic material is cooled through its Curie temperature, the previously randomly disordered paramagnetic magnetic moments become ordered over volumes containing large numbers of atoms (typically 10^{12} - 10^{18} atoms) [3.2]. These ordered volumes (where all of the magnetic moments are parallel) are called 'domains'. The direction of the spontaneous magnetisation M_s varies from domain to domain throughout the material in such a way so that the bulk magnetisation is zero.

If we consider spherical volumes of an unstrained solid within a greater solid above the Curie temperature of the material, we would have the disordered phase as shown in figure 3-

1a. In this case, the lack of ordering in the volumes results in paramagnetic behaviour for this material. When the material is cooled to below the Curie temperature, ferromagnetic ordering within the domain volumes will occur with a resultant spontaneous magnetisation and an associated strain (ϵ) or magnetostriction λ_0 . The resultant strain could be considered to be along a particular direction as shown in figure 3-1b (by assuming that the strain in the transverse direction is small compared to that along the greater longitudinal axis of a long, thin sample such as a rod).

Upon the application of a magnetic field, the domains within the material in figure 3-1 will initially be dominated by the migration of domain walls within the material in response to the external magnetic field (see section 2.2). Secondly, the domains' magnetisations will change so that they align with the applied field. These two mechanisms result in a dimensional change. Since the deformation is isochoric (a constant-volume process), there is an opposite dimensional change in the orthogonal direction. If sufficient field is applied, then saturation magnetisation will be achieved and a 'maximum' value for magnetostriction λ_{max} will result as in figure 3.1c [3.2, 3.3]. Although the material has achieved saturation magnetostriction when λ_{max} is reached; it is possible to increase the magnetisation and magnetostriction further through the application of higher applied magnetic fields. However, the increase in magnetisation and strain is very low when compared to the increases with increasing applied field before 'maximum' magnetostriction is achieved. This additional effect is only appreciable at fields of the order of 800 kA/m [3.4].

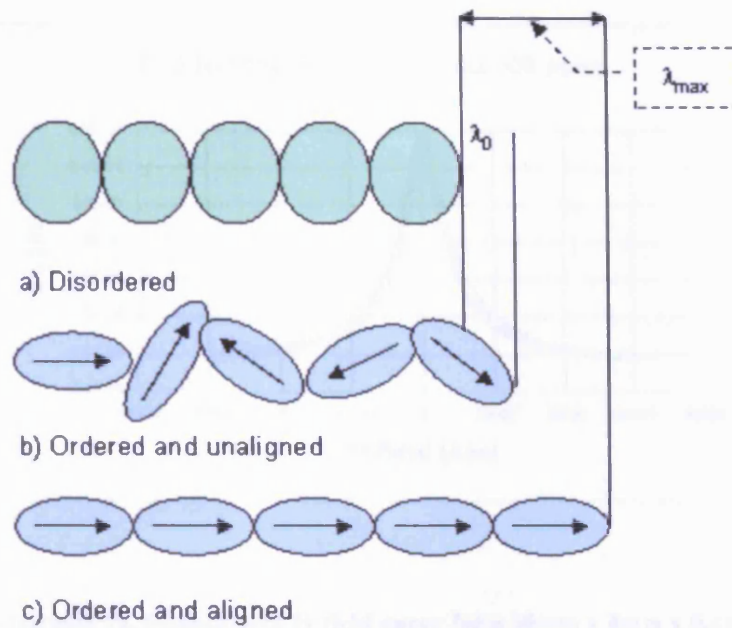


Figure 3-1 Simple schematic diagram illustrating the magnetisation in: a) the disordered (paramagnetic) case; b) the ferromagnetic but demagnetised case; c) the ferromagnetic case for saturation magnetisation. [3.4].

It is typical for ferromagnetic magnetostrictive materials to have anisotropic properties. Consequently, the saturation magnetostriction will be defined in relation to the crystal axis along which the magnetisation lies [3.5].

A typical strain vs. applied field curve for an unstressed polycrystalline nickel sample is shown in figure 3-2 where the magnetostriction can be observed to possess non-linear strain vs. applied H-field characteristics and hysteresis.

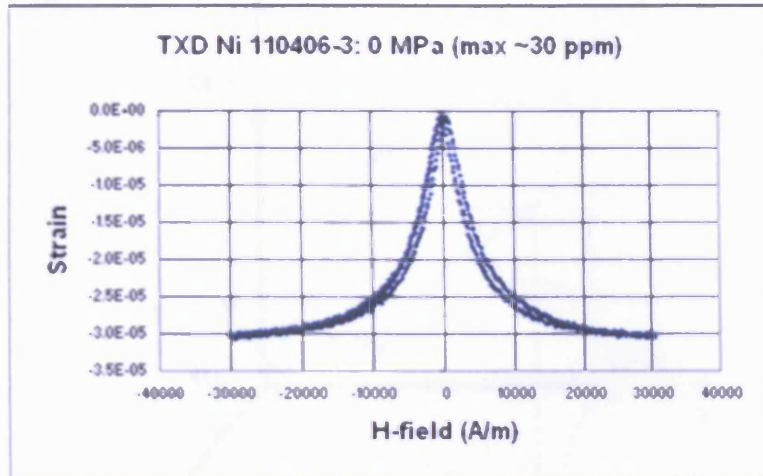


Figure 3-2 Typical λ (strain) Vs. magnetising H-field curve for a 50mm x 4mm x 0.4mm strip of negatively magnetostrictive nickel with zero pre-stress as measured by the author

The magnetic anisotropy relates the dependence of the internal energy on the direction of the spontaneous magnetisation. If the material possesses a cubic crystal structure then this energy can be expressed via direction cosines between the field and the crystallographic axis (see figure 3-3).

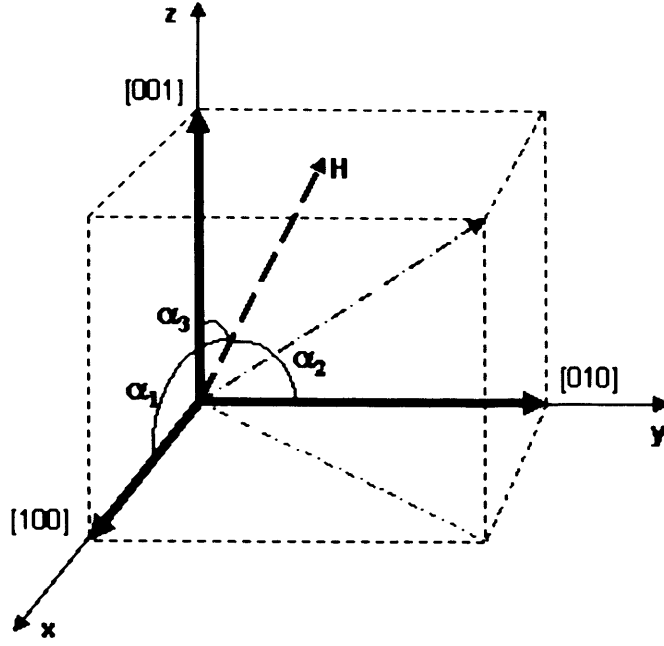


Figure 3-3 The direction cosines $\alpha_1, \alpha_2, \alpha_3$, between an applied field and the crystal axis

Assuming that the applied field makes angles a, b, c with the crystal axis $\alpha_1, \alpha_2, \alpha_3$ are the cosines of these angles and K_1 and K_2 are the ‘anisotropy constants’ for a given material then the anisotropy energy, W_k will be [3.6]:

$$W_k = K_1 (\alpha_1^2 \alpha_2^2 + \alpha_2^2 \alpha_3^2 + \alpha_3^2 \alpha_1^2) + K_2 \alpha_1^2 \alpha_2^2 \alpha_3^2 + \dots \quad (3.1)$$

As the magnetostriction of the ferromagnetic sample depends on the internal structure, then the magnetostriction in a crystalline solid will be determined by the direction cosines using the Becker-Doring equation [3.7]:

$$\lambda_s = \frac{3}{2} \lambda_{100} \left(\alpha_1^2 \beta_1^2 + \alpha_2^2 \beta_2^2 + \alpha_3^2 \beta_3^2 - \frac{1}{3} \right) + 3 \lambda_{111} (a_1 a_2 \beta_1 \beta_2 + a_2 a_3 \beta_2 \beta_3 + a_3 a_1 \beta_3 \beta_1) + \dots \quad (3.2)$$

where λ_{100} and λ_{111} are the saturation magnetostrictions measured along the [100] and [111] directions respectively when the ferromagnetic material is magnetised in these directions $\beta_1,$

β_2 and β_3 are the cosines of the angles between λ_s (the saturation magnetostriction) and the crystal axis. In the case where the induced strain is measured in the same direction as the magnetic field then [3.6, 3.7]:

$$\lambda_s = \lambda_{100} + (\lambda_{111} - \lambda_{100})(\alpha_1^2 \alpha_2^2 + \alpha_2^2 \alpha_3^2 + \alpha_3^2 \alpha_1^2) \quad (3.3)$$

and in the case of an isotropic material where $\lambda_s = \lambda_{100} = \lambda_{111}$ then Eq. (3.2) becomes [3.8]:

$$\lambda_s(\theta) = \frac{3}{2} \lambda_s \left(\cos^2 \theta - \frac{1}{3} \right) \quad (3.4)$$

References for Chapter 3

- [3.1] Jiles.D., “Introduction to magnetism and magnetic materials”, Chapman and Hall, London, 2nd Ed, 1998, p.121-129.
- [3.2] Jiles.D., “Introduction to magnetism and magnetic materials”, Chapman and Hall, London, 2nd Ed, 1998, p.122.
- [3.3] <http://aml.seas.ucla.edu/home.htm>
- [3.4] Jiles.D., “Introduction to magnetism and magnetic materials”, Chapman and Hall, London, 2nd Ed, 1998, p.123-124.
- [3.5] Chikazumi. S., “Physics of magnetism”, Krieger, Florida, 1986, p.163.
- [3.6] Katranas. G.S., “Design and development of bilayer sensor systems for biomedical and automotive applications”, Cardiff University, Ph.D Thesis, pp 32-34.
- [3.7] Chikazumi. S., “Physics of magnetism”, Krieger, Florida, 1986, p.129.
- [3.8] Jiles. D., “Introduction to magnetism and magnetic materials”, Chapman and Hall, London, 2nd Ed, 1998, pp.125-127.

4 MAGNETOSTRICTIVE TRANSDUCERS

4.1 Introduction

Transducer designers have many choices when selecting magnetostrictive materials. The starting point for any design is, in general, a demand specification in terms of currents, voltages, strains, forces, power levels, frequency characteristics, response times, and operating temperatures. [4.1]. During the design phase, these specifications, coupled to materials and electromechanical data of potential system components, must be transformed into 'construction data'. These data will enable the designer to make engineering choices so that an optimum system can be developed despite the conflicting requirements of different aspects of a device's sub-component design. In a magnetostrictive transducer, magnetic fields can be applied to the functional material via permanent magnets and/or magnetising coil arrangements [4.2]. Materials can be classified as having [4.3];

- a negative magnetostriction, where application of an increasing magnetic field results in an increasing negative strain in the field direction
- a positive magnetostriction, where application of an increasing magnetic field results in an increasing positive strain in the field direction

As the strain vs. applied H-field characteristic is non-linear, the application of a magnetic field does not result in a linear strain output for all values of the applied field [4.4]. Magnetostrictive transducers can be used to supply strains and associated forces. These can be both quasi-static and dynamic in nature.

In a transducer that is to be used for dynamic applications, the overall performance of the device will be determined by a number of the system's coupled properties including [4.5, 4.6]:

- i. Magnetostrictive material properties
- ii. Magnetic component properties
- iii. Mechanical component properties
- iv. Electrical component properties

It is important to understand the properties of each of the system components and their inherent limitations.

4.2 Basic magnetostrictive transduction concepts

Figure 3-2 showed a typical λ vs. H-field curve for an unstressed sample of nickel. From a transducer designer's point of view, this is one of the most important characteristics as it represents the 'output' strain for a given 'input field'. It represents a significant component of the overall transfer function of the transducer.

If we simplify the characteristics of such a material, it is possible to identify some of the key considerations that must be taken into account when designing a magnetostrictive transducer that will be used to produce displacement or vibration. Such a simplification is shown in figure 4-1, where a positively magnetostrictive material is shown but with the hysteresis and the higher-order non-linearities removed leaving only the main point of inflection that is a characteristic feature of magnetostrictive materials [4.7].

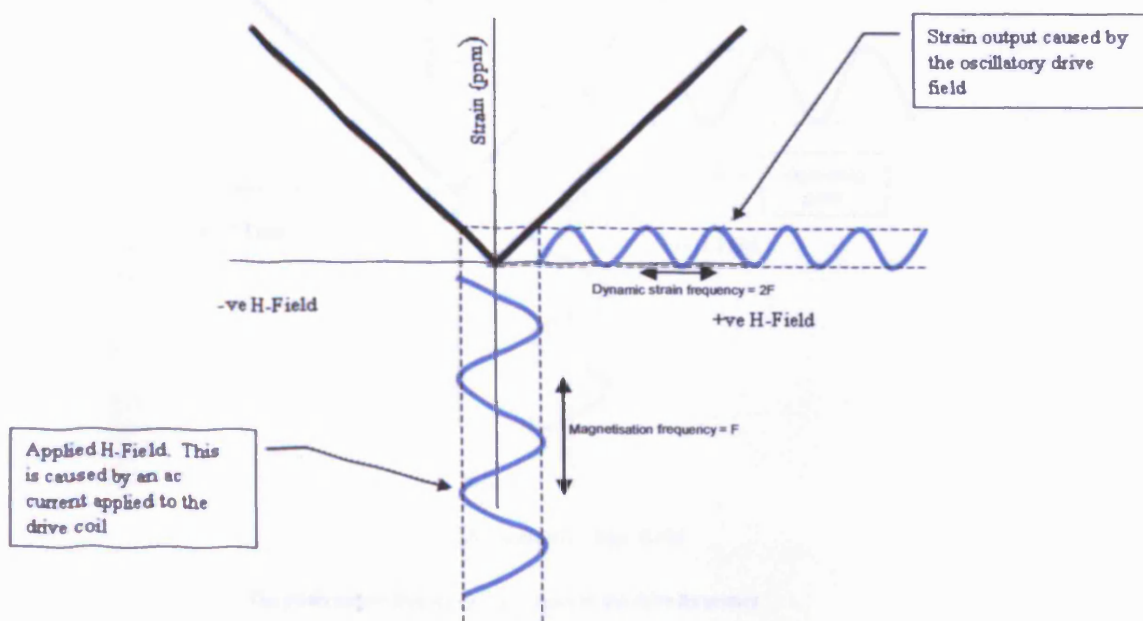
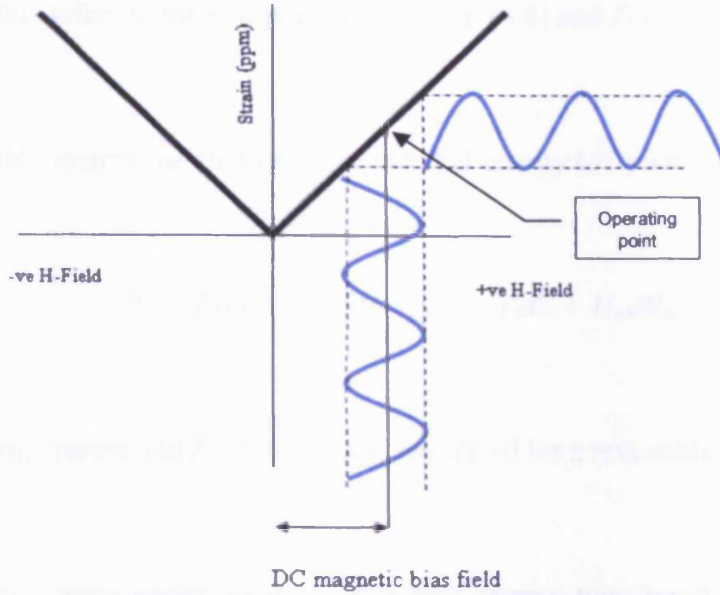


Figure 4-1 The resultant frequency doubled output of a positive magnetostrictive material as a consequence of applying a drive field without magnetic biasing

In figure 4-1, a sinusoidal H-field is applied to the magnetostrictive material. In this case, the applied H-field is supplied so that it varies with an average field value of zero. In this case there is no additional applied static H-field (usually known as the 'bias field'). A key feature of this method of excitation is that the strain output from the magnetostrictive material will have a frequency that is twice that of the applied H-field. This is the so-called 'frequency doubling effect' and it is due to the non-linearity associated with the point of inflection in the λ vs. H-field characteristic as shown in figure 4-1. In some transducers, such an effect can be desirable but in others there may be a desire to eliminate frequency doubling completely. A magnetic biasing method that achieves this is shown in figure 4-2.



Note: The strain output frequency is the same as the drive frequency

Figure 4-2 The resultant non-frequency doubled output of a positive magnetostrictive material as a consequence of applying a drive field with magnetic biasing. The DC magnetic bias establishes an operating point which the dynamic applied field is centred upon.

This has been achieved by applying a DC bias field so that the dynamic field component will be applied around an ‘operating point’ on the λ vs. H-field curve (see figure 4-2). Considering the linear case further, it is possible to identify some of the characteristics of such a magnetostrictive ‘curve’.

When a unit volume of a magnetostrictive material is magnetised, magnetic work δW_{mag} will be done [4.8]:

$$\delta W_{mag} = H_m \delta B_m \quad (4.1)$$

for an incremental magnetic flux density change; δB . ($m = 1, 2, 3$; this refers to the x, y and z directions in figure 3-3 and H_m is the applied magnetic field).

If at the same time this volume is subjected to mechanical strain δS , and this deformation process is isothermal and reversible, the mechanical work done is [4.8]:

$$\delta W_{mech} = T_i \delta S_i \quad (4.2)$$

($i = 1, 2, \dots, 6$; this refers to the components of strain [4.8] and T_i is the applied stress).

In this reversible system the change in the internal energy (dU) within the material is:

$$dU = T_i dS_i + H_m dB_m - \zeta dF = T_i dS_i + H_m dB_m \quad (4.3)$$

(where F = temperature and ζ = the entropy and $dF=0$ for a reversible system).

The Gibbs energy under adiabatic (no heat energy transferred to or from the system) conditions can be written as [4.9]:

$$G = U - T_i S_i - H_m B_m \quad (4.4)$$

where the Gibbs energy is the maximum useful work that can be obtained from a system undertaking a reversible process, whilst remaining in equilibrium with its surroundings.

Differentiating Eq.4.4 gives the change in the Gibbs energy in differential form:

$$dG = dU - dT_i S_i - dH_m B_m - T_i dS_i - H_m dB_m \quad (4.6)$$

and for reversible processes, substituting Eq. 4.3 into Eq. 4.6 gives:

$$dG = - S_i dT_i - B_m dH_m \quad (4.7)$$

which gives (using the Legendre transform):

$$S_i = \left. \frac{-\partial G}{\partial T_i} \right|_H ; \quad B_m = \left. \frac{-\partial G}{\partial H_m} \right|_T \quad (4.8)$$

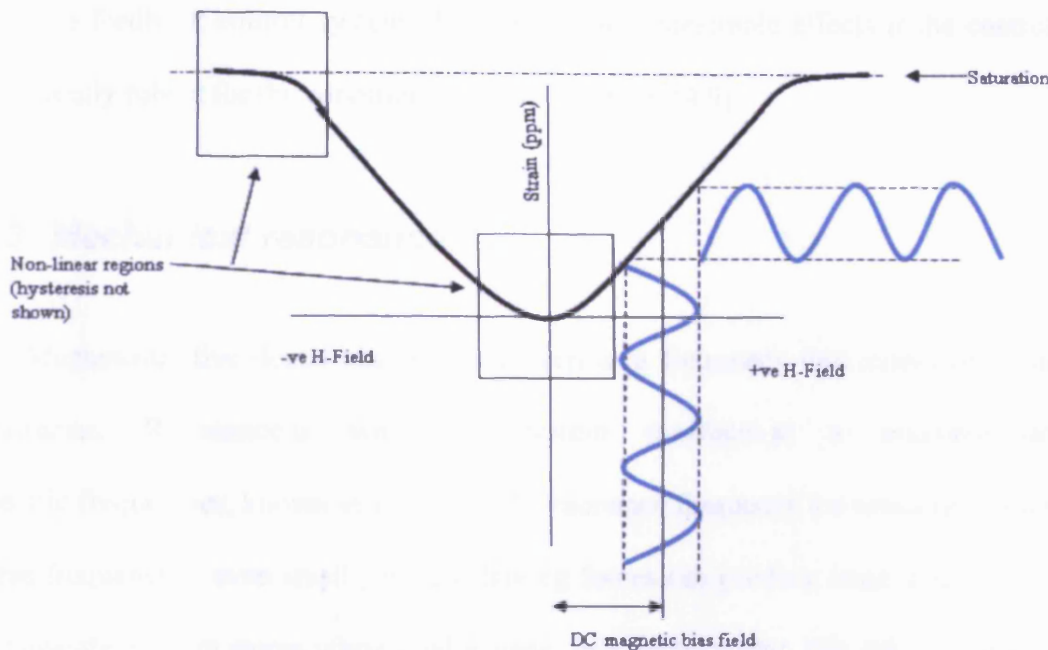
Taking the partial derivative of S_i with respect to H_m and the partial derivative of B_m with respect to T_i gives

$$\left. \frac{\partial S_i}{\partial H_m} \right|_T = \left. \frac{\partial B_m}{\partial T_i} \right|_H = d_{mi} \quad (4.9)$$

As the longitudinal operational mode for magnetostrictive materials is the most common, the applied magnetic field is applied along the longitudinal axis of the material and so magnetostrictive strains can be considered to only have components in the z-direction (also called the direction where i and $m = 3$). Hence for an actuator:

$$\left. \frac{\partial S_3}{\partial H_3} \right| = d_{33} \quad (4.10)$$

where d_{33} or d is known as the magnetostrictive constant. However, in practice there will be a volume change in dimensions. In figure 4-2, d_{33} can be determined by measuring the gradient of the λ vs. applied H-field curve. In more realistic, practical curves where d_{33} is not a constant, the maximum gradient of the λ vs. applied H-field curve may be specified. In addition, the operating point of any magnetic bias applied to the material may be selected so that a maximum value of d_{33} is achieved. In magnetostrictive transducers, it is often desirable to magnetically bias the material so that the operating point coincides with the region of the λ vs. applied H-field where d_{33} is greatest for a non-linear curve. This is shown in figure 4-3 where non-linearities (but not hysteresis) are shown for a λ vs. applied H-field curve.



Note: Biasing can also enable operation in a linear performance region that may also have the greatest gradient.

Figure 4-3 The non-linearities associated with magnetostrictive materials (hysteresis not shown). Positive magnetostrictive material shown.

Any non-linearities in the λ vs. applied H-field curve can result in a strain that incorporates frequency components other than the excitation frequency. The most significant of these is the 'frequency doubling' effect shown in figure 4-1 but it is also possible for higher harmonics to be observed when a sinusoidal H-field is applied to a magnetostrictive material. In practice, the reduction of the majority of unwanted harmonic components can be achieved by magnetically biasing the magnetostrictive material so that its operating point is on the most linear portion of the λ vs. applied H-field curve [4.10].

Hysteresis is another feature of magnetostrictive materials. The presence of hysteresis in the λ vs. applied H-field curves is due to the same physical mechanisms that produce hysteresis in B-field vs. H-field curves as the movement of domain walls causes work to be

done. The non-linearities and hysteresis present in magnetostrictive devices that are operated within a feedback control system [4.2] can cause undesirable effects if the controller is not sufficiently robust for the conditions it operates under [4.9].

4.3 Mechanical resonance

Magnetostrictive dental scalers are driven at a frequency that stimulates a mechanical resonance. Resonance is where a system oscillates at a maximum amplitude at specific frequencies, known as the system's resonance frequency (or resonant frequencies). At these frequencies, even small periodic driving forces can produce large amplitude vibrations, because the system stores vibrational energy. In a dental scaler, this driving force is supplied by the straining magnetostrictive material.

The equation of motion for a forced mechanical oscillator can be simply defined as [4.11]

$$F_0 \cos \omega_f t = m \frac{d^2 x}{dt^2} + b \frac{dx}{dt} + kx \quad (4.11)$$

Where F_0 is the maximum amplitude of the applied force, ω_f is the excitation frequency, x is the displacement of the system's mass (a combination of the load mass and the distributed mass of the magnetostrictive rod [4.10]), b is the mechanical damping coefficient for the system and k is the spring constant for the system. When the frequency of the driving force is equal to the natural frequency of the system (when damping is small $\omega_f = \omega_n = \sqrt{k/m}$, when damping is significant then $\omega_f = \omega = \sqrt{k/m - b^2}$) then the velocity, displacement amplitude and kinetic energy of the oscillating system are at a maximum. Consequently, the system is said to be resonating [4.11].

4.4 Magnetomechanical coupling

The λ -H performance of a magnetostrictive material has been shown to be stress dependent [4.12, 4.13, 4.14, and 4.15]. Therefore, it is important to have an appreciation of how a given magnetostrictive material will perform when under an external stress.

A magnetostrictive material will undergo strain when a magnetic field has been applied. In addition, the magnetisation of a magnetostrictive material will change when a stress is applied [4.16]. These coupled dependencies can be approximated by mathematical functions if it is assumed that the magnetostrictive material possesses reversible magnetomechanical properties. As the longitudinal mode is the most important for magnetostrictive materials in devices it can be assumed that the stresses, strains and magnetic field quantities are directed parallel to the z-axis (see figure 3-3). Consequently, the constitutive linearised equations that model the magnetostriction are:

$$S = s^H T + d_{33} H \quad (4.12)$$

$$B = d_{33}^* T + \mu^T H \quad (4.13)$$

In these relationships [4.17], S and T denote the longitudinal strain and axial stress in the material respectively, while s^H denotes the mechanical compliance at a fixed field strength H . Additionally, B and μ^T , respectively, denote the magnetic flux density and permeability at constant stress while;

$$d_{33} = \left. \frac{\partial S_3}{\partial H_3} \right|_T \quad (4.14)$$

and

$$d_{33}^* = \left. \frac{\partial B_3}{\partial T_3} \right|_H \quad (4.15)$$

are the magnetoelastic coupling coefficients. It must be noted that in equation (4.12) the generated strains are dependent on both the elastic properties of the material ($s^H T$) and the magnetically induced component ($d_{33} H$). Equation (4.13) incorporates the direct magnetostrictive effect in which magnetic flux is produced as a result of stressing the material. This results in magnetostrictive properties that can be used to produce sensors. Although such a linearised model is only acceptable when small values of ΔH are applied to the material so that the magnetostrictive non-linearities are not apparent in the strain output [4.17], it is sufficient to give an appreciation of the nature of the magnetomechanical coupling that is associated with magnetostrictive materials and devices. Indeed, the model does not take into account the hysteresis or non-linearities present in real magnetostrictive samples or the non-constant nature of permeability as a result of varying applied fields and stresses. In addition, the assumption of a constant Young's modulus and an associated compliance is also invalid for large field fluctuations. This situation is also compounded where a sample has a high frequency H-field applied to it as a result of skin [4.18] and inertial [4.10] effects as defined below.

The skin effect occurs when a dynamic magnetic field is applied to a conducting material. The eddy currents that are generated in the material (in the case of magnetostrictive transducers, this is initially within the material itself) are distributed in such a way that the current density near the surface of the electrically conducting magnetostrictive material is greater than that produced in the core. Such an effect causes the attenuation of the magnetic field as a result of the opposing field that is generated by the eddy currents themselves.

Consequently, the centre of a magnetostrictive component can be ‘shielded’ from the applied magnetic field and will not contribute to the production of strain [4.22]. For a rod of magnetostrictive material, it can be shown [4.23] that the so-called ‘critical frequency’ f_c above which the transducer can be considered to be operating sub-optimally as a result of skin depth screening is;

$$f_c = \frac{1}{2\pi\mu\sigma r^2} \quad (4.16)$$

where r , represents the radius of the cylinder, σ the magnetostrictive material’s electrical conductivity, and μ is the value of the permeability that would be expected for the operating conditions. Although care must be taken when using this equation (due to any assumptions made about the value of the permeability for a given pre-stress), it can nevertheless give an indication of whether the dimensions of the magnetostrictive sample to be used are acceptable for the proposed operating frequency.

Inertial effects are those associated with a magnetostrictive material supplying a dynamic force to a load mass (that will include the distributed mass of the magnetic material itself) [4.24].

As the magnetising frequency increases, the ability of the magnetic material to supply the required strain will reduce. This is a direct consequence of the limited maximum force that can be produced by a given magnetostrictive drive element. Indeed, such a dynamic variable force can also change the value of the prestress that the magnetostrictive material experiences and consequently d_{33} [4.24]. This will have an influence in the strain output as:

$$S = s^H T + d_{33} H \quad (4.17)$$

Hence, a given drive field will not result in the same strain output as the drive frequency increases. The implications of coupled magnetomechanical systems on transducer performance are discussed further in chapter 2.5 from the perspective of the system's overall electrical impedance.

Applying a pre-stress can have a distinct influence on the performance of a given magnetostrictive material. By applying an appropriate level of pre-stress (tension for a negative magnetostrictive material and compression for a positive magnetostrictive material) the maximum strain output from a sample can be optimised. This is due to the pre-stress causing domain alignment in a direction that is close to or on the easy axis of the sample concerned. Consequently, the subsequent application of an applied field will result in coherent domain rotations from one direction to another yielding a greater overall strain. However, too much pre-stress will introduce a 'retarding force' that will require greater H-fields to be applied to cause the domains to rotate to the same strain levels [4.19].

A magnetostrictive transducer should be considered as a system. The magnetostrictive material within the transducer contributes to the overall transfer function of the device but the nature of the mechanical sub-system, other magnetic materials and the solenoid supplying the H-field to the magnetostrictive sample will have an influence on issues such as [4.2, 4.20, and 4.21]:

- i. The overall electrical impedance of the device (including impedances due to magnetomechanical coupling with the magnetostrictive component).
- ii. The overall mechanical compliance of the device (again influenced by the magnetomechanical coupling with the magnetostrictive component).
- iii. The resonant characteristics of the whole transducer (this includes the magnetostrictive component and any other mechanical components it is connected to).
- iv. The flux levels and flux uniformity as a result of the full magnetic circuit.

- v. The thermal characteristics of the transducer and the magnetostrictive material concerned (as the magnetostrictive performance of a device is also temperature dependent with the Curie temperature being the ultimate limit for transducer functionality).

An example of such a transducer system is the ultrasonic dental scaler. The magnetostrictive components of such a dental scaler are excited via the application of a magnetic field so that a tip (that is used to ‘clean’ a tooth’s surface) exhibits ultrasonic vibrations that assist in the removal of unwanted dental deposits.

4.5 The electrical impedance of magnetostrictive dental scalers

From an engineering viewpoint a magnetostrictive transducer can be considered to be a R-L circuit. In its simplest form, the electrical impedance of which is [4.25];

$$Z = R + j\omega L \approx R + j\omega\mu n^2 V \quad (4.18)$$

Where R is the resistance of the coil, n is the number of turns of the coil, μ is the permeability of the core material and V is the volume of the coil. As R , n and V are all real valued constants, any changes in the impedance in these transducers with frequency must be due to variations in the magnetic permeability with frequency and load.

It is possible to develop a magnetomechanical model of magnetostriction that can identify the impedance that would be expected to be measured at the terminals of a transducer. This can take into account the changes in impedance that are due to changes in the frequency dependent variables associated with Eq. 4.18.

Equations 4.12 and 4.13 are useful to understand how magnetostrictive materials work but they neglect dynamic effects [4.25]. The following will present a magnetomechanical model that will take into account dynamic effects that will influence the impedance of magnetostrictive dental scaler systems.

The transduction equations for an electromechanical transducer can be stated to be [4.25];

$$V = Z_e I + T_{em} v \quad (4.19)$$

$$F = T_{me} I + z_m v \quad (4.20)$$

where V is the voltage measured across the electrical input terminals of the transducer, Z_e is the blocked electrical impedance¹ of the transducer, I is the current passing through the transducer's solenoid, T_{em} is the transduction coefficient for electrical effects from the mechanical velocity, v is the transducer output velocity, F is the output force of the transducer, T_{me} is the transduction coefficient for mechanical effects from the electrical current and z_m is the mechanical impedance of the transducer.

To solve these equations, all of the coefficients of v and I must be known along with two of the four state variables (V , F , I and v). The coefficients represent the 'effective' parameters for the transducer. This includes the effects of eddy currents, leakage flux and all of the detrimental effects of the overall magnetic circuit on the performance of the magnetostrictive material within the transducer [4.25, 2.26].

¹ The blocked electrical impedance is the impedance of the transducer when motion is inhibited by the application of a force that has the same magnitude as the force produced by the transducer.

The dependence of transducer performance on the load can be included using;

$$F_{load} = z_L v \quad (4.21)$$

where z_L is the mechanical impedance of the load. If the velocity of the load is the same as that of the transducer then the output force of the transducer must be equal and opposite to F_{load} so F (in Eq. 4.20) is;

$$F = -z_L v \quad (4.22)$$

So Eq. 4.20 becomes;

$$0 = T_{me} I + (z_m + z_L) v \quad (4.23)$$

Rearranging gives;

$$\frac{v}{I} = \frac{-T_{me}}{(z_m + z_L)} \quad (4.24)$$

The electrical impedance is obtained by dividing Eq. 4.19 by the current I and substituting for

$\frac{v}{I}$ giving;

$$\frac{V}{I} = Z_e - \frac{T_{em} T_{me}}{(z_m + z_L)} \equiv Z_{ee} \quad (4.25)$$

where Z_{ee} is the electrical impedance that would be measured experimentally for a given transducer. This impedance must contain a combination of the blocked electrical impedance (where the output velocity of the transducer is held at zero) and the impedance due to motional effects. This impedance is known as Z_{mot} and is defined as [4.25]:

$$Z_{mot} = \frac{-T_{em} T_{me}}{(z_m + z_L)} \quad (4.26)$$

Consequently,

$$Z_{ee} = Z_{mot} + Z_e \quad (4.27)$$

To calculate Z_{ee} the coefficients in Eq.s 4.19 and 4.20 must be determined. To do so, Eq.s 4.12 ($S = s^H T + d_{33} H$) and 4.13 ($B = d_{33}^* T + \mu^T H$) must be compared to Eq.s 4.19 and 4.20.

A magnetostrictive transducer has a magnetostrictive bar of length l_b and area A surrounded by a solenoid of N turns. If it is assumed that the bar and the solenoid are of the same length ($l_b = l_s$) then [4.25];

$$H = nI = \frac{NI}{l_s} \quad (4.28)$$

It must be noted that Eq. 4.28 does not take into account demagnetisation effects and so this equation will only be considered valid if length l_b is significantly larger than the bar/rod width/diameter. If this is not the case then a correction will have to be applied as specified by Eq. 2.9. This analysis will continue assuming that the demagnetisation correction need not be applied.

The magnetic flux is;

$$\Phi_m = BA \quad (4.29)$$

As all of the turns have the same magnetic flux linkage then the total flux linkage is $N\Phi_m$ and $B = \mu H$. Consequently [4.25],

$$L \approx \mu n^2 A l_s \quad (4.30)$$

If it is also assumed that stress and strain are spatially independent then;

$$F = TA \quad (4.31)$$

and

$$u = Sl_p \quad (4.32)$$

where u is displacement due to the increase in length of the magnetostrictive bar.

For the purposes of this analysis it is assumed that the magnetostrictive component behaves as an ideal spring [4.25] and that B, H, S, T, V, I, F and v all vary with $e^{j\omega t}$. Therefore, displacement and velocity are related by;

$$v = j\omega u \quad (4.33)$$

Eq.s 4.12 and 4.13 can be arranged so that they can be compared with Eq.s 4.19 and 4.20;

$$B = \mu^T (1 - k^2)H + \frac{d_{33}S}{s^H} \quad (4.34)$$

$$T = \frac{-d_{33}H}{s^H} + \frac{S}{s^H} \quad (4.35)$$

where

$$k^2 = \frac{d_{33}^2}{\mu^T s^H} \quad (4.36)$$

k is called the magnetomechanical coupling coefficient and is a figure of merit for magnetostrictive materials [4.25].

Using Eq.s 4.28, 4.22 and 4.23 then 4.34 becomes;

$$B = [\mu^T (1 - k^2)n]I + \left[\frac{d_{33}}{j\omega l_b s^H} \right] v \quad (4.37)$$

and Eq. 4.35 becomes;

$$T = \left[\frac{-d_{33}n}{s^H} \right] I + \left[\frac{1}{j\omega l_b} \right] v \quad (4.38)$$

The voltage drop across a solenoid is:

$$V = R_{IX'} + \frac{d(NAB)}{dt} = R_{IX'} + j\omega NAB \quad (4.39)$$

so substituting Eq. 4.39 with 4.37 gives;

$$V = [R_{IX'} + j\omega \mu^T (1 - k^2)n^2 Al_b]I + \left[Nd_{33} \frac{A}{l_b s^H} \right] v \quad (4.40)$$

and comparing with Eq 4.20 gives;

$$V = [Z_e]I + [T_{em}]v \quad (4.41)$$

Therefore, the blocked electrical impedance is;

$$Z_e = R_{IX'} + j\omega \{ \mu^T (1 - k^2)n^2 Al_b \} = R_{IX'} + j\omega L_{blocked} \quad (4.42)$$

where $\{\mu^T(1-k^2)n^2Al_b\}$ can be considered equivalent to the blocked inductance of the transducer with the blocked permeability $\mu^S = \mu^T(1-k^2)$ [4.25].

Similarly Eq. 4.21, 4.31 and 4.38 give;

$$F = TA = \left[\frac{-d_{33}An}{s^H} \right] I + \left[\frac{A}{j\omega l_b s^H} \right] v \quad (4.43)$$

so

$$F = [T_{me}]I + [z_m]v \quad (4.44)$$

therefore

$$T_{me} = -Nd_{33} \frac{A}{s^H l_b} = -Nd_{33} k_m^H = -T_{em} \quad (4.45)$$

where k_m^H is the mechanical stiffness for the magnetostrictive bar. T_{me} is negative with respect to T_{em} as a result of the spatial orthogonality of current and magnetic field [4.25].

Also,

$$z_m = \frac{1}{j\omega} \frac{A}{s^H l_b} = \frac{k_m^H}{j\omega} \quad (4.46)$$

However, equation 4.46 only contains a stiffness term and does not contain the mass and damping terms that would be expected in a dynamic system. Consequently, this equation could only be used at frequencies below the first longitudinal resonance (for a given load) where the stiffness term would be dominant in the equation of motion [4.26].

Consequently, an equation for the electrical impedance of a magnetostrictive transducer (Z_{ee}) will be developed that will take into account motional effects. Using Eq. 4.26 and substituting and re-arranging gives (noting that $l_s = l_b$) [4.25];

$$Z_{mot} = \frac{N^2 d_{33}^2 k_m^H}{(z_m + z_l)} = \frac{\left(\frac{n^2}{l_s^2}\right) d_{33}^2 \left(\frac{A^2}{l_b^2 s^H}\right)}{(z_m + z_l)} = \frac{d_{33}^2}{s^H} \left(\frac{A/l_b s^H}{z_m + z_l}\right) \frac{l_s}{l_b} n^2 A l_s \quad (4.47)$$

$$= j\omega \mu^T \frac{d_{33}}{\mu^T s^H} \frac{k_m^H}{j\omega(z_m + z_l)} n^2 A l_s \quad (4.48)$$

$$= j\omega \mu^T k^2 \frac{k_m^H}{j\omega(z_m + z_l)} n^2 A l_s \quad (4.49)$$

Using Z_e from Eq. 4.42 and Z_{mot} from Eq. 4.49, Eq 4.27 becomes;

$$Z_{ee} = R_{IX} + j\omega \{ \mu^T (1 - k^2) n^2 A l_s \} + j\omega \left\{ \mu^T k^2 \frac{k_m^H}{j\omega(z_m + z_l)} n^2 A l_s \right\} \quad (4.50)$$

$$= R_{IX} + j\omega \left\{ \left[\mu^T \left(1 + k^2 \left(\frac{k_m^H}{j\omega(z_m + z_l)} - 1 \right) \right) \right] n^2 A l_s \right\} \quad (4.51)$$

In Eq. 4.51, the term within the braces is the electrical impedance that would be measured at the terminals of the transducer that is not due to the resistance of the solenoid. It is clear that it comprises both real and imaginary components. The bracketed term is the complex magnetic permeability (μ_r) of the magnetostrictive element as determined by the mechanical impedances of the transducer and the load. This dynamic permeability as a function of material coupling and mechanical impedances is:

$$\mu_r = \mu^T \left(1 + k^2 \left(\frac{k_m^H}{j\omega(z_m + z_l)} - 1 \right) \right) \quad (4.52)$$

The magnetomechanical coupling coefficient k is sensitive to any changes in d_{33} , μ^T and k_m^H as specified in Eq.4.36. This means that any frequency dependence can be incorporated into this model as modifiers of the values of these parameters.

This linear model does not take into account the influence of hysteresis or demagnetisation on the transducer's performance. Consequently, it does not represent all of the loss mechanisms associated with magnetostrictive transducers. However, it does suggest a power-circuit option that has introduced a step forward in dental-scaler system design:

For most transducer designs, the 'imaginary' component of the transducer's impedance would be a problem for a device designer, as an increase in excitation frequency would increase Z_{ee} . However, magnetostrictive dental scalers are resonant devices and so this feature of their operation can be used to the designer's advantage.

Eddy current losses can also influence the value of Z_{ee} . Eddy currents are generated in the conducting core of a solenoid when dynamic magnetic fields are applied to it. Their presence tends to decrease the applied field's penetration of the core material. Consequently, the inner part of the rod is 'shielded' from the applied magnetic field.

For a laminated magnetostrictive stack (rather than a rod), the 'critical frequency' f_c above which the effect of eddy currents is considered to be significant is [4.28, 4.29];

$$f_c = \frac{\rho_c}{\pi \mu t^2} \quad (4.53)$$

where ρ_c is the magnetostrictive material's resistivity, μ is the material's permeability and t is the thickness of a lamination. The critical frequency is used to calculate the eddy current factor χ for an applied magnetic field of frequency f where [4.29];

$$\chi = \chi_R - j\chi_L = \frac{\tanh \sqrt{jf / f_c}}{\sqrt{jf / f_c}} \quad (4.54)$$

at low frequencies [4.28];

$$\chi_R = 1 - \frac{2}{15} \left(\frac{f}{f_c} \right)^2 + \frac{62}{2835} \left(\frac{f}{f_c} \right)^4 \quad (4.55)$$

$$\chi_L = \frac{1}{3} \left(\frac{f}{f_c} \right) - \frac{17}{315} \left(\frac{f}{f_c} \right)^3 \quad (4.56)$$

and at high frequencies (where $ff_c \gg 1$) [4.28.4.29];

$$\chi_R \rightarrow \chi_L \rightarrow \frac{1}{\sqrt{\frac{2\omega}{\omega_c}}} = \chi_b \quad (4.57)$$

So in the case where $ff_c \gg 1$, Eq. 4.54 becomes:

$$\chi = \frac{1}{\sqrt{\frac{2\omega}{\omega_c}}} - j \frac{1}{\sqrt{\frac{2\omega}{\omega_c}}} \quad (4.58)$$

In the presence of eddy currents μ_T becomes $\mu_T \chi$ and the square of the coupling coefficient k^2 becomes $k^2 \chi$ [4.29].

Therefore Eq. 4.51 becomes

$$Z_{ee} = R_{IX} + j\omega \left\{ \left[\mu^T \chi \left(1 + k^2 \chi \left(\frac{k_m^H}{j\omega(z_m + z_L)} - 1 \right) \right) \right] n^2 A l_s \right\} \quad (4.59)$$

If

$$Z_m = j\omega m_m + b_m (k_m^H + k_{mps}) / j\omega \quad (4.60)$$

$$Z_L = j\omega m_L + b_L + k_L / j\omega \quad (4.61)$$

where ω is the frequency that the transducer is operating at and the subscripts m and L refer to the transducer and the load respectively. m is the mass, b is the damping coefficient and k is the linear stiffness of the components. k_{mps} represents the linear stiffness of an prestress mechanism. If $m = m_m + m_L$, $b = b_m + b_L$, $\omega_n^2 = (k_m^H + k_{mps} + k_L) / m$, and $2\xi\omega_n = b / m$ (where ξ is known as the damping ration) then Eq. 4.52 can be written as [4.25]:

$$\mu_{reddy} = \mu^T \chi \left\{ 1 + k^2 \chi \left(\frac{\left(\frac{k_m^H}{k_m^H + k_{mps} + k_L} \right)}{\left(1 - \left(\frac{\omega}{\omega_n} \right)^2 + j2\xi \frac{\omega}{\omega_n} \right)} - 1 \right) \right\} \quad (4.62)$$

This theoretical treatment has been extended for resonant dental scalers for this programme:

As these are operated at resonance and they possess no prestress mechanism, Eq. 4.62 becomes (using Eq. 4.36);

$$\mu_{reddy, res} = \mu^T \chi \left\{ 1 + \frac{d_{33}^2}{s_{11}} \left(\frac{\left(\frac{k_m^H}{k_m^H + k_L} \right)}{j2\xi} - 1 \right) \right\} \quad (4.63)$$

Expanding χ means that Eq. 4.63 becomes:

$$\mu_{r_{\text{eff}}} = \mu^T (\chi_R - j\chi_L) \left\{ 1 + \frac{d_{33}^2}{s_H} \left(\frac{\left(\frac{k_m^H}{k_m^H + k_L} \right)}{j2\xi} - 1 \right) \right\} \quad (4.64)$$

And so Eq.4.59 becomes:

$$\begin{aligned} Z_{ee} = R_{DC} + \omega \left(\frac{N^2 \mu^T A \chi_L}{l_s} - \frac{N^2 d_{33}^2 A \chi_L}{l_s s_H} + \frac{N^2 d_{33}^2 A k_m^H \chi_R}{2\xi(k_L + k_m^H) l_s s_H} \right) \\ + j\omega \left(\frac{N^2 \mu^T A \chi_R}{l_s} - \frac{N^2 d_{33}^2 A \chi_R}{l_s s_H} - \frac{N^2 d_{33}^2 A k_m^H \chi_L}{2\xi(k_L + k_m^H) l_s s_H} \right) \end{aligned} \quad (4.65)$$

Consequently, it can be seen that the impedance of a magnetostrictive transducer, operating at mechanical resonance, will have both real and imaginary components that are influenced by the frequency of excitation. Eq. 4.65 can be considered as an extension of Eq. 4.18 that takes into account these frequency dependent parameters.

In both the real and imaginary components of Eq.4.65, the first term is an impedance contribution due to eddy current losses that are not directly linked to magnetostrictive effects. Whereas, the second and third terms are a result of both eddy current effects and the mechanical losses that contribute to the overall impedance due the magnetomechanical coupling. If d_{33} is small, then there will be no contribution to the impedance via magnetomechanically coupled mechanical components. This analysis shows that the performance of a resonant magnetostrictive device is determined by the coupled interaction between the mechanical, electrical and magnetic components.

References for Chapter 4

- [4.1] Engdahl. G., "Handbook of giant magnetostrictive materials", 1st Ed, Academic Press, San Diego, 2000, pp 217-263.
- [4.2] Bartlett. P.A., et al, "High-power, low frequency magnetostrictive actuation for anti-vibration applications", Sensors and Actuators A: Physical, Volume 91, Number 1, June 2001, pp. 133-136(4).
- [4.3] Chikazumi S., "Physics of magnetism", Krieger, Florida, 1986, p.173.
- [4.4] Smith R.C. et al., "A free model for hysteresis in magnetostrictive transducers", Journal of Applied Physics, 93(1), pp. 458-466, 2003.
- [4.5] Smith. R.J.E., et al, "Magnetostrictive actuation performance under digital variable structure control", Journal of Alloys and Compounds. Vol. 258, 1997, pp 101-106.
- [4.6] Engdahl. G., "Handbook of giant magnetostrictive materials", 1st Ed, Academic Press, San Diego, 2000, pp 207-263.
- [4.7] Engdahl. G., "Handbook of giant magnetostrictive materials", 1st Ed, Academic Press, San Diego, 2000, pp 185-186.
- [4.8] Engdahl. G., "Handbook of giant magnetostrictive materials", 1st Ed, Academic Press, San Diego, 2000, pp129-131.
- [4.9] Pitt. V.H., "Dictionary of physics", Penguin, Hamondsworth, 1987, p.169.
- [4.10] Bartlett. P.A., "Properties and applications of magnetostrictive materials", MSc Thesis, University of Hull, 1997.
- [4.11] Alonzo. M., Finn. E.J., "Physics", Addison-Wesley, Reading, Mass, 1970, pp168-172.
- [4.12] Engdahl. G., "Handbook of giant magnetostrictive materials", 1st Ed, Academic Press, San Diego, 2000, pp 78-81.
- [4.13] Hernando. A., "Influence of the tensile stress on the magnetostriction, resistivity and magnetic anisotropy of Co-rich metallic glasses. TSRO abd CSRO correlation", Physica Scripta, Vol. T24, 11-21, 1998.
- [4.14] Bozorth. R.M., "Ferromagnetism", IEEE Press: New Jersey, 1993, pp. 595-712.
- [4.15] Chikazumi. S., "Physics of magnetism", Kreiger: New York, 1978, p182.
- [4.16] Engdahl. G., "Handbook of giant magnetostrictive materials", 1st Ed, Academic Press, San Diego, 2000, pp 131-135.
- [4.17] Dapino. M.J. et al, "Structural magnetic strain model for magnetostrictive Transducers", IEEE Trans Mag, Vol. 36, No.3, 2000, pp 545-556.
- [4.18] Engdahl. G., "Handbook of giant magnetostrictive materials", 1st Ed, Academic Press, San Diego, 2000, pp 164-165.
- [4.19] Engdahl. G., "Handbook of giant magnetostrictive materials", 1st Ed, Academic Press, San Diego, 2000, pp 79-81.
- [4.20] Engdahl. G., "Handbook of giant magnetostrictive materials", 1st Ed, Academic Press, San Diego, 2000, pp 135-146.
- [4.21] Engdahl. G., "Handbook of giant magnetostrictive materials", 1st Ed, Academic Press, San Diego, 2000, pp 257-265.
- [4.22] Jiles D, "Introduction to magnetism and magnetic materials", Chapman and Hall, London, 2nd Ed, 1998, p.57-59.
- [4.23] Engdahl. G., "Handbook of giant magnetostrictive materials", 1st Ed, Academic Press, San Diego, 2000, pp 257-265.
- [4.24] Bartlett. P.A., "Properties and applications of magnetostrictive materials", MSc Thesis, University of Hull, 1997, pp 46-61.

- [4.25] Hall L.H., Flatau A.B., "One-dimensional constant parameter linear electromagnetic-magnetomechanical models of a cylindrical magnetostrictive (Terfenol-D) transducer", J. Intelligent. Material. Systems and Structures, Vol 6, 1995, pp315-328.
- [4.26] Hunt F.V., "Electroacoustics; the analysis of transduction, and its historical background", Woodbury, NY, Acoustical Society of America, 1954.
- [4.27] Bartlett. P.A., "Properties and applications of magnetostrictive materials", MSc Thesis, University of Hull, 1997.
- [4.28] Ensminger. D., Stulen. F.B., "Ultrasonics", CRC Press, 2008, p251.
- [4.29] Meeks. S.W., "Acoustic resonance of a rare earth iron magnetostrictive rod in the presence of large eddy currents", IEEE Trans. Sonics and Ultrasonics, Vol. SU-27, No.2, 1980.

5 MAGNETOSTRICTIVE DENTAL SCALERS

5.1 Introduction

Ultrasonic dental scalers are commonly used in dentistry as a clinical tool for use in the field of periodontology. Periodontal disease is the primary cause of tooth loss in adults and the instrument is used during professional cleaning to remove soft and hard deposits from the teeth, such as bacterial plaque and mineralised plaque known as calculus. The first ultrasonic scaler was developed in the mid 1950's after the use of ultrasound for cavity preparation was made redundant by the development of the high-speed rotary drill [5.1]. Commercial scalers have not significantly changed in design for many years although both magnetostrictive and piezoelectric materials-based units are now available. Clinical research shows that the instrument is an acceptable alternative to hand-held mechanical scalers for effective removal of plaque and calculus [5.2].

The following sections describe the components that comprise a typical magnetostrictive scaler system and discuss initial studies that were conducted to identify features of their operation.

5.2 Dental scaler system components

The widely used scaler variant consists of a magnetostrictive drive unit which is excited via the application of a dynamic magnetic-field that induces vibration of a de-scaling tool known as an 'insert'. This insert will oscillate at maximum amplitude at a resonant frequency determined by the mechanical properties and geometry of this component.

This magnetostrictive material is located within an energising coil which creates the dynamic magnetostriction that causes the tip of the insert to vibrate. A typical magnetostrictive dental scaler system is shown in figure 5-1.

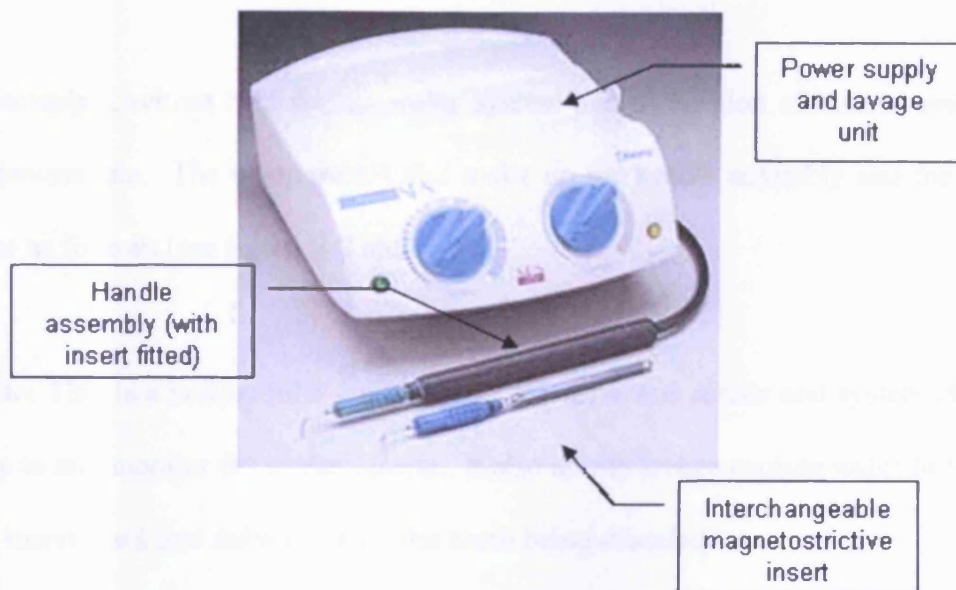


Figure 5-1 Typical Dentsply™ Cavitron SPS® dental scaler system.

Such a magnetostrictive dental scaler typically comprises three components:

- a. The power supply and water cooling 'lavage' system.
- b. The handle assembly.
- c. Interchangeable magnetostrictive inserts.

The power supply provides an alternating current to the dental scaler handle assembly. This current passes through a solenoid arrangement producing the dynamic magnetic-field that causes magnetostrictive strain to occur. The power supply also supplies a flow of water to the handle assembly. This 'lavage' system enables water to be passed through the handle assembly to cool a nickel stack. This water exits from a small hole in the tip that causes it to

flow on the tooth surface when scaling is taking place. This ensures that the tooth remains cool during physical scaling and enables cavitation to take place as a result of the ultrasonic output of the scaler system [5.3]. It is possible for the clinician to set the current level (and hence the level of tip vibration) and the lavage water flow rate by adjusting dials on the front of the power supply unit.

A Dentsply Cavitron SPS dental scalar system and a selection of inserts were obtained for this programme. The components that make up the handle assembly and the associated inserts are as follows (see figure 5-2 and 5-3):

- **Handle:** This is a hollow tube that contains the drive and sensor coil systems that supply energy to and monitor the scalar inserts. It also allows lavage cooling water to be supplied to the insert stack and subsequently, the tooth being descaled.
- **Insert:** This is the complete interchangeable magnetostrictive unit that can be slotted into the scaler handle. It comprises the tip assembly, stack and grip.
- **Tip Assembly:** This is the stainless steel component of the insert that is used to remove calculus from a tooth. The tip is connected to the stack via a braised/soldered joint and has a plastic grip moulded onto it.
- **Tip:** This is the stainless steel component of the Tip Assembly that terminates it and is used to descale teeth.
- **Grip:** A plastic grip is moulded to the tip assembly and features an O-ring which clamps the insert in the handle and also acts as a water seal. The user holds the exposed part of the grip when using the insert.
- **Stack:** This is the magnetostrictive drive element of the insert that is energised by the drive coils in the scalar handle. Vibrations generated by the stack are used to cause

sympathetic vibrations of the tip itself. It must be noted that the stack laminae are not under any mechanical prestress.

- **Socket:** This connects the handle system to the power, sensing and water cables/tubes that connect it to the power/lavage system.

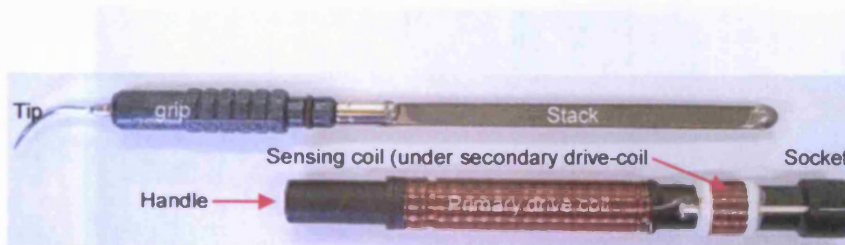


Figure 5-2 Typical magnetostrictive insert and handle (handle cover removed to show solenoid system). The insert and handle are arranged in the image to show the location of the insert when fitted into the handle assembly.

5.3 Dental scaler system

A typical commercial Dentsply™ insert, designed to operate at 30 kHz is shown in figure 5-1. It comprises a steel tip that is attached to a laminated stack of magnetostrictive strips (figure 5-3). This stack is brazed or soldered at both ends. One of these joints is used to affix the stack to the tip assembly and the other is used to ensure the stack behaves as a single mechanical structure. Although the laminate surfaces have been shown to have a high-resistivity coating through contact resistance measurements with a Draper DMM1A multimeter, this has been removed in the region of the end-joints prior to bonding.

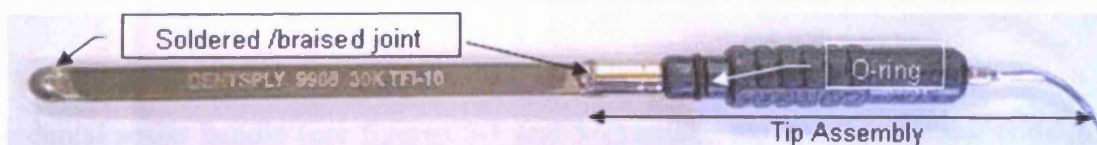


Figure 5-3 Typical Dentsply 'Slimline' dental scaler insert

Dental hygienists and researchers have commented on the variability in performance between scalar inserts [5.4, 5.5]. Part of the reason for this is the properties associated with tips of different geometries (see figure 5.4).

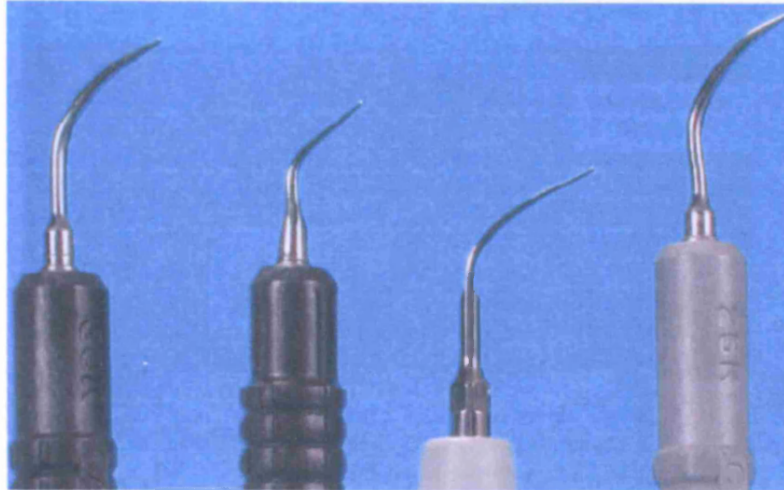


Figure 5-4 Typical dental scaler tip geometries [5.5]

However, identical designs of dental inserts also seem to have performance variability. It has been found that, even when using identical scaling inserts of the same style of tip in the same power supply/lavage system, the displacement outputs produced were statistically different under the same drive conditions [5.6]. It must be noted that the geometry of the insert tips have been developed as a result of the technical needs of dental practitioners over a long period of time [5.7]. Researchers at the University of Birmingham School of Dentistry have also stated [5.7] that autoclaving of inserts can introduce deformations in the stacks.

The dental scaler handle (see figures 5-1 and 5-2) houses the drive and sensor coils that are the key to the Dentsply system's operation.

To assemble a dental scaler, a selected insert is pushed into the handle so that the O-ring seals the inner axial-chamber. This chamber is flooded with water as part of the combined cooling/lavage system. The user of a dental scaler system will select the levels of required power and lavage via the front panel of the power supply unit (see figure 5-5).

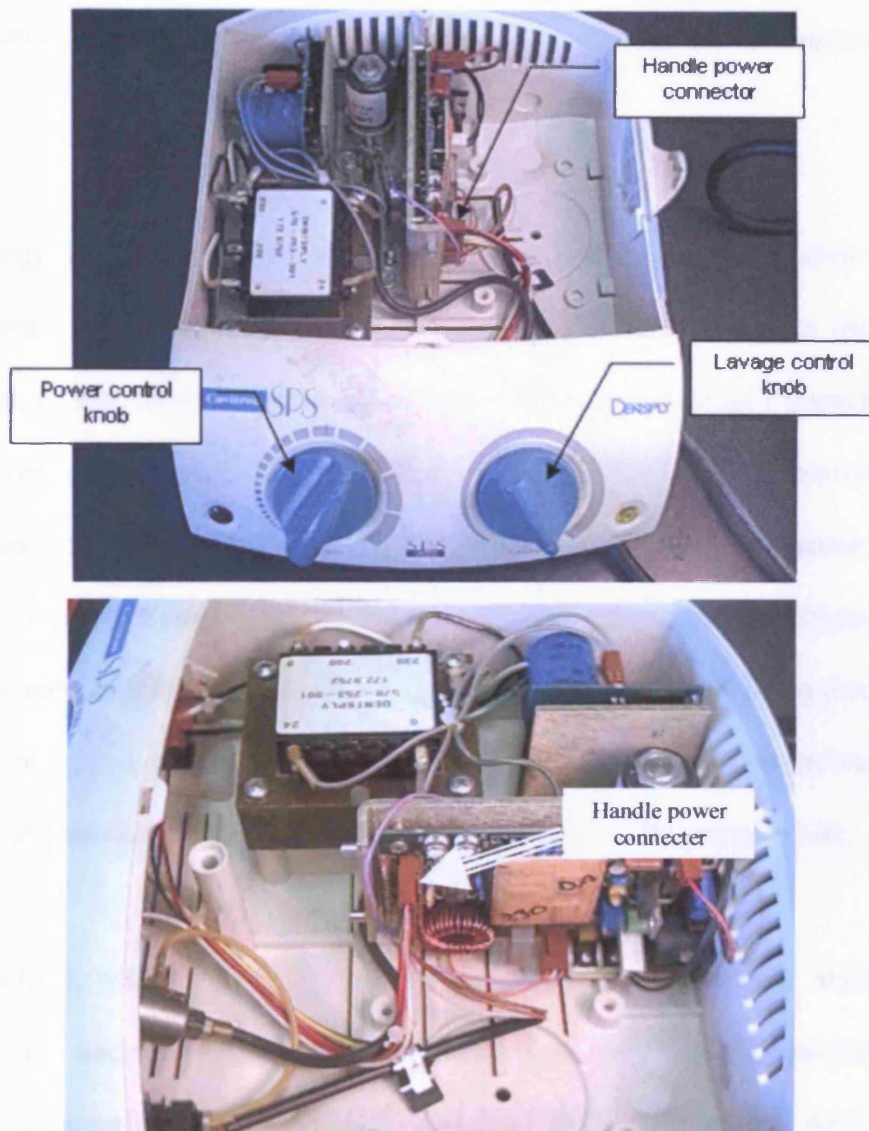


Figure 5-5 Dentsply Cavitron SPS power unit.

However, although the user can set the power and lavage levels via the front of the control panel, the power and water are not supplied to the handle until a foot pedal is depressed so that both are switched on.

5.4 Dental scaler component analysis

It was assumed [5.7] that Dentsply dental scaler magnetostrictive ‘stacks’ were likely to have been made from a nickel-iron alloy. However, a WINEDS® X-Ray microanalysis system was used to make an energy dispersive spectroscopy analysis of samples of magnetostrictive stack laminae, by Mr. R. Jones of the School of Engineering, Cardiff University.

By Energy Dispersive Spectroscopy (EDS), it is possible to stimulate a measurable response from a specimen, if an electron or photon beam is incident on the sample to be characterised. At rest, an atom within the sample contains ground state (‘unexcited’) electrons situated in concentric shells around the nucleus. The incident beam, however, excites an electron in an inner shell, prompting its ejection and resulting in the formation of an electron hole within the atom’s electronic structure. An electron from an outer, higher-energy shell then fills the hole, and the excess energy of that electron is released in the form of an X-ray. The release of X-rays creates spectral lines that are highly specific to individual elements; thus, the X-ray emission data can be analysed to characterise the sample [5.8].

This method, when applied to the dental scaler stack material, indicated that the magnetostrictive stack of ‘slimline’ dental scaler inserts comprised 99% nickel (see figure 5-6). By undertaking this process, confirmation of the nature of the stack material was achieved without having to rely on 3rd party information.

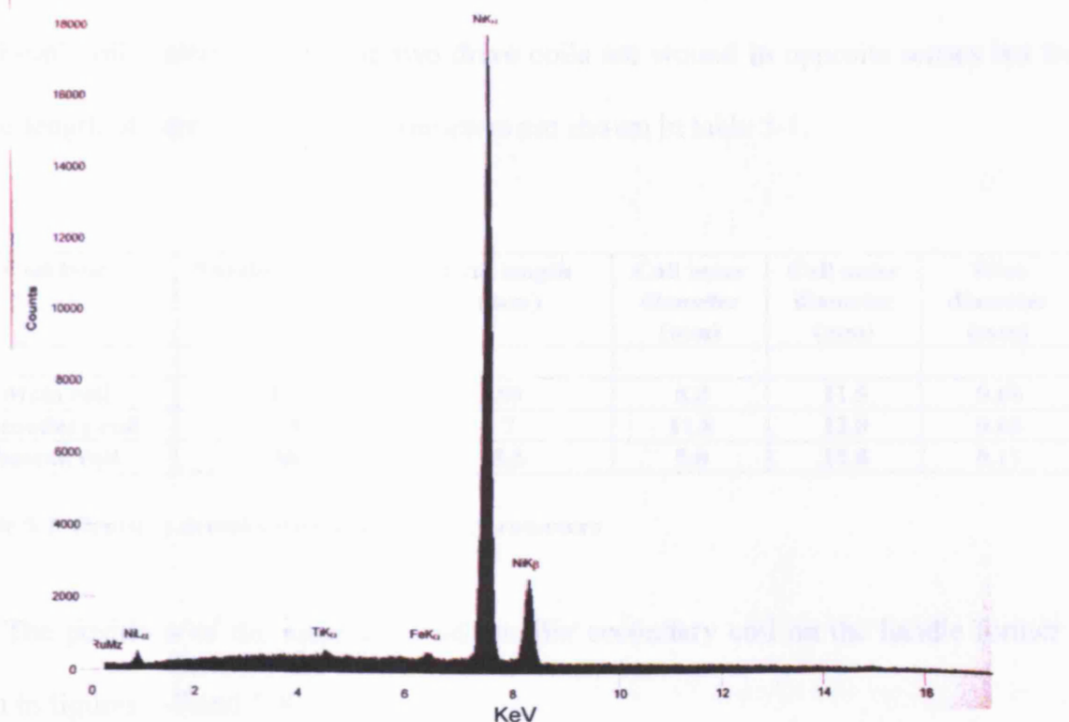


Figure 5-6 EDS X-ray analysis of stack material with the main peak indicating that it composed of predominantly nickel

Figure 5-2 showed both a typical insert and the handle with its outer cover removed. The device was subjected to a ‘reverse engineering’ process that would aid understanding of the construction and operation of the system in conjunction with patent information presented in section 5.5.

Coil and water supply connections are made to the handle via a plug that is attached to the female connection sockets on the right-hand side of the handle as shown. The handle comprised two drive-coils of the same diameter wire (0.68mm) but the left-hand ‘main’ coil is much longer and comprised two layers (see figure 5-7).

It was found that the smaller single-layer ‘secondary’ coil had, what seemed to be, a ‘pick-up’ coil underneath it. The two drive coils are wound in opposite senses but from the same length of wire. The coils’ parameters are shown in table 5-1.

Coil type	Number of turns	Coil length (mm)	Coil inner diameter (mm)	Coil outer diameter (mm)	Wire diameter (mm)
Main coil	140	50	8.8	11.5	0.68
Secondary coil	10	7	11.8	12.0	0.68
Search coil	300	5.5	9.0	10.8	0.11

Table 5-1 Dentsply dental scaler handle coil parameters

The positions of the main coil and smaller secondary coil on the handle former can be seen in figures 5-7 and 5-8.

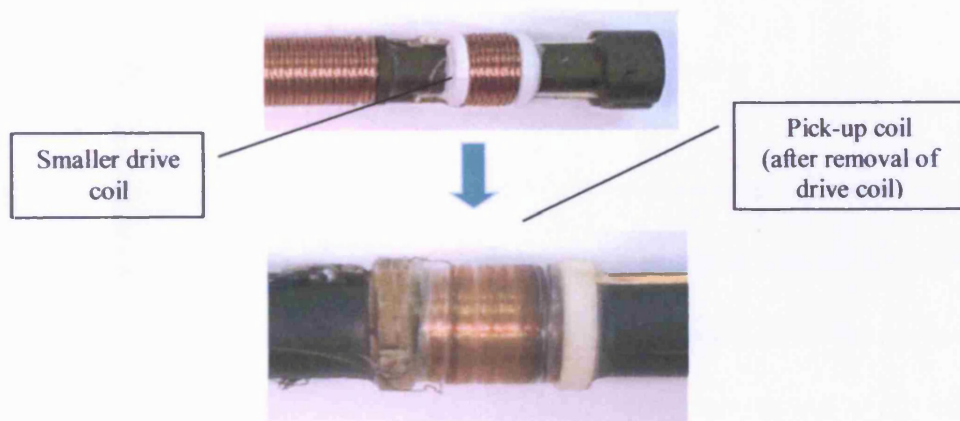


Figure 5-7 Image showing the ‘pick-up’ coil under the smaller ‘secondary’ drive coil

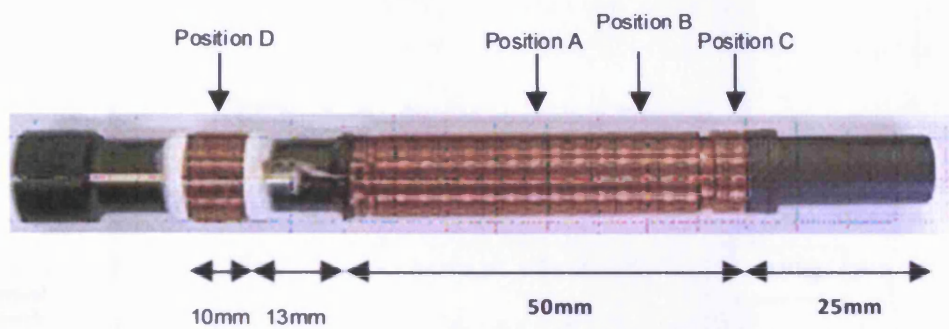


Figure 5-8 Dentsply handle coil configuration

It was noted that there was some resistance to the insertion of an insert into the handle. It was possible that the insert was not only clamped by the O-ring but was also clamped inside the handle assembly. Consequently, a handle had its coil components removed and was split down the main axis so that the insert fixing arrangement could be identified (see figure 5-9).

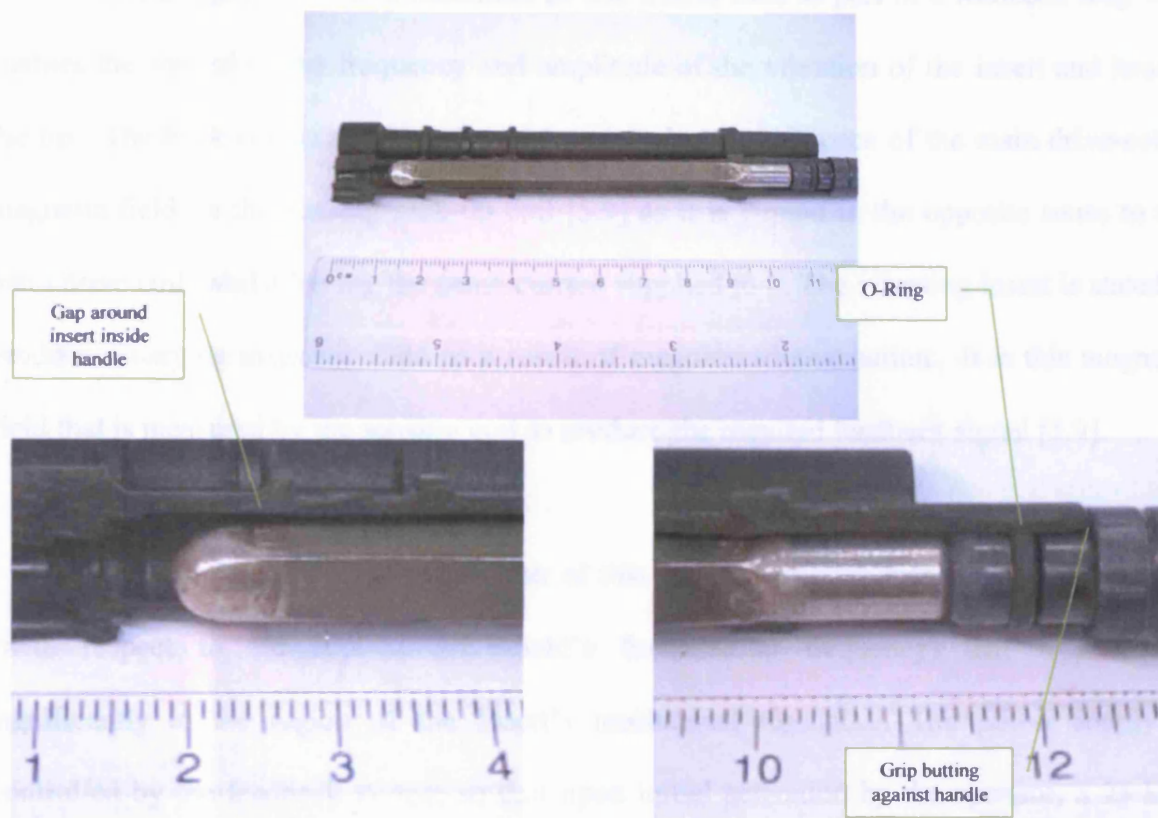


Figure 5-9 The position of a typical insert when inside the Dentsply handle

It was found that the rubber O-ring was the main source of the resistance to insertion as at no other point along the stack's length was there any pinching contact between the insert and the inner walls of the handle. However, an additional constraint on the movement of the insert was established by the butting of the handle grip up against the end of the handle.

5.5 Dentsply Dental Scaler Systems

The operation of this type of magnetostrictive dental scaler follows that identified in a Dentsply patent application filed in 1998 [5.9]. In this patent, a main drive-coil is described as supplying the field required for magnetostrictively derived vibration generation and the secondary drive-coil is described as a 'buck coil' (see figure 5.2).

The sensing pick-up coil is identified as one that is used as part of a feedback loop that enables the control of the frequency and amplitude of the vibration of the insert and hence, the tip. The buck coil is said to be used to minimise the influence of the main drive-coil's magnetic field on the sensing pick-up coil [5.9] as it is wound in the opposite sense to the main drive coil, whilst having the same current supplied to it. The vibrating insert is stated to produce a varying magnetic field as a result of magnetostrictive action. It is this magnetic field that is measured by the sensing coil to produce the required feedback signal [5.9].

The fundamental frequency vibration of this magnetostrictive insert will have a phase (with respect to the applied drive-field's fundamental frequency) that will change significantly in the region of the insert's mechanical resonance. The power supply is controlled by the feedback system so that upon initial activation by the operator, a 25 kHz signal (in this case) is applied to the drive coil and this frequency is increased until a resonance is identified by the control system. Once this resonance is identified, the applied frequency is locked at one that will maintain this resonance.

The amplitude of the feedback signal is claimed [5.9] to be proportional in amplitude and phase to both the electronic drive signal applied to the drive coil and the magnetostrictive transducer characteristics. Any variation in the produced vibration amplitude and frequency for a particular transducer are minimised by continuously using a direct comparison of the feedback signal amplitude and phase characteristics with respect to the user-applied applied drive current amplitude and phase (at the fundamental frequency). This enables the control of the tip vibration amplitude.

The feedback signal phase variation from the ‘pick-up coil’ (when compared to that of the applied drive-signal fundamental frequency phase) is used in conjunction with a phase-locked loop circuit to effectively maintain a nearly 0° phase shift between the two identical frequency signals. A phase detector generates an error voltage that results in a change in a voltage-controlled oscillator’s frequency that will stop only when a 0° phase shift between its two identical frequency inputs is detected. This will only occur when the system is at resonance. This ensures that the drive-circuit frequency tracks the resonant frequency of the magnetostrictive transducer. Indeed, this would ensure that the resonant frequency of operation would be maintained despite changes in the value of this resonance due to external conditions (such as changes in load or operating temperature) [5.9].

In this design [5.9], the magnitude of the tip vibration can be controlled by applying a pulse-width modulated drive signal from the power amplifier stage. This would control the duty cycle and the average power applied to the drive coil system. However, the transducer’s vibration amplitude control can also be achieved by amplitude control of the applied drive signal. In this way, the average power applied to the drive coil system is controlled. As the applied drive signal was noted to be sinusoidal, rather than pulse-width modulated, this second power-control method seems to be being utilised in the Cavitron system under investigation.

5.6 Initial dental scaler analysis

In this section, the operation of the dental scaler system is discussed based on observations made during operation. This was undertaken to gain an appreciation of the performance of the system.

To investigate the signal supplied to a dental scaler handle/insert system, a Hameg HM 205-3 oscilloscope was utilised to identify the frequency of the excitation signal supplied by a Dentsply Cavitron SPS power unit to a standard Slimline handle system with a Dentsply 9908 30K TFI-10 insert located in the handle. This was achieved by monitoring the voltages applied to the scaler drive-coil system via the power connector cable attached to the Cavitron SPS unit (see figure 5-5).

It was found that when an insert was present, the power supply would settle on an operating frequency of 29 kHz but would change to 42 kHz when an insert was not present (air-cored handle-system) or was removed. Indeed, placing other ferromagnetic materials (such as mild steel rods) in the handle did not enable the power supply system to settle on the same 29 kHz operating frequency but would behave as if there was an air-core present and would settle on an applied frequency of 42 kHz.

The sinusoidal signal that is supplied to the dental-scaler coil system by the power supply (when a nickel insert is in place) is close to the stated operating frequency of 30 kHz. Based on this analysis, the scaler power-supply seemed to be able to distinguish between the nickel and non-nickel insert materials.

If the dental-scaler system was operating in a resonant mode, it would be important to supply a drive current at a frequency that would stimulate this resonance. Supplying a drive current away from this resonant frequency would not achieve this. Consequently, it would be important for the power supply to sense the resonant frequency for the insert concerned and supply a drive current that would stimulate this resonance.

A dental scaler coil system was analysed to identify the nature of the field magnitudes at four positions along its length (see figure 5-8). A FW Bell Series 9950 with a PAA99-1908 axial probe was placed so that the probe sensor was placed at the positions indicated in figure 5-8. When the probe was located in the handle at the appropriate measurement position, a relative peak H-field measurement was made that eliminated the contribution as a result of external magnetic fields (such as earth's magnetic field).

A d.c. current produced by a Farnell TOPS 3D power supply (with integrated current meter) was passed through the two coils. The axial peak H-field outputs at each of the positions shown in figure 5-8 are shown in figure 5-10.

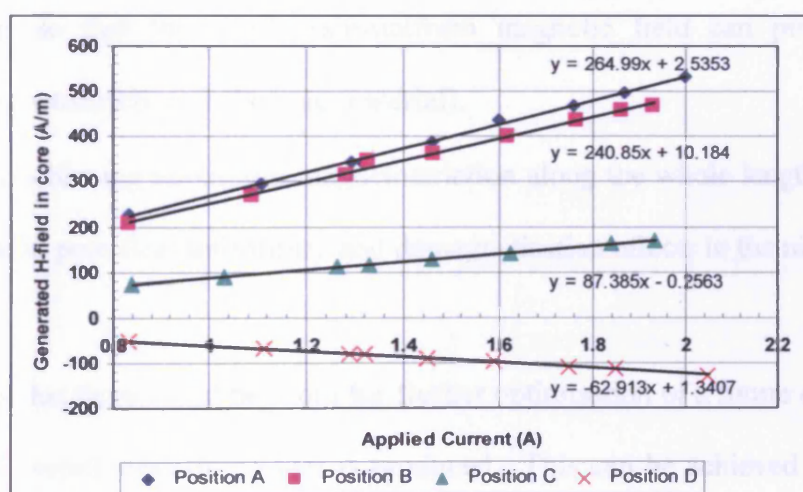


Figure 5-10 H-fields produced at the positions shown in figure 5-8 for as drive current is increased.

Equipment	Error
FW Bell Series 9950 Gauss Meter	± 0.01 mT (90%) (± 7.96 A/m)
Farnell TOPS 3D Power Supply	± 0.01 A (90%)

Table 5-2 Errors associated with the measurements taken and displayed in figure 5-10

Figure 5-10 shows that the two coils produce fields that are in the opposite directions. It also shows that the field is non-uniform along the length of the longer coil. In addition, the field produced by the smaller coil is $\sim 1/5$ of the maximum field produced by the main coil. This shows that the main coil is operating with a significant non-uniformity in the field that is applied to the magnetostrictive material it influences. The overall magnetostrictive strain is dependent on the sum of the individual strains produced in the material along its length. The maximum strain that can be achieved is dependent on applying a magnetic field that creates the condition of saturation magnetostriction. If the magnetic field applied along the length of a magnetostrictive material is non-uniform, then either magnetostriction is;

- being achieved inefficiently (due to excessive current being applied to the field coil so that the whole non-uniform magnetic field can produce saturation magnetostriction in the core material),
- not achieving maximum magnetostriction along the whole length of the material due to poor field uniformity and demagnetisation effects in the nickel stack.

This means that there could be room for further optimisation of a future drive coil system to increase the overall strain/force that is produced. This can be achieved by changing the profile of the drive coil so that there are more turns at the end of the coils (thereby improving H-field uniformity) or ensuring that the magnetostrictive sample is placed within a longer drive coil so that it is in a more linear field-region [5.10]. In addition, changing the geometry of the stack could result in a reduction of the significance of demagnetisation effects.

Based on Eq. 2.12, the demagnetisation factor for a 5mm x 5mm x 80mm nickel stack, the demagnetisation factor would be:

$$N_z = \frac{1}{\left[2\left(\frac{2n}{\sqrt{\pi}}\right) + 1\right]} = 0.0303$$

as $n=16$ for this geometry (see fig. 2-3) and N_z is the demagnetisation factor along the long axis of the stack. Consequently, from Eq. 2.10, the demagnetising field H_d will be ~3% of H_a . Increasing the length to width ratio of the stack would reduce the significance of demagnetisation effects, improve field uniformity and thereby increase overall strain for the stack.

5.7 Initial resonance measurements

Initial measurements were undertaken with a typical dental scaler insert (Dentsply 9607 30K FSI-SLI-10R) when housed within a typical ‘handle’ coil system and also when located in an in-house solenoid (see figure 5-11 and table 5-3 for experimental set up and equipment). The purpose of this experiment was to identify the vibrational behaviour of a dental scaler insert using a Polytec OFV-303 Single Point Laser Vibrometer head and associated 3001 Controller System. The ultimate objective being the identification of the frequency of any mechanical resonances produced by the dental scaler insert when stimulated by a dynamic applied H-field.

The Polytec single-point vibrometer used was an instrument for non-contact measurements based on laser vibrometry. A beam of a helium-neon laser light was focused on the object under investigation. The beam was scattered back from it and some returned to the sensor head (which also houses the emitting laser). An interferometer compares the phase and frequency of the object beam with that of an internal reference beam. The frequency difference is proportional to the instantaneous velocity and the phase difference is

proportional to the instantaneous position of the object. In the controller, these data were analysed and outputted so that it can identify the velocity and displacements associated with an illuminated object [5.11].

As the laser vibrometer used was a 'single-point' device, the insert tip was removed so that there would be a flat face for beam reflections. This was because a laser vibrometer of this type would be unable to measure vibrations off the laser beam axis.

In each case, a constant current was maintained in both coils whilst the drive frequency was decreased from a maximum value. This was to replicate the sinusoidal drive current that was applied by the dental scaler power-supply to the handle drive coil assembly. However, it was noted that the supply of a sinusoidal drive current would not ensure that the shape of the flux density waveform, B remained constant [5.12]. However, as control of the input drive sinusoid was not modified to achieve a sinusoidal flux density waveform in the commercial device, this was not replicated for these experiments.

The control of the applied drive current magnitude was achieved by maintaining a constant 9.0 mV peak-to-peak voltage across a $0.236\ \Omega$ non-inductively wound resistor (equivalent to 0.038A peak-to-peak) that was placed in series with the respective coil systems.

Based on the coil parameters specified in table 5-3 and using Eq. 2.1 this equated in an applied H-field of 180 A/m (peak-to-peak) for the 400 turn in-house coil and a maximum applied H-field of 107 A/m (peak-to-peak) for the Dentsply coil. It must be noted that the length of the main coil of the Dentsply coil was less than that of the 'in-house' coil.

However, the Dentsply coil did have a field contribution supplied by the smaller secondary coil that produced 54 A/m (peak-to-peak).

As a result of the application of these dynamic fields, it was possible to identify the positions of the resonances that occurred as a result of excitation in both coil systems. The voltage was maintained at this low level so that the amplifier could maintain this output across the whole frequency range (0-55 kHz) for both coil systems. Figure 5-12 shows both the 'in-house' drive coil with the test insert in situ and the LM12 Op-Amp based power supply schematic (see figure 5-13) that was used to excite the coil system. The equipment used in the measurements is shown in table 5-3.

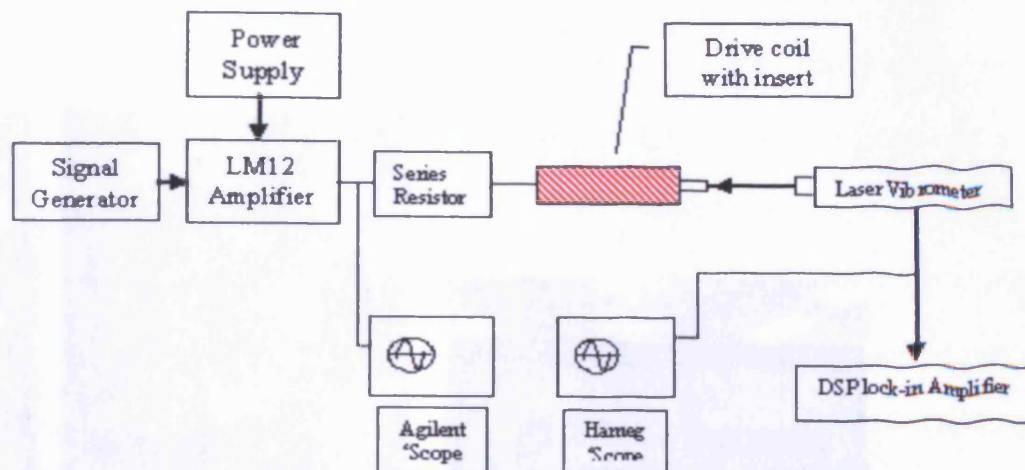


Figure 5-11 Experimental set-up for resonance investigation

Equipment Item	Purpose/Specification
Feedback FG600 Signal Generator	To supply sinusoidal signal to the LM12-Based Amplifier
Farnell TOPS 3D Bi-polar Power Supply	To supply ± 25 V to the LM12-Based Amplifier
LM12 Op-Amp Based Amplifier	To supply sinusoidal current to drive coils
Agilent 5462A Oscilloscope	To monitor voltage across 0.236Ω resistor in series with the drive coils
Hameg HM 205-3 Oscilloscope	To monitor the output voltage from the Laser Vibrometer
Signal Recovery 7265 DSP Lock-in Amplifier	To monitor voltage output signal from Laser Vibrometer (also measures TTL reference frequency from Feedback FG600 signal generator)
Polytec OFV-303 Single Point Laser Vibrometer head and associated 3001 Controller System ($5\mu\text{m}/\text{V}$ sensitivity, displacement mode)	To measure vibration of the insert caused by magnetostriction
Dentsply Drive Coil System (30k Cavitron 134° SSS) Main Coil	140 turns, length: 50mm, ID: 8.8mm, OD: 11.5mm, wire thickness = 0.68mm, Resistance: 0.9Ω (main and secondary coils) Z: 33.58Ω , θ : 77.75° @ 20 kHz Z: 48.21Ω , θ : 73.98° @ 30 kHz (in main and secondary coils)
Dentsply Drive Coil System (30k Cavitron 134° SSS) Secondary Coil	10 turns, length: 7mm, ID: 11.8mm, OD: 12mm, wire thickness: 0.68mm, Z: 33.58Ω , θ : 77.75° @ 20 kHz Z: 48.21Ω , θ : 73.98° @ 30 kHz (in main and secondary coils)
Dentsply Drive Coil System (30k Cavitron 134° SSS) Pick-up Coil	300 turns, length: 5.5mm, ID: 9mm, OD: 10.8mm coil, wire thickness: 0.11mm
'In-House' Drive Coil System	470 turns, length: 100mm, ID: 5mm, OD: 13mm, wire thickness: 0.78mm, Z: 209.13Ω , θ : 76.16° @ 20 kHz Z: 297.93Ω , θ : 72.75° @ 30 kHz

Table 5-3 Equipment used in the resonance identification experiments (impedance measured via Agilent 4284A Precision LCR Meter)



Figure 5-12 'In-House' drive coil with tip-removed insert installed and LM12 Op-Amp based Amplifier

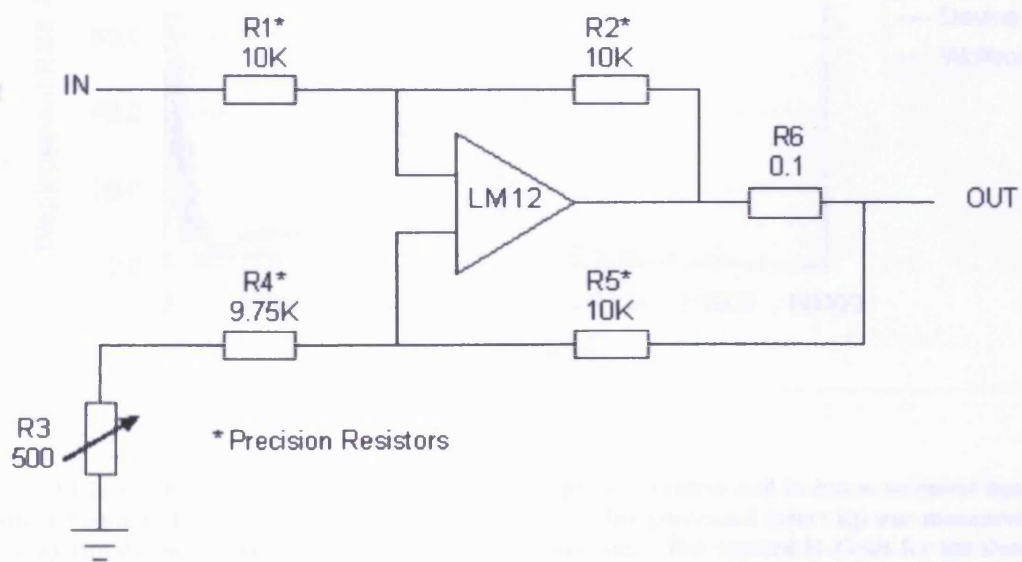


Figure 5-13 LM12 Op Amp circuit diagram. Current mode configuration.

As a result of scanning the drive frequency that was applied to both solenoid systems, resonances were identified for the Dentsply 9607 30K FSI-SLI-10R nickel insert (see figure

5-14). In both drive-coil cases, significant resonances were observed at 21.3 kHz and 31.4 kHz for the 'in-house' and Dentsply coil systems. Both coil systems stimulate the same mechanical resonances in the dental scaler stack. Consequently, it would be expected that vibration resonances would be observed at the same frequencies. The second resonance at 31.4 kHz would seem to be the one that is excited in dental scaler inserts for clinical operation. It was also found that the two coils, despite their different electrical properties (see table 5.3), produced very similar resonant frequencies and phase changes across the measured frequency range (see figs. 5.15 and 5.16) where these significant phase changes can be observed in the region of the resonances.

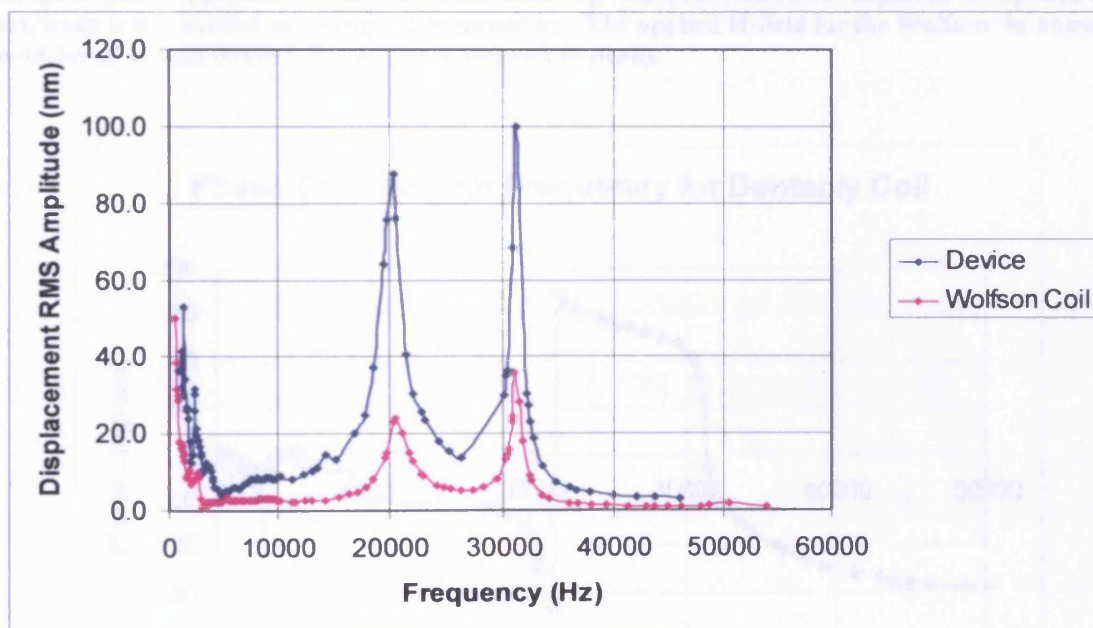


Figure 5-14 Initial Frequency analysis between Dentsply coil system and in-house solenoid-based transducer system, where the displacement amplitude of the truncated insert tip was measured when it is excited by two different drive coils at a range of frequencies. The applied H-fields for the Dentsply 'Device' coil and Wolfson 'in-house' solenoid (table 5-3) were 107 A/m and 180 A/m respectively (peak to peak).

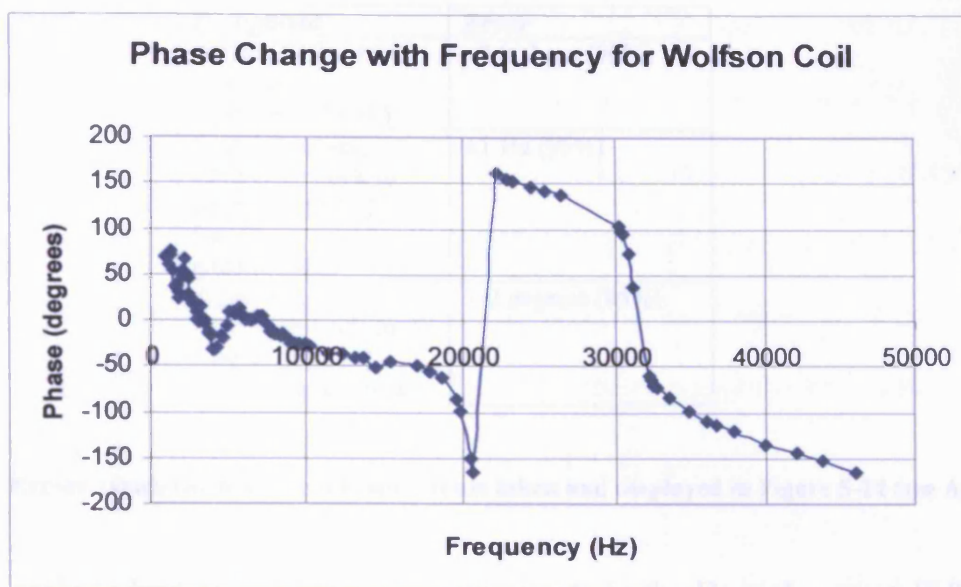


Figure 5-15 Change in phase with frequency for the Wolfson house solenoid-based transducer system where the displacement phase of the truncated insert tip was measured (with respect to the applied drive phase), when it was excited at a range of frequencies. The applied H-field for the Wolfson 'in-house' solenoid-based system (table 5-3) was 180 A/m(peak to peak).

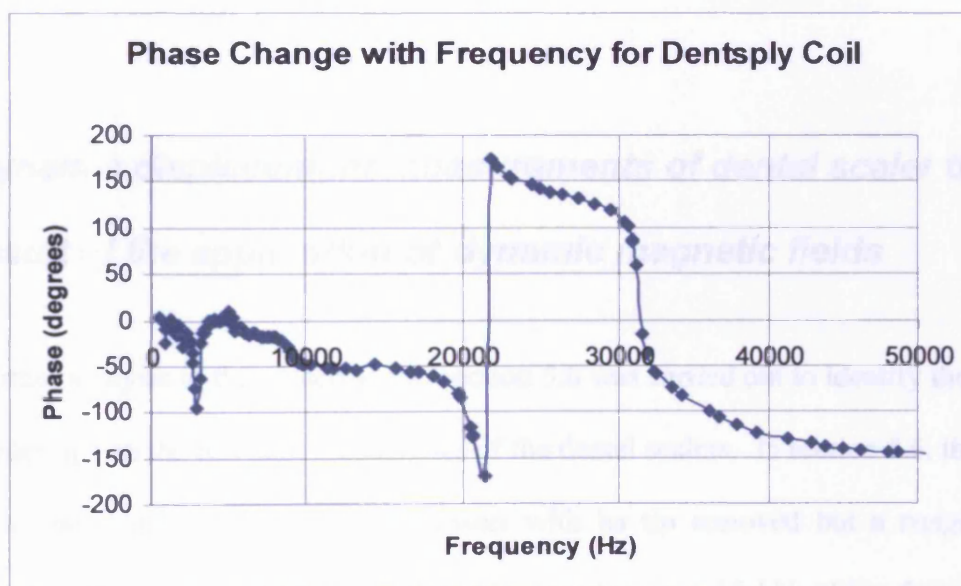


Figure 5-16 Change in phase with frequency for the Dentsply solenoid-based transducer system where the displacement phase of the truncated insert tip was measured (with respect to the applied drive phase), when it was excited at a range of frequencies. The applied H-field for the Dentsply solenoid-based system (table 5-3) was 107 A/m (peak to peak).

Equipment	Error
Polytec OFV-303 based laser Vibrometer [5.10]	$\pm 0.002 \mu\text{m}$ (90%)
Signal Recovery 7265 DSP Lock-in Amplifier [5.11] frequency measurement	$\pm 1 \text{ Hz}$ (95%)
Signal Recovery 7265 DSP Lock-in Amplifier [5.11] phase measurement	$\pm 2 \text{ degrees}$ (95%)

Table 5-4 Errors associated with the measurements taken and displayed in Figure 5-14 (see Appendix A)

This analysis lends credibility to the statements in the Dentsply patent [5.9] where it states that a measured phase of zero degrees in the region of the resonance point (31.4 kHz in the case of the system under investigation) is used to enable the control electronics of the scaler system to ‘lock on’ to a particular insert’s resonance and stimulate it.

5.8 Dynamic displacement measurements of dental scaler tips as a result of the application of dynamic magnetic fields

A further analysis to that described in section 5.6 was carried out to identify the influence of the scaler tips on the resonant frequencies of the dental scalers. In section 5.6, the resonant frequencies were only observed for an insert with its tip removed but a *range* of drive frequencies were applied to the insert. In this experiment, a 15 kHz drive frequency (107 kA/m peak-to-peak field) was applied to the insert so that the expected main resonant peak could be stimulated as a result of frequency doubling (for a magnetostrictive element lacking an applied biasing field). In this case, the Dentsply drive coil used in section 5.7 was used to produce the applied field.

Two inserts (of type Dentsply 9607 30K FSI-SLI-10R) were examined. Both were identical in design but for one, the curved portion of the tip was removed so that a flat face of circular cross-section could be placed orthogonal to the vibrometer's laser-beam path. The laser beam was then focused on the target face so that the magnitude of the reflected and detected light would be at a maximum, as specified in the Polytec OFV 303 Operator's Manual [5.11]. This enabled the measurement of vibrations along the longitudinal axis of the dental scaler inserts. The experimental set-up is shown in figure 5-17.

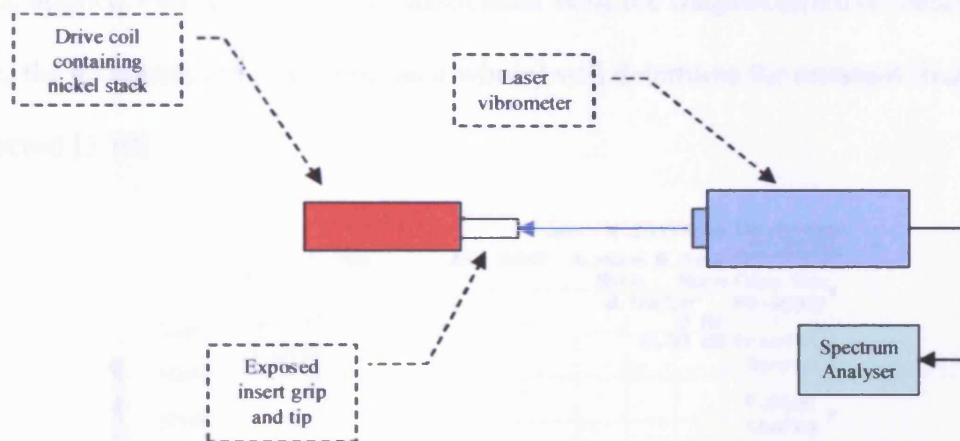


Figure 5-17 Schematic diagram of the equipment used for a frequency analysis of inserts with and without tips

In addition to the equipment shown in table 5.3, an Advantest R3131A spectrum analyser was used to monitor the output from the Polytec OFV 303 laser vibrometer analysis so that resonances could be observed for the two types of insert. The bandwidth of this spectrum analyser was quoted to be 9 kHz to 3 GHz [5.11]. As this lower frequency value for the operational bandwidth was somewhat close to the drive frequency of 15 kHz the spectrum analyser was only used to identify the frequencies that were being established in the transducer when resonating rather than measuring the displacement amplitude. However, it was possible to indicate an indicative relative magnitude (in dB) between the different peaks.

In figure 5-18, the vibration measured by the laser vibrometer for the insert with its tip removed is shown. It comprises of a small peak at the drive frequency of $15.2 \pm 1\text{kHz}$ and a larger peak at $31.0 \pm 1\text{ kHz}$. Although it would be expected that all of the applied field would be frequency doubled, any residual magnetisation or unwanted bias fields will inhibit 'perfect' frequency doubling and a proportion of the applied drive-field frequency will be present in the dynamic strain output. The magnitude of any subsequent strain peaks will be determined by the magnetomechanical transfer function and that will be determined by the strain vs. applied field characteristics associated with the magnetostrictive material used. In addition, the geometry of the system (as a whole) will determine the resonant frequencies that are observed [5.10].

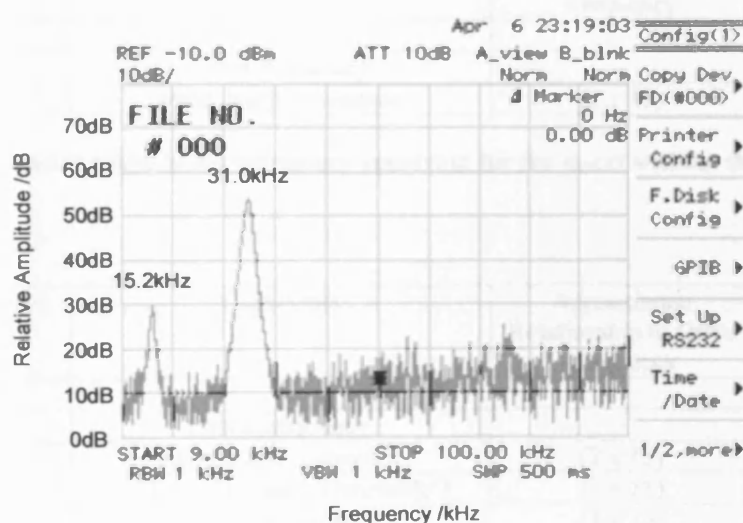


Figure 5-18 Vibration measured from an insert without a tip. Resonances observed at 15.2 kHz and 31.0 kHz when stimulated by a 107 kA/m applied field.

When the insert with the tip still attached was examined under the same drive conditions (107 kA/m applied field) there still is a 15.0 kHz component and the main resonant peak at 29.9 kHz but a number of additional peaks were also observed (see figure 5-19).

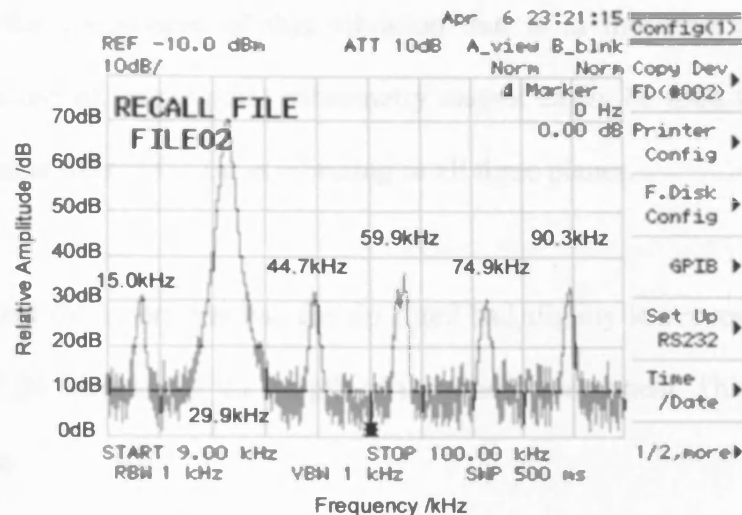


Figure 5-19 Vibration measured from an insert with a tip. Multiple resonances observed when stimulated by a 107 kA/m applied field.

The frequency peaks for the insert with and without the tip attached were as follows:

Peak Frequency (kHz)	Comments	Approximate Relationship to Drive Frequency	Amplitude relative to main resonance (dB)
± 1 kHz			
15.2	Drive frequency	-	-23
31.1	Main insert resonance	(2 x 15)	0

Table 5-5 The measured peaks in the frequency spectrum for the insert without the tip attached

Peak Frequency (kHz)	Comments	Approximate Relationship to Drive Frequency	Amplitude relative to main resonance (dB)
± 1 kHz			
15.0	Drive frequency	-	-38
29.9	Main insert resonance	(2 x 15)	0
44.7	First tip resonance ('unstable')	(3 x 15)	-37 to -70
59.9	Second tip resonance	(4 x 15)	-33
74.9	Third tip resonance (unstable)	(5 x 15)	-40 to -70
90.3	Forth tip resonance	(6 x 15)	-37

Table 5-6 The measured peaks in the frequency spectrum for the insert with the tip attached

It was noted during measurement that the 44.7 kHz and 74.9 kHz peaks seemed to be 'unstable' in that their amplitudes changed with respect to time whilst the other peaks were stable (see table 5-6). The most likely cause of this instability is the result of the complex oscillation of the tip in more than one direction/plane. The laser vibrometer would only be

able to measure the component of this vibration that is in the same axis as the beam. Consequently, the use of single point vibrometry cannot easily be used to identify all axis vibrations at the same time if the tip is vibrating in all three planes.

It was noted that the insert that had the tip fitted had slightly lower resonant frequencies. This is a result of the increase of the length of the whole component. This will be discussed later in this section.

As a result of this analysis four conclusions were drawn:

- 1) The dental scaler inserts produce resonances that can be utilised in the Dentsply scaler systems with the largest resonance component at ~30 kHz.
- 2) The single-point laser vibrometer is not suitable for identifying all aspects of the tip's vibrations.
- 3) The dental scalers were functioning as a result of a resonance of the insert as a whole as removal of the tip did not significantly change the main resonant frequency of the modified insert.
- 4) A 15 kHz applied magnetic field can be used to stimulate a 30 kHz resonance via frequency doubling.

Although complete commercial dental scaler inserts had been assessed, in sections 5.7 and 5.8, (where Dentsply scaler insert resonant frequencies were identified) there was a question on how the geometry of the stack would influence its dynamic strain output under magnetic field excitation. To this end, a further series of experiments were conducted with stacks with different geometries. These additional nickel stacks were produced by either

cutting down existing commercial stacks to $2/3$ or $1/3$ of their original length or by reducing the number of laminae in a stack (see figure 5-20). This was achieved by sawing the stacks to the appropriate length or by removing laminae by sawing them away from the main insert stack (with care being taken so that the remaining laminae were not damaged by the cutting process).

By doing this, it would be possible to identify if the length of the stack or the number of laminae in a stack would influence resonant behaviour or the strains that would be produced, when excited by an external dynamic magnetic-field.

The truncated and 'reduced laminae' stacks were then fixed into a non-magnetic stack holder with Araldite and placed in a tube that would hold the sample-stack in the central portion of a solenoid as shown in figures 5-21 and 5-22. In the case of the truncated insert stacks, the sawn end of the insert was used to fix it in the sample holder. This ensured that the un-modified end of the insert would be exposed to the Polytec laser vibrometer's beam so that any longitudinal vibrations produced as a result of the application of a dynamic magnetic field could be observed.

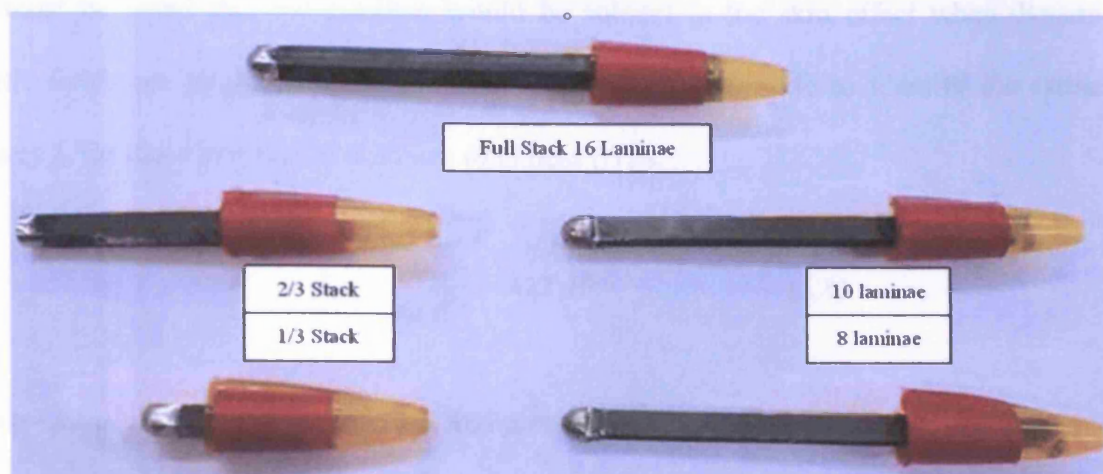


Figure 5-20 Nickel stacks modified so that the length and number of laminae were reduced to identify the influence of geometric factors on magnetostrictive performance. Stacks fitted into sample holders prior to insertion into sample holding assembly.

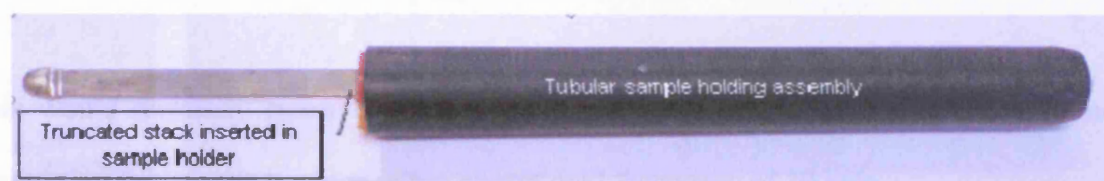


Figure 5-21 Sample holding assembly prior to insertion into solenoid. The truncated stacks are inserted into the tubular plastic sample holder so that the stack could be located in the centre of the solenoid.

These truncated stacks possessed the geometric parameters specified in table 5-7.

Stack Number	Cross-section (mm)	Length (mm)	Number of Laminae
1	4 x 5	80 (full stack length)	16
2	4 x 5	53 (2/3 stack length)	16
3	4 x 5	23 (1/3 stack length)	16
4	2.5 x 5	80 (full stack length)	10
5	2.0 x 5	80 (full stack length)	7

Table 5-7 Geometries and laminae numbers for truncated, laminated stacks

It must be noted that the laminae would be subject to the skin effect when dynamic magnetic fields are applied to them. Using Eq. 4.53 it is possible to identify the critical frequency f_c for these laminae of 0.30mm thickness (t) as:

$$f_c = \frac{\rho_c}{\pi \mu t^2} = 422 \text{ Hz} \quad (5.1)$$

Where $\mu = \mu_r \mu_0$, $\mu_r = 600$, $\rho_c = 9 \times 10^{-8} \Omega \text{m}$, and $\mu_0 = 4\pi \times 10^{-7} \text{Hm}^{-2}$ [5.15, 5.16].

Also, at 30 kHz, the skin depth would be expected to be (from Eq. 4.53):

$$t = \sqrt{\frac{\rho_c}{\pi \mu f}} = 3.6 \times 10^{-5} \text{ m} \quad (5.2)$$

This would normally mean that the dynamically changing magnetic field would not be penetrating far into the laminae at the operational frequency of 30 kHz.

Consequently, based on this simple analysis, the commercial dental scaler stacks are operating significantly beyond what would normally be expected to be their critical frequency. However, that they still function at 30 kHz suggests that operating at resonance is changing the behaviour of the system in such a way that eddy currents do not inhibit the production of magnetostrictive strains that produce vibrations used for descaling.

The dimensions of the solenoid shown in figure 5-22 were: length 280mm and bore inner diameter 23mm.

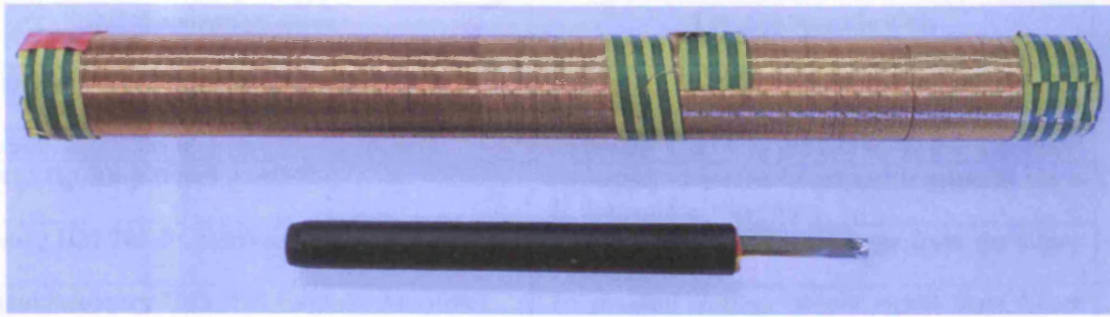
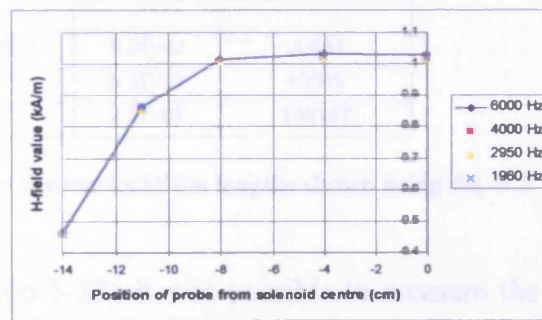
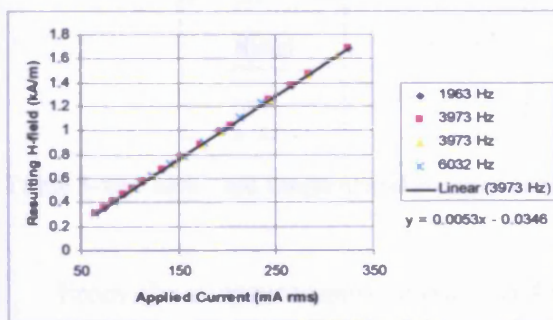


Figure 5-22 Solenoid used to apply excitation field to the magnetostrictive stacks shown with the a stack inserted in the sample holder (2/3 length insert shown).

This solenoid was selected as it had a sufficiently wide bore inner diameter and length to accommodate the stack samples and holder. Although the number of turns of the solenoid was unknown, the coil was calibrated so that the H-field output against applied drive current. In addition, the field uniformity was checked with respect to the position of the field measurement. The field measurement was undertaken with an F.W. Bell Series 9950 Tesla/Gaussmeter and a PAA99-1908 1x axial probe. With this system, it was possible to measure dynamic fields from dc to 50 kHz. The equipment used during the calibration procedure and for further dynamic vibration measurements of the truncated stacks is listed in table 5-8.

Equipment Item	Purpose/Specification
Feedback FG600 Signal Generator	To supply sinusoidal signal to the LM12-Based Amplifier
Farnell TOPS 3D Bi-polar Power Supply	To supply ± 25 V to the LM12-Based Amplifier
LM12 Op-Amp Based Amplifier	To supply sinusoidal current to solenoid via a dc decoupling capacitor.
Hameg HM 205-3 Oscilloscope	To monitor the output voltage from the Laser Vibrometer
Signal Recovery 7265 DSP Lock-in Amplifier	To monitor voltage output signal from Laser Vibrometer (also measures TTL reference frequency from Feedback FG600 signal generator)
Polytec OFV-303 Single Point Laser Vibrometer head and associated 3001 Controller System ($5\mu\text{m/V}$ sensitivity, displacement mode)	To measure vibration of the insert caused by magnetostriction
Keithley 2001 Multimeter (20Hz – 100kHz ACI bandwidth)	To measure RMS value of drive current through solenoid

Table 5-8 Equipment used in the truncated stack experiments



(a)

(b)

Figure 5-23 (a) Resultant H-field produced as a result of an applied ac current to the solenoid shown in fig. 5-22 at various drive frequencies (b) The H-field profile for the solenoid shown in fig. 5-22 at various drive frequencies where the zero position is the centre of the solenoid.

Equipment	Error
FW Bell Series 9950 Gauss Meter	± 0.01 mT (90%) (± 7.96 kA/m)
Keithley 2001 Multimeter	± 1 mA (90%) (1 kHz – 10 kHz)
Measured position of probe	± 1 mm (90%)

Table 5-9 Errors associated with the measurements taken and displayed in Figure 5-22 (see Appendix A).

As the fundamental resonance of a rod is [5.14]:

$$f_r = \frac{v}{2l} \quad (5.3)$$

where

$$v = \sqrt{\frac{E}{\rho}} \quad (5.4)$$

then the expected longitudinal fundamental resonances for the truncated stacks would be expected to be found at those frequencies shown in table 5-10

Stack Type	Young's modulus	Density Kg/m ³	Length m	Fundamental Resonance F _r Hz
Nickel	2.10E+11	8800	8.0E-02	30531
	"	"	5.3E-02	46085
	"	"	2.3E-02	106197

Table 5-10 Calculated longitudinal resonances for the stacks of the lengths shown using Eq. 5.3

From the measurements shown in figure 5-23a it was possible to measure the H-fields applied to the truncated stack samples for a given drive current. In addition, as the longest stack sample was 80mm long, figure 5-23b showed that the uniformity of the applied H-field would not change significantly along this length. After this coil calibration routine, single-point vibrometry studies of the influence of stack geometry were undertaken. An experimental set-up was used as shown in figure 5-17 but in this case, the laser vibrometer was measuring the longitudinal vibrations produced in truncated and 'reduced laminae' stacks when stimulated by the solenoid shown in figure 5.22

By utilising the Signal Recovery 7265 DSP Lock-in Amplifier, it was possible to monitor the drive frequency and the harmonic content of the dynamic displacements produced by the vibrating stacks in the range 2 kHz to 6 kHz. This frequency range was selected as a result

on the current limits that were imposed on the power supply system as a consequence of rising impedances with increasing frequency. This enabled the application of a dynamic H-field across the frequency range with a sufficient displacement output for laser vibrometry measurements. As can be seen in table 5-10, this frequency range is below the calculated fundamental resonances for the truncated stacks. Consequently, these resonances will not influence the strain output of them.

Although a large proportion of first and second harmonic outputs were expected to be measured via the laser vibrometer, it is not unusual to find higher harmonic components in the output displacement waveform [5.12, 5.17]. This can be due to non-linearities in the effective transfer function of the transducer under investigation.

The subsequent output strain will clearly have a waveform that is a synthesis of all of the harmonic components identified through this method.

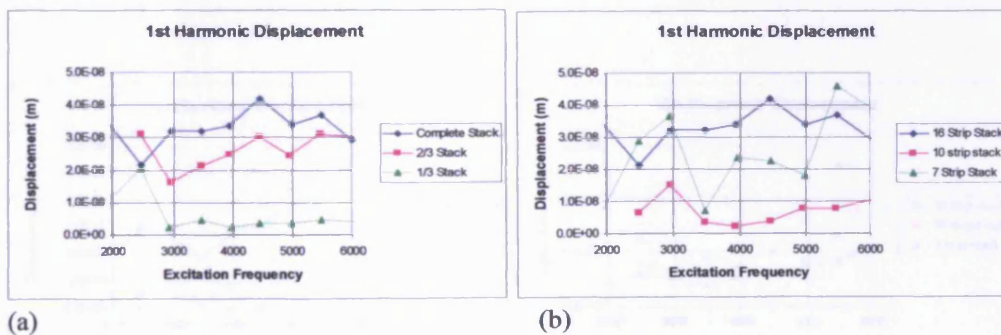
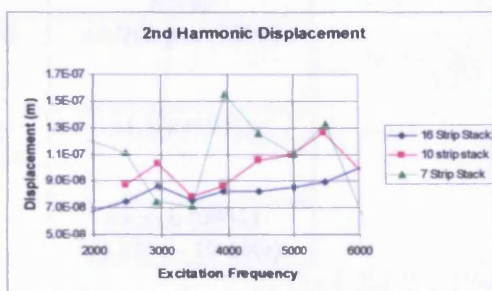
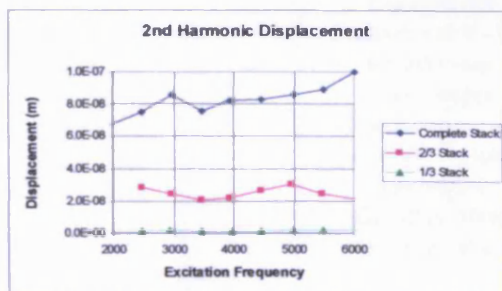
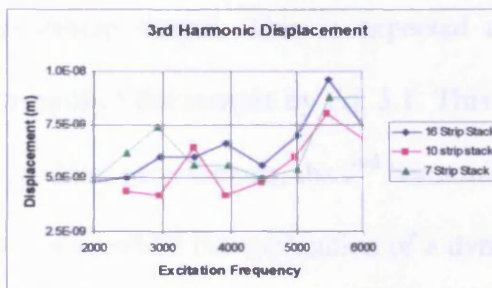
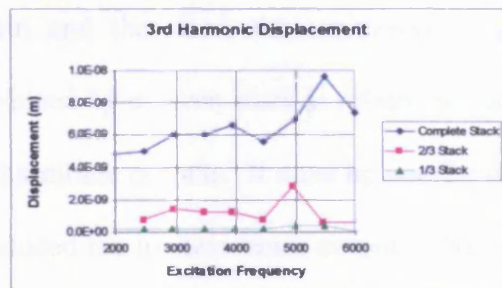


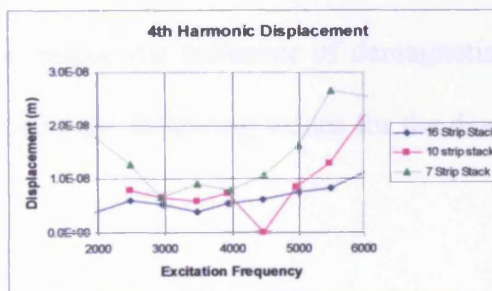
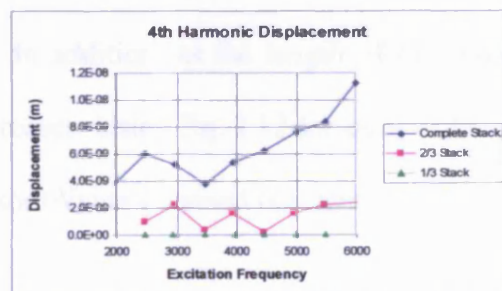
Figure 5-24 (a) 1st harmonic displacement output from stacks of reducing length as a result of an applied H-field of 0.65 kA/m (rms) in the range 2 kHz to 6 kHz (b) 1st harmonic displacement output from stacks with reducing laminae as a result of an applied H-field of 0.65 kA/m (rms) in the range 2 kHz to 6 kHz (laminae thickness 0.30mm).



(a) (b)
Figure 5-25 (a) 2nd harmonic displacement output from stacks of reducing length as a result of an applied H-field of 0.65 kA/m (rms) in the range 2 kHz to 6 kHz (b) 2nd harmonic displacement output from stacks with reducing laminae as a result of an applied H-field of 0.65 kA/m (rms) in the range 2 kHz to 6 kHz (laminae thickness 0.30mm).



(a) (b)
Figure 5-26 (a) 3rd harmonic displacement output from stacks of reducing length as a result of an applied H-field of 0.65 kA/m (rms) in the range 2 kHz to 6 kHz (b) 3rd harmonic displacement output from stacks with reducing laminae as a result of an applied H-field of 0.65 kA/m (rms) in the range 2 kHz to 6 kHz (laminae thickness 0.30mm).



(a) (b)
Figure 5-27 (a) 4th harmonic displacement output from stacks of reducing length as a result of an applied H-field of 0.65 kA/m (rms) in the range 2 kHz to 6 kHz (b) 4th harmonic displacement output from stacks with reducing laminae as a result of an applied H-field of 0.65 kA/m (rms) in the range 2 kHz to 6 kHz (laminae thickness 0.30mm).

Equipment	Error
Polytec OFV-303 based laser vibrometer	$\pm 0.002 \mu\text{m}$ (90%)
Signal Recovery 7265 DSP Lock-in Amplifier	$\pm 1 \text{ Hz}$ (95%)
Keithley 2001 Multimeter	$\pm 1 \text{ mA}$ (90%) (1 kHz – 10 kHz)

Table 5-11 Errors associated with the measurements taken and displayed in Figure 5-23 to 5-26 (see Appendix A).

In figures 5-24(a) to 5-27(a) with stacks with the same number of laminae but of varying lengths, the experimental data showed that a reduction in length produced a reduction in strain and therefore, the maximum displacement output. This is expected as the strain produced by a given stack is related to the length of the sample by Eq. 3.1. This occurred for all harmonic outputs. It must be noted that in these experiments, the 2nd harmonic component produced the highest strain output. This is as a result of the application of a dynamic H-field to the solenoid without an accompanying biasing field (see figures 4-1 to 4-3). The 3rd and 4th harmonic dynamic displacement components were an order of magnitude lower than those of the 1st and 2nd.

In addition, as the length of the stacks reduce the influence of demagnetisation factors increases. Using Eq. 2.12 for each of the stacks the following values for the demagnetisation factor (N) are obtained (see table 5-12).

Stack Length (mm)	Demagnetisation Factor (N)	Effective Applied Field H (compared to H_a)
80	0.0303	97%
53	0.0450	95%
23	0.0980	90%

Table 5-12 Calculation of the demagnetisation factors for the stacks of different lengths using Eq. 2.10 and Eq. 2.12.

As a result, a reduction of the stack length will reduce the maximum strain output (and therefore the output displacement, δx) as a result of both the action of the reduction of straining magnetostrictive material and the effective applied magnetic field.

In figures 5-24(b) to 5-27(b) stacks, with the varying numbers of laminae but of the same length, the experimental data also showed that the largest strain outputs for the three stack geometries were still the 2nd harmonic component. However, in these experiments, the size of the soldered joints holding the ends of the stacks together varied from sample to sample. As a result, the effective 'load mass' being actuated differed from stack to stack and may have influenced these results.

Figures 5-28 to 5-31 show the harmonic displacements when an applied H-field of 0.65 kA/m (rms) was applied to full scaler stack in the range 2 kHz to 6 kHz five times. This was undertaken to identify the consistency for repeated measurements. The results show that the repeated measurements are within the maximum expected error of the vibrometer system ($\pm 0.002 \mu\text{m}$).

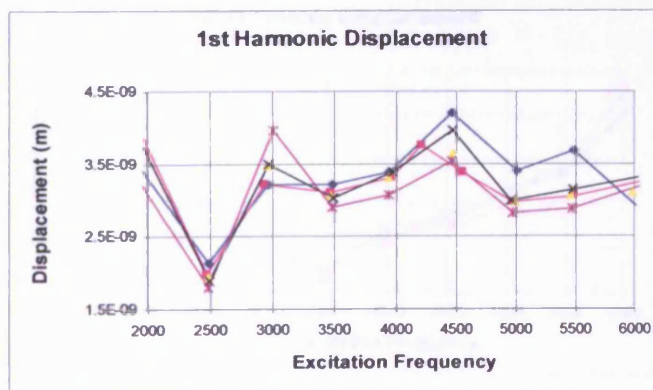


Figure 5-28 1st harmonic displacement output from a full stack as a result of an applied H-field of 0.65 kA/m (rms) in the range 2 kHz to 6 kHz: 5 repeats

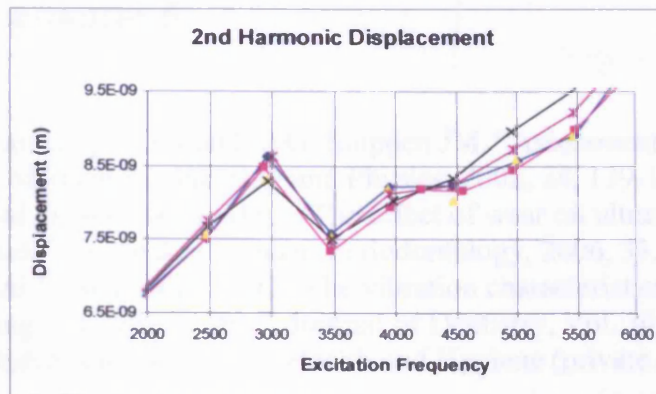


Figure 5-29 2nd harmonic displacement output from a full stack as a result of an applied H-field of 0.65 kA/m (rms) in the range 2 kHz to 6 kHz: 5 repeats

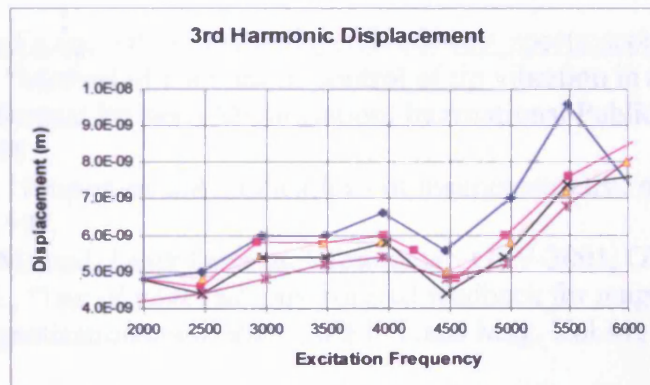


Figure 5-30 3rd harmonic displacement output from a full stack as a result of an applied H-field of 0.65 kA/m (rms) in the range 2 kHz to 6 kHz: 5 repeats

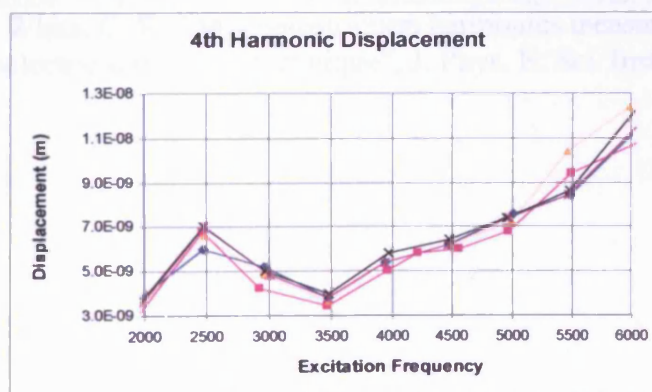


Figure 5-31 4th harmonic displacement output from a full stack as a result of an applied H-field of 0.65 kA/m (rms) in the range 2 kHz to 6 kHz: 5 repeats

References for chapter 5

- [5.1] Trenter SC, Walmsley AD, Landini G, Shippen JM. "Assessment of the ultrasonic dental scaler insert". Medical Engineering and Physics, 2002, 24, 139-144.
- [5.2] Lea SC, Landini G, Walmsley AD., "The effect of wear on ultrasonic scaler tip displacement amplitude". Journal of Clinical Periodontology, 2006, 33, 37-41.
- [5.3] Lea SC, Landini G, Walmsley AD., "The vibration characteristics of ultrasonic scalers assessed with scanning laser vibrometry", Journal of Dentistry, Vol. 30, 2002, 147–151.
- [5.4] Pinder. J., British Society of Dental Health and Hygiene (private communication), 2005.
- [5.5] Lea. S.C. Landini G. Walmsley A.D., "Ultrasonic scaler tip performance under various load conditions", J Clin Periodontol 2003; 30: 876–881.
- [5.6] Lea. S.C. S.C. Landini G. Walmsley A.D., "Displacement amplitude of dental scaler inserts", J Clin Periodontol 2003; 30: 505–510.
- [5.7] Lea. S.C., The Dental School, The University of Birmingham, (private communication), 2005.
- [5.8] http://en.wikipedia.org/wiki/Energy-dispersive_X-ray_spectroscopy
- [5.9] Javanovic. V., "Method of continuous control of tip vibration in a dental scaler system", World Intellectual Property Organisation, International Publication Number WO 98/11844, March 1998.
- [5.10] Bartlett. P.A., "Properties and applications of magnetostrictive materials", MSc Thesis, University of Hull, 1997.
- [5.11] Polytec User Manual, Laser Doppler Vibrometer, OFV-3001, OFV-303.
- [5.12] Zurek. S. et al., "Use of novel adaptive digital feedback for magnetic measurements under controlled magnetization conditions", IEEE Trans Mag. Vol.41, No.11, 2005, pp 4242 – 4250.
- [5.13] Signal Recovery 7265 DSP Lock-in Amplifier User Manual.
- [5.14] Blitz. J., "Ultrasonics", Physics Education, Vol 2, p 269, 1969.
- [5.15] <http://info.ee.surrey.ac.uk/Workshop/advice/coils/mu/>
- [5.16] http://www.kayelaby.npl.co.uk/general_physics/2_6/2_6_6_6.html
- [5.17] Mapps. D. J., White. C. E., "Magnetostriction harmonics measurement using a double piezoelectric transducer technique", J. Phys. E: Sci. Instrum., Vol. 17, 1984, 472-476.

6 MEASUREMENTS OF QUASI-STATIC MAGNETOSTRICTION OF ALTERNATIVE SCALER STACK MATERIALS

6.1 *Introduction*

Any material substitution for enhancement of current dental scalers, must offer advantages over laminated nickel stacks. Therefore, it is necessary to have an understanding of the magnetostrictive properties of candidate material, particularly, the quasi-static strain vs. applied field and associated stress and temperature performance.

It must be noted that the frequency related performance of a magnetostrictive element used to produce transduction is a result of the combined magnetic, magnetostrictive, electrical and mechanical components of this element. Also, the overall transfer function of a transducer will not be determined by the properties of the magnetostrictive material alone but will be influenced by all of the components that comprise the transducer. Despite this, initial measurements of the frequency performance of a material may give an indication of its suitability for high-frequency applications. However, such measurements would have to take into account the sample geometry which may have an influence on the response of the core material for given applied dynamic magnetic fields. This can be illustrated in the current dental scalers where a laminated stack of electrically insulated nickel strips is used to supply the dynamic stimulus to the scaler tips. The performance of this stack of strips would, clearly, be different to an equivalent solid bar of nickel as a result of eddy current effects.

Therefore a characterisation of material samples must be undertaken and compared with nickel-stacks. The geometry of these newer ‘stacks’ and rods will have to be determined based on what can be manufactured or obtained.

Magnetostrictive metallic alloys were identified as candidate materials based on their quasi-static saturation magnetostriction as a result of a survey of the literature. The materials selected were:

- Nickel iron (Radiometal 2550: 45% Ni) [6.1, 6.2]
- 3% Grain-oriented silicon iron [6.3, 6.4]
- Cobalt iron (Hyperco50: 49% Co) [6.5, 6.6]
- Cubex (doubly grain oriented 3% silicon iron) [6.7]
- Terfenol-D (15mm diam x 50mm long rod) [6.8]

In the literature, it was clear that cobalt iron and nickel iron alloys had been successfully used in non-dental ultrasonic systems before and so these seemed to be a logical choice for potential candidate materials [6.9, 6.10, 6.11, 6.12].

All but the Terfenol-D sample were cut from sheets of the metal. The strip sample dimensions and post-cutting annealing information is shown in table 6-1.

Material	Sample length and width (mm)	Sample Thickness (mm)	Anneal time and temperature
Ni	50 x 4	0.25	815°C for 4 hrs [6.1]
Cubex	50 x 4	0.35	900°C for 4 hrs [6.6]
3% GO Steel	50 x 4	0.31	750°C for 4 hrs [6.3]
Hyperco50	50 x 4	0.36	850°C for 4 hrs [6.4]
Radiometal 4550	50 x 4	0.35	1180°C for 4 hrs [6.4]

Table 6-1 Table showing the strip sample dimensions and vacuum annealing times and temperatures.

Measurements made on samples of these materials were compared to the accepted values and signs for their saturation magnetostrictions.

As the dental scaler lavage system supplies water to the teeth via the central void of the handle and over the stack, it must only produce water that will not be so hot that it presents a scald hazard to the patient. Tables 6-2 and 6-3 indicate the temperature limits and exposure times for skin contact with water.

Temperature, °C	Exposure time
44	6 h
49	9 min
51	2–6 min
52	2 min
55	20–30 s
60*	5–6 s
66	2 s
70	1 s

*Usual temperature of home water heaters.

Table 6-2 Exposure time at given temperatures that causes deep second-degree burn injury in adults [6.15]

Temperature, °C	Activity
32–41	Infant's and toddler's bath
34–45	Adult's bath
39–41	Adult's shower
41–42	Hot tub
42–45	Too hot for activities; threshold for sensation of pain in adults

Table 6-3 Typical hot water temperatures in daily living [6.15]

As a result, it would be wise to ensure that the stack operates at a temperature below 40°C if it is not to result in patient discomfort due to over-heated lavage water. Any materials that may be considered as a substitute to the current nickel stacks need only be characterised below this temperature.

An in-house DC permeameter system [6.16] (see figure 6-1) based on 'Labview' control software was modified so that it could measure magnetostriction under linear tensile stresses up to 10 MPa at temperatures up to 40°C. Magnetising current was supplied by a pair of

Kepeco bipolar DC power supplies. These were controlled by a PC via a 16 bit digital to analogue converter giving a resolution ~ 0.2 mA. Two methods for measuring the applied magnetic field strength were used. A Lakeshore 480 gaussmeter with a Hall probe was utilised when a sample was placed in a Newport Instruments Type AE4 electromagnet and a Agilent 34401A DC voltmeter (DVM) was used to measure the voltage across a precision 0.1 Ohm resistor in the ground return of the primary circuit with the magnetic field strength being calculated using Eq. 2.1 when a solenoid was used. It was possible to measure the magnetic field directly (with the gaussmeter) for the electromagnet as the space between the pole pieces was accessible. This was not the case for those samples that were placed inside a solenoid. Consequently, measuring the current supplied to the solenoid would enable the calculation of the applied field that was applied to a sample (see figure 6-1).

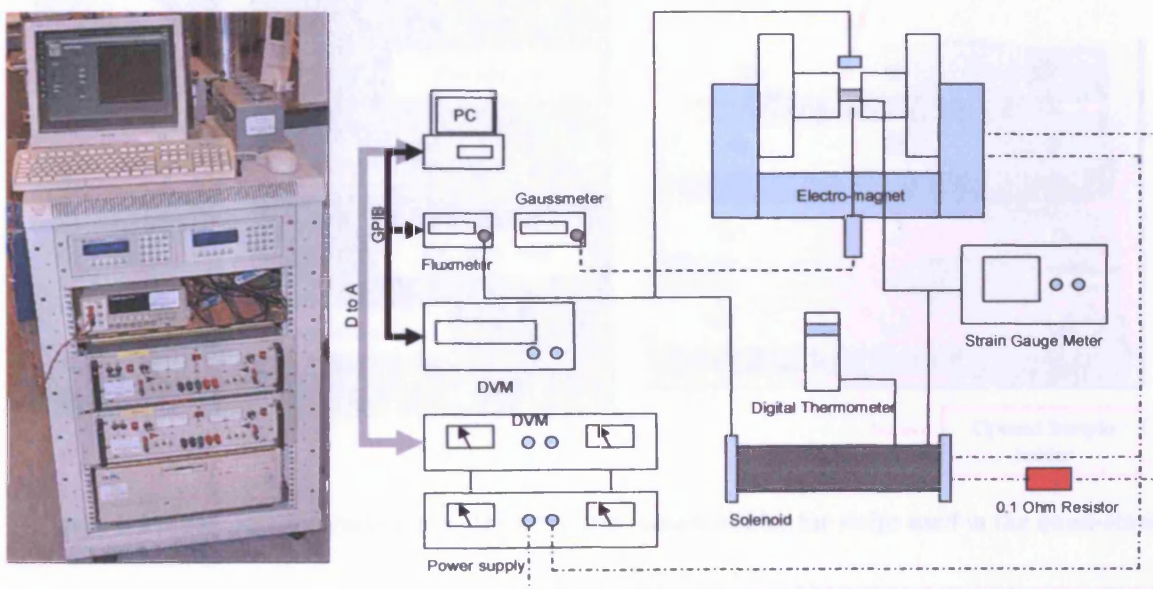


Figure 6-1 DC permeameter system used to obtain strain vs. applied H-field characteristics of materials [6.16]

The fluxmeter and volt meter were connected to the PC via a GPIB bus. This enabled the full control of the instruments and the transfer of the measurement data. Foil Resistance strain gauges (RS 632-146) were fixed (with cyanoacrylate adhesive) to each sample and

connected to an EMS MAS 010 strain gauge meter in a Wheatstone bridge configuration with a temperature compensation strain gauge included in the circuit. This temperature compensation strain gauge was fixed to the sample holding stage. A digital K-type thermocouple thermometer was used to monitor the sample temperature. The thermocouple was fixed in thermal contact with the sample holder.

The solenoid based measurement system was used to measure the properties of the metallic strips identified in table 6-1. The size of these was chosen to be similar to that of strips in commercial nickel-based scaler stacks. The strip under test was placed in a custom made brass sample-holder such that a compressive prestress could be applied (see figure 6-2 and 6-3).

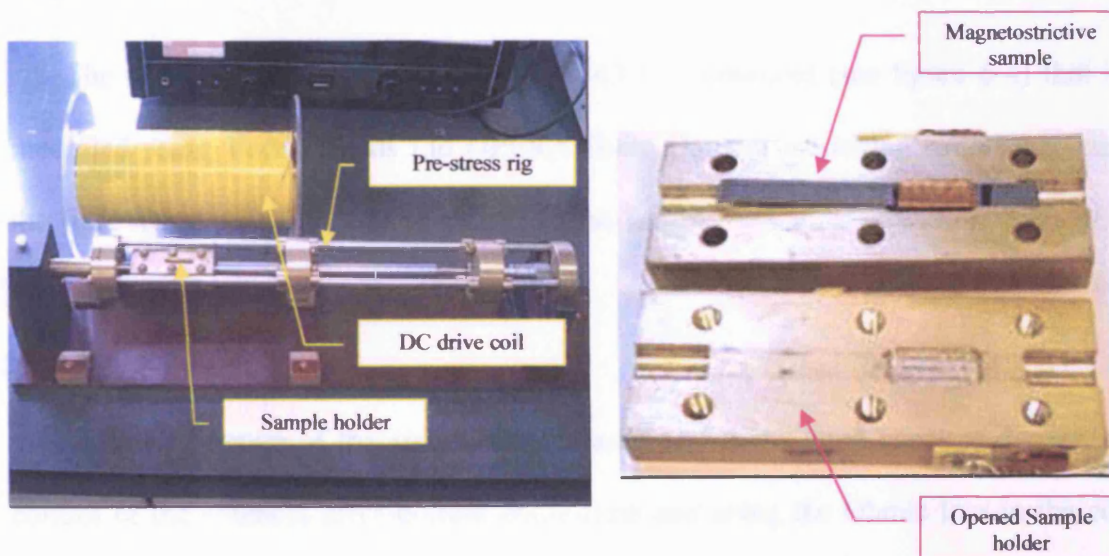


Figure 6-2 Solenoid, compressive pre-stress rig and sample holder for strips used in the quasi-static magnetostriction study

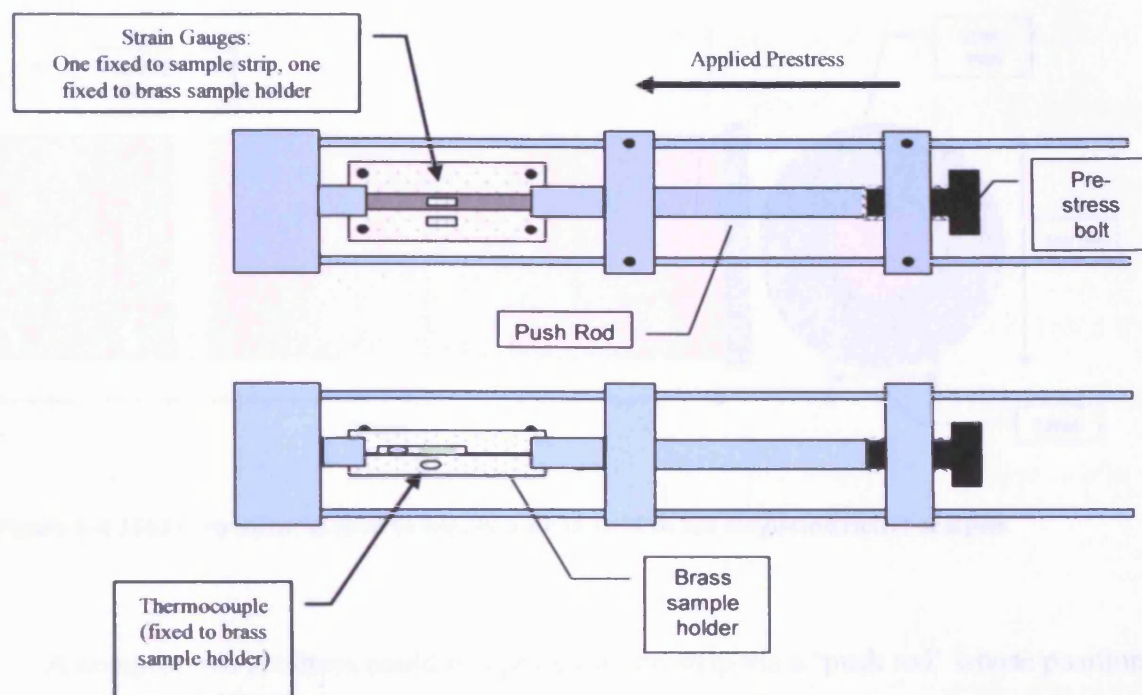


Figure 6-3 Schematic of the stress rig used to hold the 50 mm long samples during the quasi-static magnetostriction study

The test rig was then inserted into a 1563 turn solenoid (see figure 6-4) that had been modelled using Vector Fields Ltd OPERA finite element modelling software to ensure that the field was uniform in the region where the sample was located within 2.2% of the field value at the centre of the solenoid.

The temperature of the strip was increased and maintained constant during testing by control of the solenoid drive-current cycle-time and using the Ohmic loss in the coil as the heat source. The cycle time was selected so that the temperature measured by the brass sample-holder thermocouple would only increase by more than 1°C after the Strain vs. H loop was cycled over 5 times. By continuing the cycling of subsequent Strain vs. H-field loops it was possible to measure the DC magnetostrictive properties of the test materials up to 40°C.

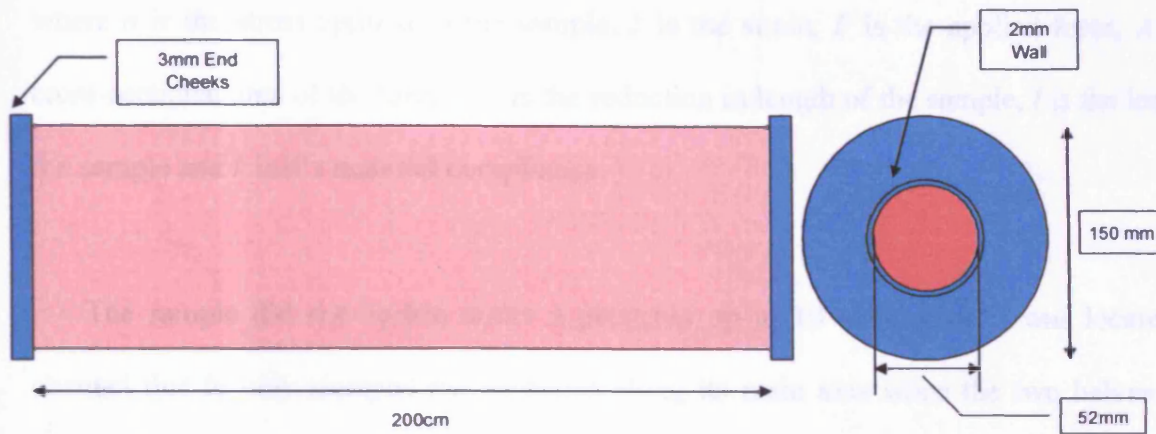


Figure 6-4 1563 turn solenoid used to supply a dc H-field to the magnetostrictive samples

A compressive prestress could be applied to the strip via a ‘push rod’ whose position was controlled by a vernier screw mechanism. The push rod enters the brass sample holder via a recess so that it can be placed in contact with the end of the sample strip. The other end of the sample strip butts against an equivalent rod that is fixed to the body of the stress rig as shown in fig. 6.2.

The amount of prestress was calculated based on the amount of strain that was measured, via the strain gauge meter, when the stress was applied to a strip with a known Young’s Modulus E where:

$$E = \sigma / \lambda \quad (6.1)$$

$$\text{and} \quad E = F / A / x / l \quad (6.2)$$

$$\text{so} \quad E = kx / A / x / l \quad (6.3)$$

$$\text{leading to} \quad k = EA / l \quad (6.4)$$

where σ is the stress applied to the sample, λ is the strain, F is the applied force, A is the cross-sectional area of the sample, x is the reduction in length of the sample, l is the length of the sample and k is it's material compliance.

The sample did not buckle under a prestress up to 10 MPa since it was located in a channel that loosely clamped the its edges along its main axis when the two halves of the brass sample holder were screwed together prior to installation in the sample holder (see figure 6-2).

An output voltage from the strain-gauge meter was connected to the permeameter system so that it could be stored or displayed via LabView. In order to calibrate the system, a strain was simulated by switching in an additional resistance in parallel with the strain gauge that would be used to measure magnetostriction when a quasi-static field is applied (see figure 6-4).

If δR is the change in resistance of the strain gauge, (resulting in a change in the output voltage of the strain gauge meter), then the strain λ can be calculated as:

$$\lambda = \frac{\delta R / R_g}{G} \quad (6.5)$$

where G is the gauge factor, δR is the change in resistance due to a strain (or simulated change in strain due to an external resistor bank as show in figure 6-5) and R_g is the resistance of the strain gauge.

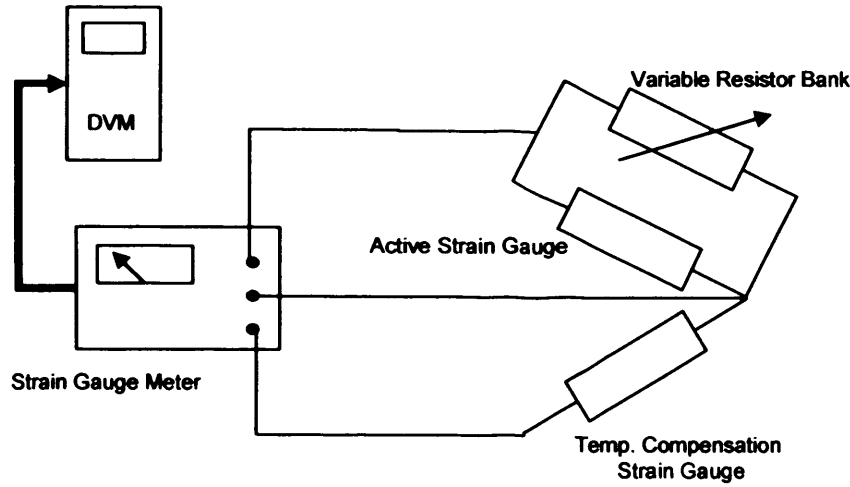


Figure 6-5 Arrangement of the strain gauge meter calibration system

By connecting a Draper DMM1A digital voltmeter to the output of the EMS MAS 010 strain gauge meter it was possible to identify the relationship between the change in resistance (simulating an applied strain to the ‘active’ strain gauge) and the strain gauge voltage output (from the meter) that would be subsequently related to this strain. The calibration factor (G) obtained relates a change in voltage in the bridge circuit to a change in strain as measured via the strain gauge so

$$\lambda = \frac{\delta R}{R_g} \cdot \frac{V}{G \cdot \delta V} \quad (6.6)$$

where V is the initial voltage output from the strain gauge meter and δV is the change in voltage due to the change in magnetostrictive strain when a magnetic field is applied.

A separate sample holder and field source were required for a 15 mm diameter Terfenol-D sample of length 50 mm used for comparison tests. This was undertaken purely to compare

the strain output performance of the Terfenol-D sample for a given applied field (without an optimising pre-stress) with that of the other candidate materials. However, Terfenol-D was not considered to be a potential replacement material for dental scalers of this topology as they rely on the production of flexural resonances in the stack. Such resonances would damage Terfenol-D as it cannot withstand transverse or torsional loads [6.17]. Initial measurements on this sample were undertaken with it held in a plastic tube between the poles of the Newport Instruments AE4 Electromagnet so that there were no air-gaps between the Terfenol-D sample and the pole-pieces. In this case the Terfenol-D rod was instrumented with the same type of strain gauge used in the single-strip measurements with a reference strain gauge on the plastic tube. The same permeameter system was used to energise the electromagnet and undertake measurements (see figure 6.6) under zero prestress.

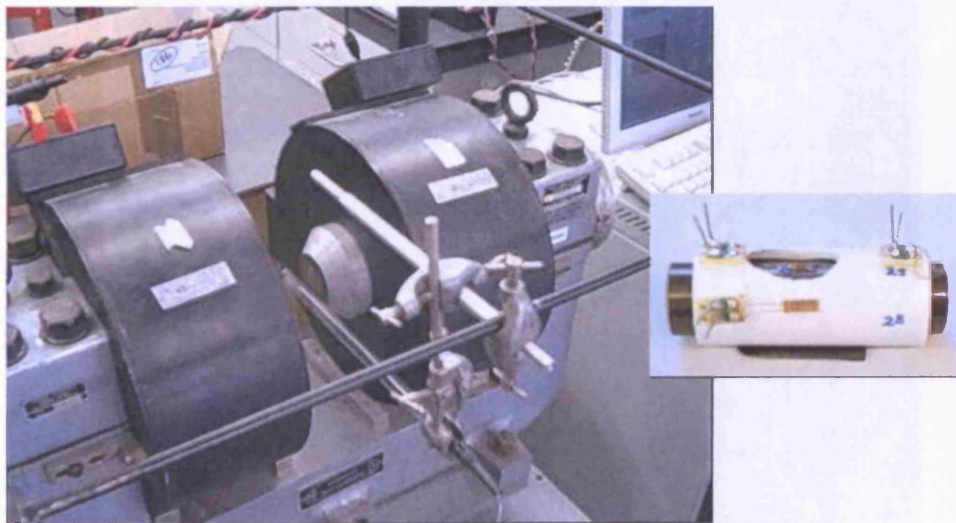


Figure 6-6 Newport magnet-based Terfenol-D strain measurement system and Terfenol-D sample in a sample sleeve.

The same strain measurement system and techniques were used for characterising the Terfenol-D sample as was used for measurement in the previous magnetostrictive strip

measurements. A 'Rare Earth Products Ltd. 'Reacton' Terfenol-D sample² was available for comparison testing. The sample was suspended between the pole-pieces of the Newport electromagnet so that the main axis of the rod was aligned with the axis of the electromagnet. In this case the Terfenol-D rod was instrumented with the same strain gauges as used in the single strip measurements. The same permeameter system was used to power and control the Newport magnet and undertake strain measurements (see figure 6-1).

A LabView virtual instrument (figure 6-7) was developed so that the strain data obtained using this method could be saved as a data file for analysis via a Microsoft Excel package.

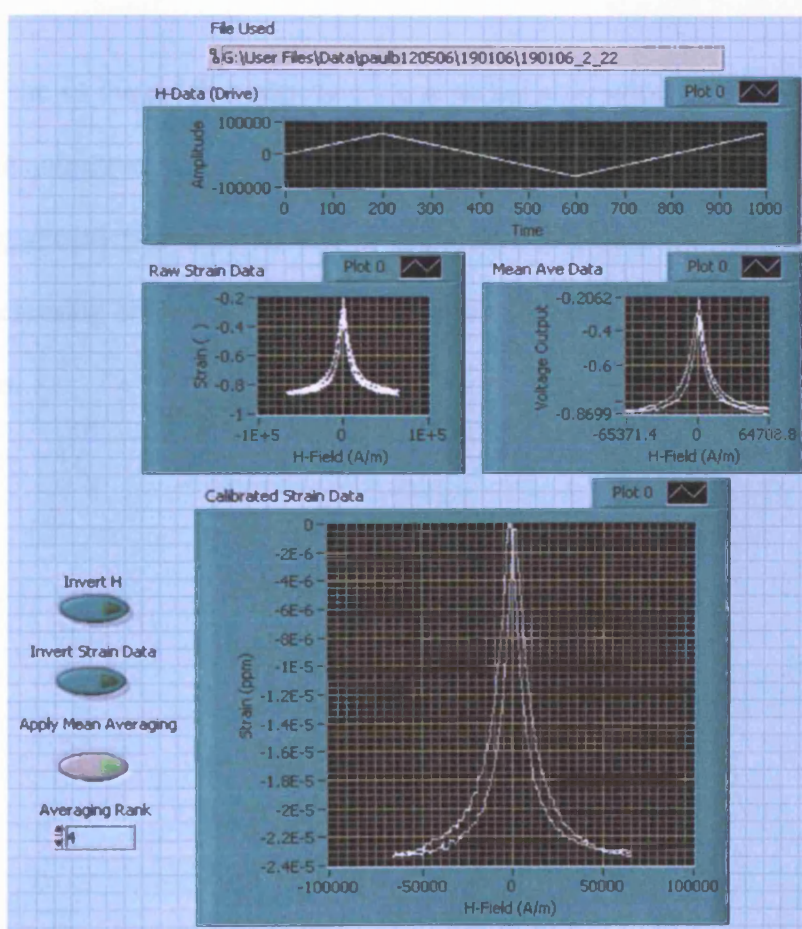


Figure 6-7 LabView virtual instrument front panel for processing strain data

² Originally purchased by the University of Hull and donated to Cardiff University by Mr. S. Eaton of QinetiQ Ltd.

6.2 Results

Plots of quasi-static strain vs. applied H-field for the different magnetostrictive materials are shown in this chapter together with peak strain output as the sample temperature was increased. The strain vs. applied field data represents the transfer function of the materials concerned. Demagnetisation corrections have not been applied to these data so that a direct comparison can be made between the materials. This is because the applied field *requirements* to achieve maximum strain are what are most important to the transducer designer. Consequently, an output strain vs. applied field comparison could be made between the candidate materials.

Figure 6-8 shows the magnetostriction for a nickel strip which is used as a reference for the other magnetostrictive materials to match or exceed. It must be noted that the material is negatively magnetostrictive and so has a reduction in saturation magnetostriction when subjected to increasing compressive stresses. Saturation strain was achieved with an applied field $\sim 30 \text{ kA/m}$.

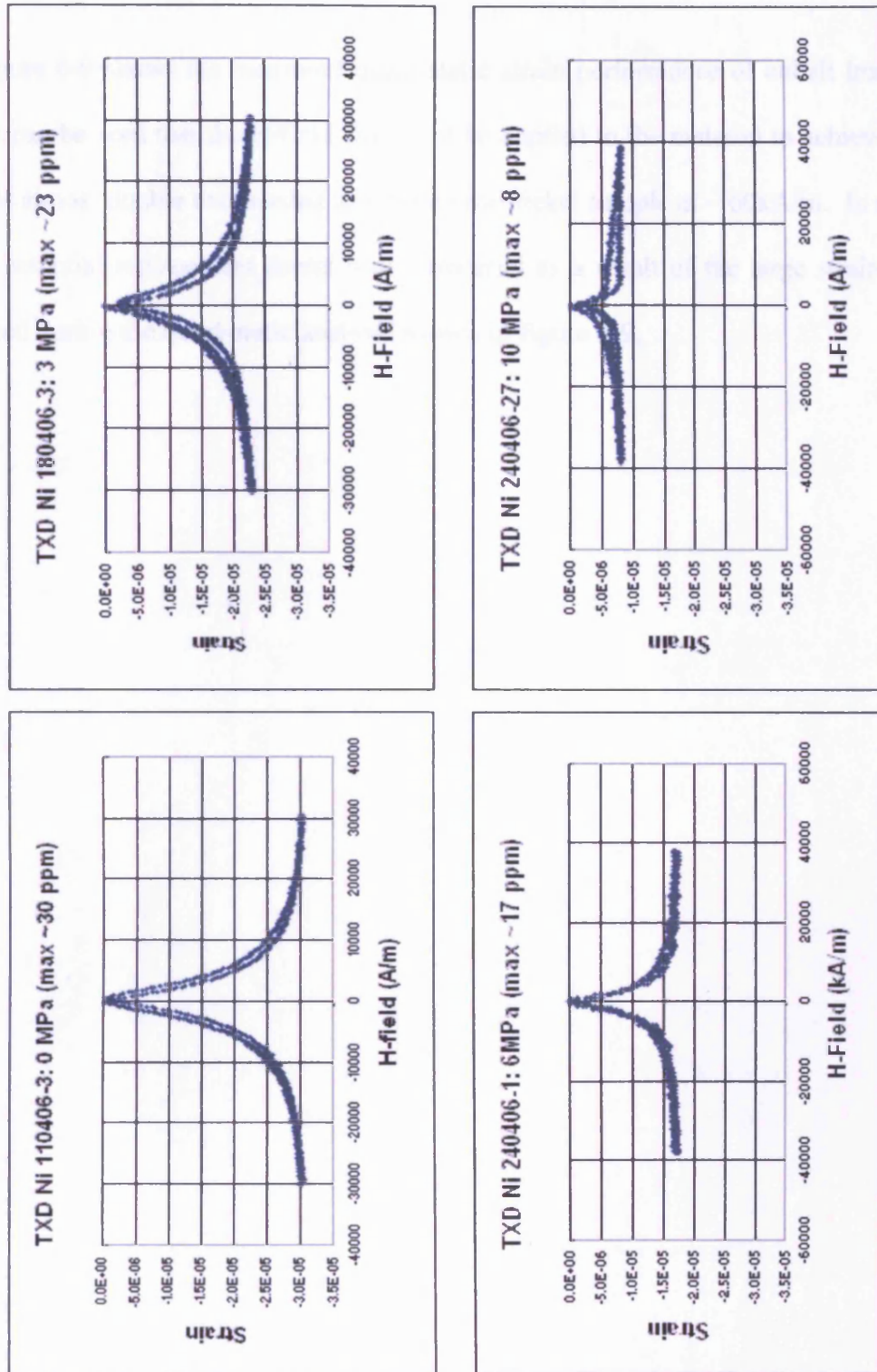


Figure 6-8 Variation of strain with applied H-field for a nickel strip subjected to compressive pre-stresses of 0, 3, 6 and 10 MPa.

This compares to a maximum saturation magnetostriction of -25 to -47 ppm as stated by Bozorth [6.18].

Figure 6-9 shows the measured quasi-static strain performance of cobalt iron (Hyperco 50). It can be seen that the H-field that must be applied to the material to achieve saturation strain is almost double that needed to saturate the nickel sample at $\sim 60\text{kA/m}$. In spite of this it is a potential replacement dental scaler material as a result of the large strains that were produced during the quasi-static analysis shown in figure 6-9.

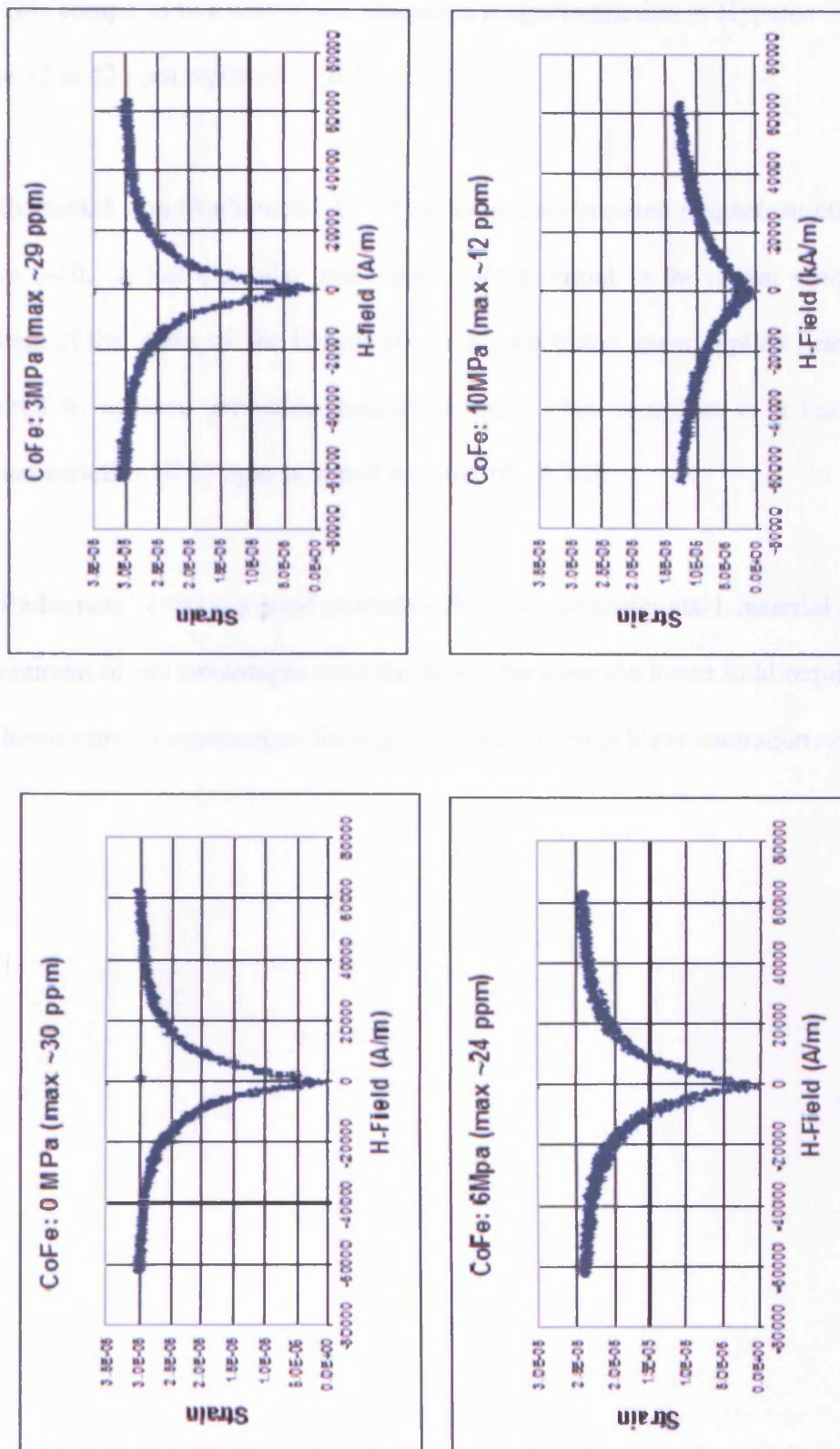


Figure 6-9 Variation of strain with applied H-field for a Cobalt Iron (Hyperco 50) strip subjected to compressive pre-stresses of 0, 3, 6 and 10 MPa.

This compares to a maximum saturation magnetostriction of Hyperco 50 measured in the range 32 to 42 ppm reported in [6.19].

For the nickel iron (Radiometal 4550) material the measured magnetostriction can be seen in figure 6-10. It has a similar quasi-static strain output to the nickel sample but the initial gradient of the strain vs. the H-field curve is such that a lower applied field (~ 15 kA/m) was required to achieve saturation magnetisation. This compares to a maximum saturation magnetostriction of 27 ppm as stated by Bozorth [6.20].

Radiometal 4550 is a good candidate for a dental scaler stack material as this lower field requirement offers advantages over the nickel because the lower field requirement will result in a lower current requirement for a given drive coil to achieve saturation strain.

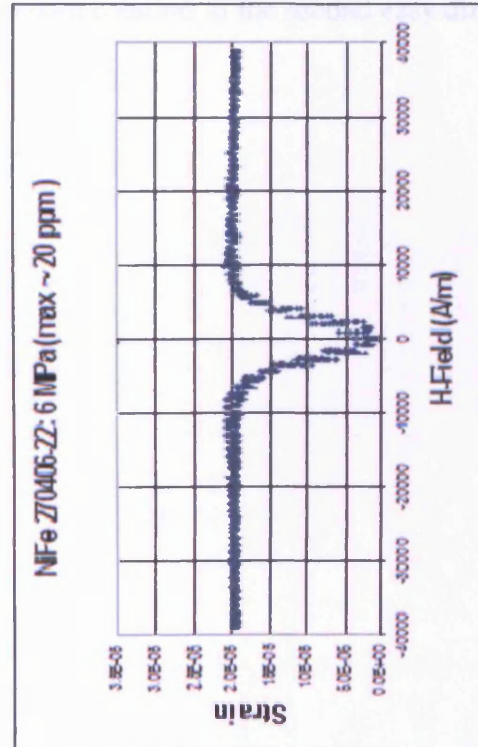
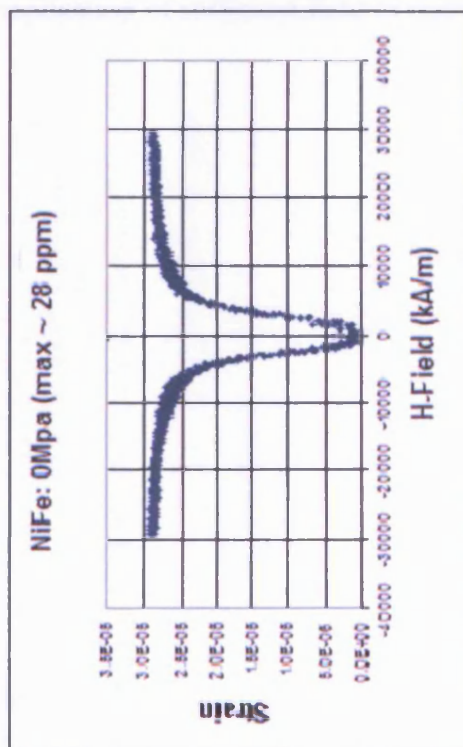
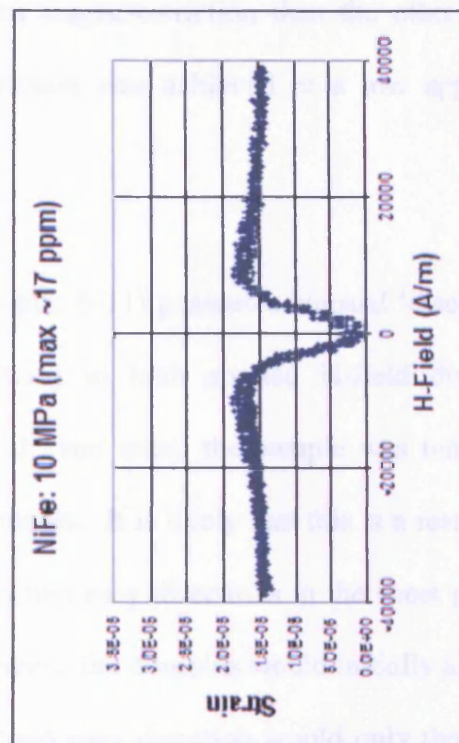
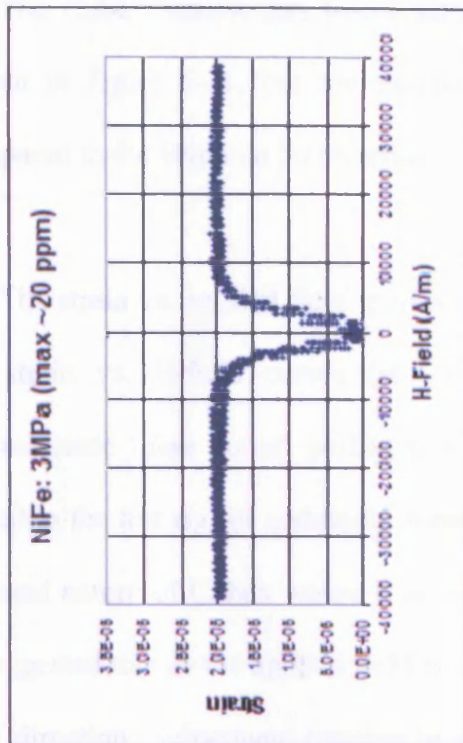


Figure 6-10 Variation of strain with applied H-field for a nickel-iron (Radiometal 4550) strip subjected to compressive pre-stresses of 0, 3, 6 and 10 MPa.

The Cubex sample has lower saturation magnetostriction than the other materials, as shown in figure 6-11, but the magnetostriction was achieved at a low applied H-fields compared to the Hyperco 50 material.

The strain vs. applied field graphs (in figure 6-11) possesses unusual 'discontinuities' in the strain vs. H-field curves (at 2500 A/m) in both applied H-field directions. This characteristic 'deer horns' profile was noted even when the sample was removed and re-seated in the test rig for additional measurements. It is likely that this is a result of the cube oriented nature of Cubex where it possesses two easy directions in the sheet plane [6.6]. It is suggested that as the applied field is increased, the domains would initially align along one easy direction. Subsequent rotation to a second easy direction would only then be achieved the application of sufficient field to enable domain rotation to the second easy direction.

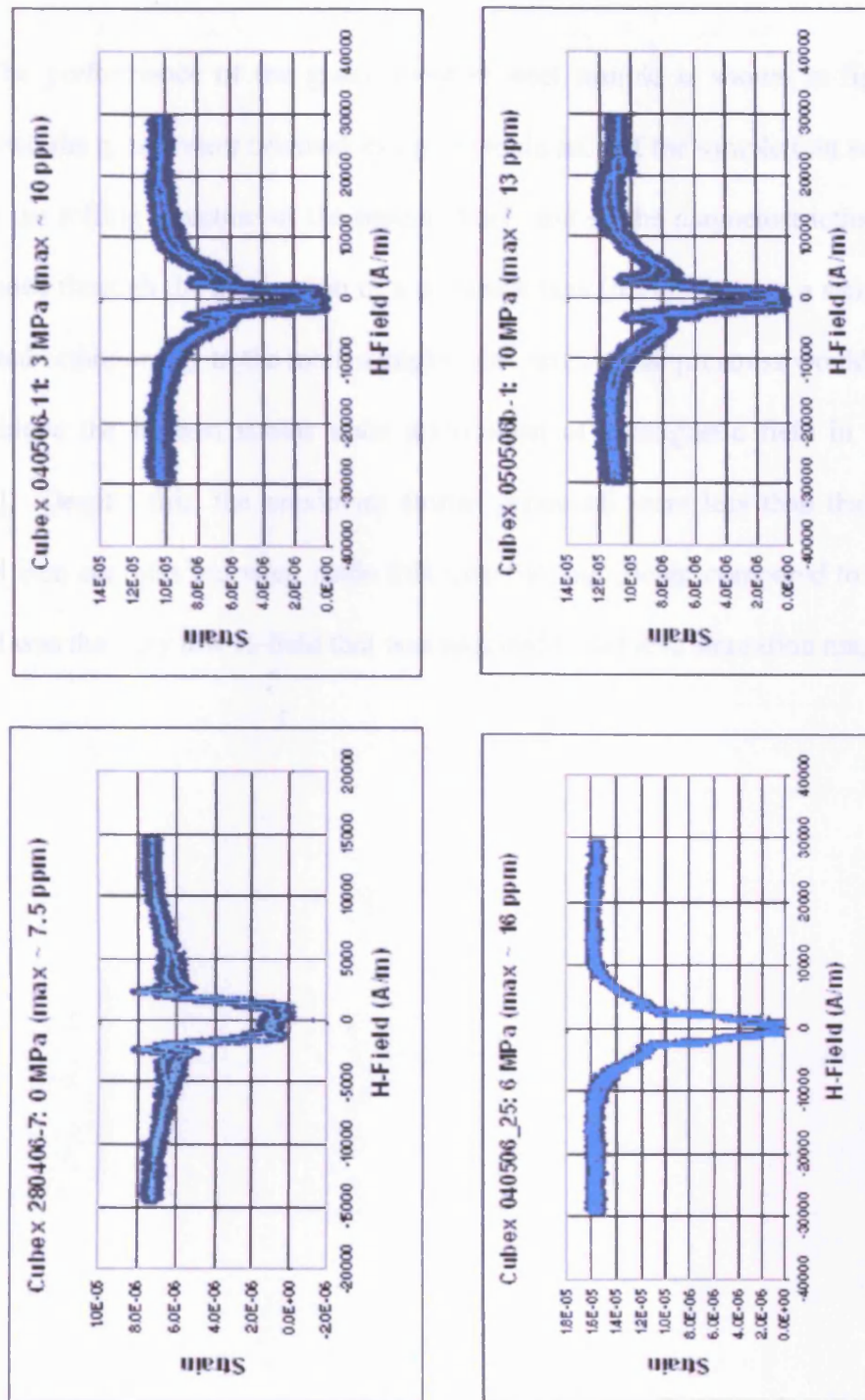


Figure 6-11 Variation of strain with applied H-field for a Cubex strip subjected to compressive prestresses of 0, 3, 6 and 10 MPa.

The performance of the grain oriented steel sample is shown in figure 6-12. In this material, the grains were oriented along the main axis of the sample (cut so the main axis was along the rolling direction of the parent sheet) and so the magnetostriction performance was enhanced through the application of a prestress bias [6.21]. Having a sample with the grains oriented orthogonally to the main sample axis, no external prestress would need to be applied to achieve the highest strains upon application of a magnetic field in the same direction [6.20]. Despite this, the maximum strains produced were less than that of the nickel and nickel iron samples but what made this material significant compared to the other materials tested was the very low H-field that was required to achieve saturation magnetostriction.

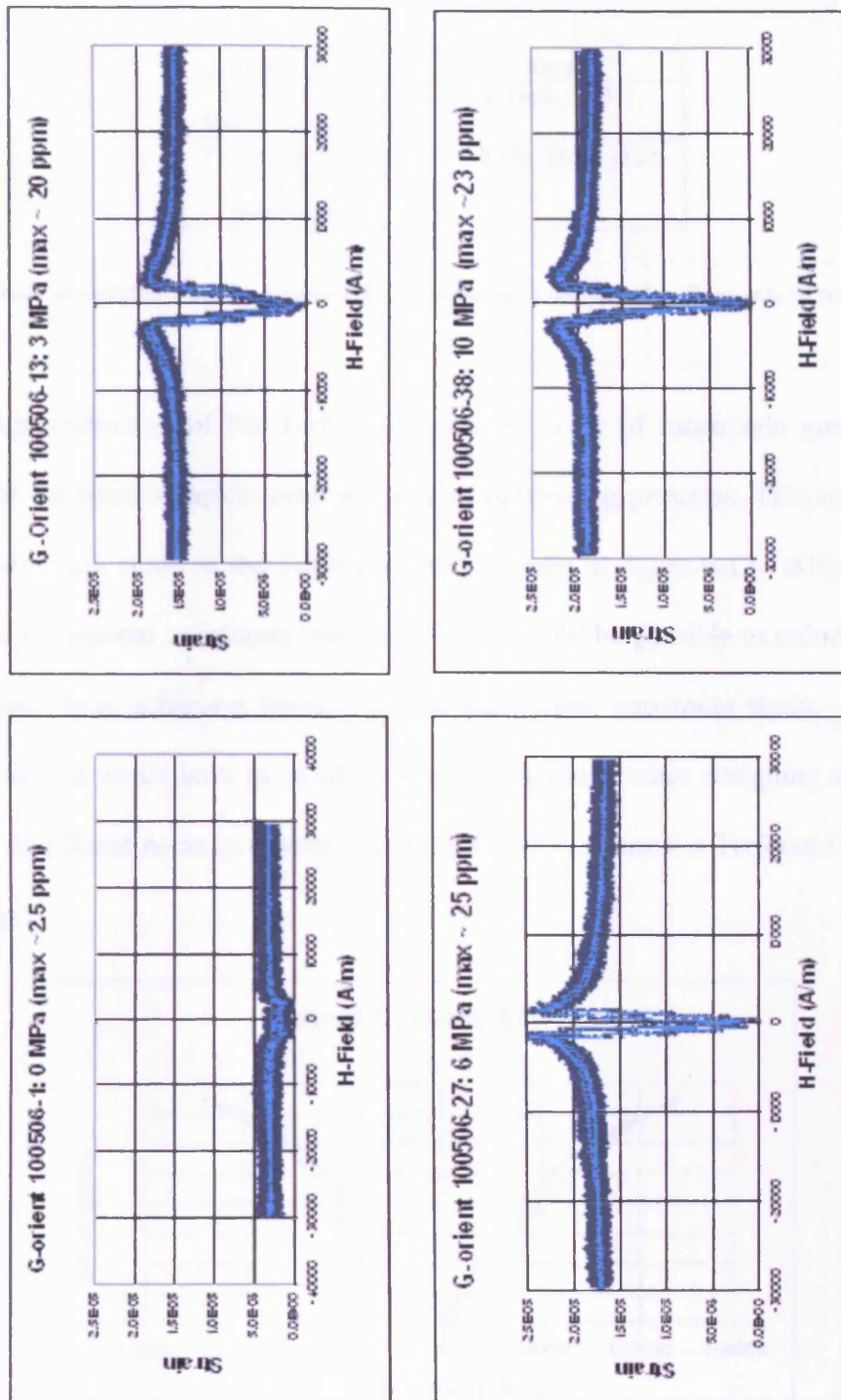


Figure 6-12 Variation of strain with applied H-field for a grain-oriented steel strip subjected to compressive pre-stresses of 0, 3, 6 and 10 MPa.

Equipment	Error
EMS MAS 010 Strain Gauge Meter	$\pm 1 \text{ ppm}$ (80%)
Permeameter system H-field measurement	$\pm 0.6\%$ (80%) [6.2]

Table 6-4 Errors associated with the measurements taken and displayed in figures 6-10 to 6-14 (see Appendix A).

The magnetostriction of the Terfenol-D was an order of magnitude greater than that measured for the other samples, even without an optimising prestress. This was despite not achieving saturation strain in the Terfenol-D rod as seen in figure 6-13. Although a higher applied field is required to saturate this material, it would be possible to reduce the ultimate field requirements to achieve a lower, but still significant, maximum strain. Terfenol-D is expensive³, so this would have to be taken into consideration when designing a dental scaler. However a significant re-design, would be required to implement a Terfenol-D based dental scaler design.

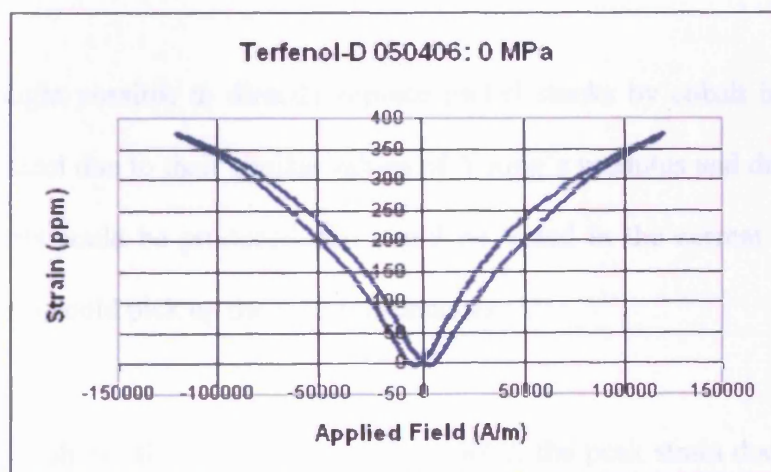


Figure 6-13 Terfenol-D strain output with applied field with zero pre-stress

³ The cost of 2.5" diameter rod (which only comes in 10" cast lengths) is approximately \$60 per mm or \$926 per lb (Jan 2009).

Equipment	Error
EMS MAS 010 Strain Gauge Meter	$\pm 1\text{ppm}$ (80%)
Permeameter system H-field measurement	$\pm 0.6\%$ (80%) [6.2]

Table 6-5 Errors associated with the measurements taken and displayed in Figure 6-15 (see Appendix A).

In addition, it was clear that the use of a Terfenol-D rod of these dimensions would be limited by eddy current losses [6.22] but successful composite 1-3 magnetostrictive materials have been produced from identical rods as those used in this investigation (indeed from the same manufacturing batch from Rare Earth Products Ltd). A 1-3 material is one where small ‘pillars’ of magnetostrictive material are set equidistant from each other in a polymer matrix. These Terfenol-D 1-3 composites were found to have a high frequency capability while maintaining the benefits of continuous anisotropic Terfenol-D in the direction of actuation [6.22]. However, as a result of the problem associated with generating flexural modes in this brittle material, Terfenol-D was not taken forward as a candidate replacement material.

It was thought possible to directly replace nickel stacks by cobalt iron, nickel iron or grain oriented steel due to their similar values of Young’s modulus and density. This would mean that inserts could be produced that could be tested in the current commercial scaler system to see if it could pick up the insert resonances.

Figure 6-14 shows that in the range 28° to 40°C, the peak strain does not significantly alter with temperature in all the materials examined.

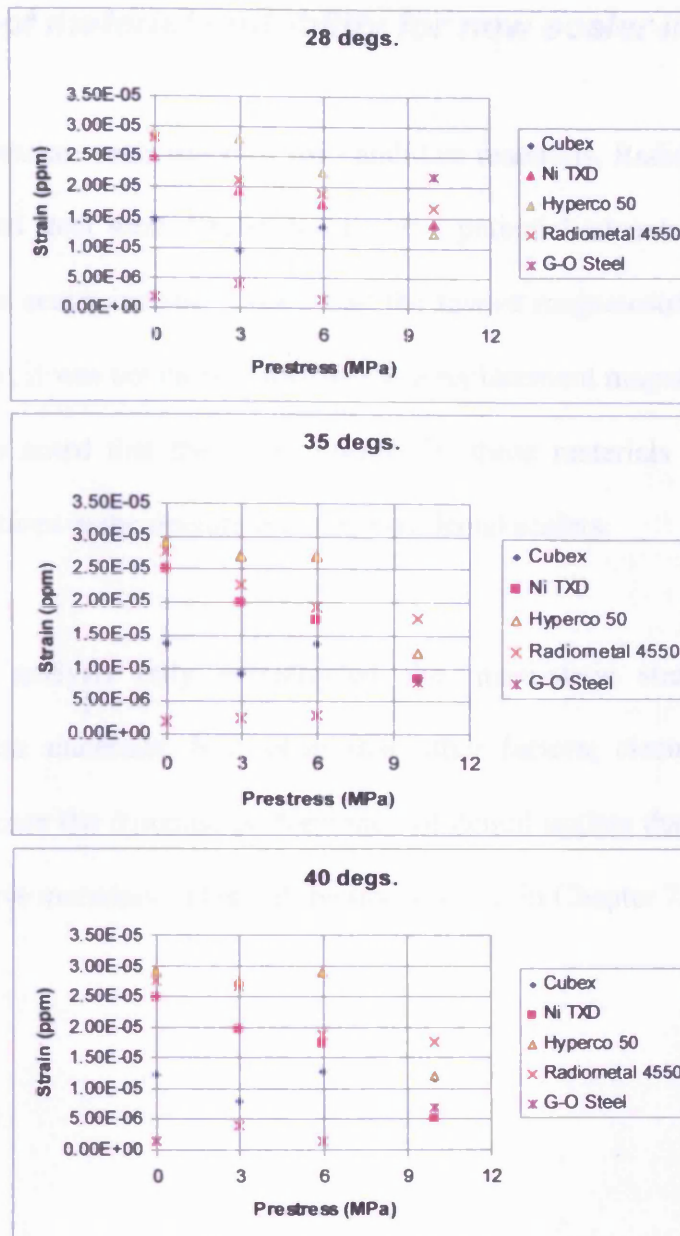


Figure 6-14 Peak magnetostriction measured for the sample materials at different pre-stresses at 28, 35 and 40 °C showing that there is not a significant influence of operating temperature on the peak strain produced when a magnetic field is applied.

Equipment	Error
EMS MAS 010 Strain Gauge Meter	± 1ppm (80%)
Thermocouple	0.25°C (80%)

Table 6-6 Errors associated with the measurements taken and displayed in Figures 6-16 to 6-18 (see Appendix A).

6.3 Summary of material suitability for new scaler inserts

Based on the measurements made of the candidate materials, Radiometal 4550, Hyperco 50 and grain oriented steel were determined to offer potential advantages over the standard nickel used in dental scaler inserts. Cubex had the lowest magnetostriction of the materials tested. Consequently, it was not carried forward as a replacement magnetostrictive material in further tests. It was noted that the strain output for these materials was not significantly affected by temperatures in the operational range of dental scalers.

However, this analysis only investigated the quasi-static strain vs. applied field performance of these materials. It is clear that other factors; electrical, mechanical and magnetic will influence the dynamic performance of dental scalers that are constructed with these magnetostrictive materials. This will be investigated in Chapter 7.

References for chapter 6

- [6.1] <http://nonferrous.keytometals.com/Articles/Article32.htm>
- [6.2] Bozorth R.M., "Ferromagnetism", 2nd Ed. IEEE Press Reissue, 1993, p. 664-672
- [6.3] Yamamoto Y and Yamashiro Y., "Effect of compressive stress on hysteresis loss and magnetostriction of grain oriented Si-Fe sheets", J. Appl. Phys., Vol 93, No.10, 2003, p. 6683-6685.
- [6.4] Anderson P.I., Moses A.J., Stanbury H.J., "An automated system for the measurement of magnetostriction in electrical steel sheet under applied stress", J. Magnetism and Mag. Mats. 215-216, 2000 p.714-716.
- [6.5] Bozorth R.M., "Ferromagnetism", 2nd Ed. IEEE Press Reissue, 1993, p.672-674
- [6.6] Tomida T. and Uenoya. S., "Cube oriented 3%Si-1%Mn soft magnetic steel sheets with fine grain structure", IEEE Trans. Mag., 37 (4), July 2001, 2318-2320.
- [6.7] Foster K., Seidel J., Shilling J.W., "effect of coating induced stresses on properties of cube textured 3% SiFe sheets", AIP Conf. Proc., J. Magnetism and Mag. Mats. Vol. 10. 1973, p.971-975.
- [6.8] Claeysen.F., et al "Actuators, transducers and motors based on giant magnetostrictive materials", Journal of Alloys and Compounds, Volume 258, Number 0, 1 August 1997 , pp. 61-73(13).
- [6.9] Crawford A.E., "Magnetostriction transducers for ultrasonic power generation", Ferroelectrics, Vol. 228, 1999, p.321-332.
- [6.10] Mason T.J., "Advances in sonochemistry", Vol.5, JAI Press, 1999, p.258-260.
- [6.11] Organ R.M., "Treatment using ultra-sonic vibrations", Studies in Conservation, Vol. 4, No.1. 1959, p.35-38.
- [6.12] Goldman A., "Handbook of modern ferromagnetic materials", Vol. 505, Springer, 1999, p.571.
- [6.13] Nakano M. et al., "New production method of 100-mm-thick grain-oriented 3% silicon steel sheets", J. App. Phys. 81(8), Apr 97, pp4098-4100.
- [6.14] Hart. E., Carpenter Technology (UK) Ltd, mar 06, private communication.
- [6.15] Huyer D.W, Corkum S. H., "Reducing the incidence of tap-water scalds: strategies for physicians", Can Med Assoc J, 15 MARS 1997; 156 (6) 841-844.
- [6.16] Anderson P., " A Universal DC characterization system for hard and soft magnetic materials", J. Mar. and Mag. Mat, in press.
- [6.17] Bartlett. P.A., "Properties and applications of magnetostrictive materials", MSc Thesis, University of Hull, 1997.
- [6.18] Bozorth R.M., Ferromagnetism, 2nd Ed, IEEE Press Re-Issue, 1993, p 659.
- [6.19] Lorenz B.E. and Graham C.D., "High temperature magnetostriction in polycrystalline Fe-Co alloys" IEEE Trans. Mag.,40 (4), July 2004, pp2751-2753.
- [6.20] Bozorth R.M., Ferromagnetism, 2nd Ed, IEEE Press Re-Issue, 1993, p 669.
- [6.21] Yamamoto K. and Yamashiro Y., "Effect of compressive stress on hysteresis loss and magnetostriction of grain oriented Si-Fe sheets", J. Applied Physics, 93(10), May 03, pp6683-6685.
- [6.22] Thomas O.J, et al "Magnetostrictive 1-3 composites with internal field biasing", IEEE Trans. Mag., Vol.40, No.4, 2004.

7 MEASUREMENT OF THE DYNAMIC MAGNOSTRICTION OF DENTAL SCALER STACK MATERIALS

7.1 Introduction

In this chapter, a series of measurements are presented to compare the dynamic performance of samples of the magnetostrictive materials selected from those discussed in chapter 6. The materials that were chosen were those that presented the highest magnetostriction and so represented the most likely candidates for inclusion in a dental scaler insert assembly.

The materials tested were 3% grain oriented silicon steel, Radiometal 4550, Hyperco 50 and standard nickel taken from a dental scaler insert. A laser-vibrometer based measurement system was used to measure the properties of strips of these materials (with the dimensions shown in table 6-1) This size was chosen so that they would be similar to the size of strips that could be obtained by cutting existing nickel-based scaler stacks.

7.2 Single strip measurements

The strips were investigated using a Polytec OFV-303 Single Point Laser Vibrometer head and associated 3001 Controller System (Polytec GmbH, Germany) [7.1]. A low power (<1mW), Helium-Neon (He-Ne) laser with a wavelength of 633nm was used (see fig. 7-1 and 7-2). The other test equipment that was used is shown in table 7-1.

Equipment Item	Purpose/Specification
Feedback FG600 Signal Generator	To supply sinusoidal signal to the LM12-Based Amplifier
2x Kingshill Model 10A05C Power Supplies	To supply ± 25 V to the LM12-Based Amplifier
LM12 Op-Amp Based Amplifier	To supply sinusoidal current to drive coils
Yokogawa DC708E Digital Oscilloscope	To monitor Lock-in Amplifier outputs
Keithley 2001 multimeter	To monitor the current supplied to the Drive Solenoid
Hameg HM 205-3 Oscilloscope	To monitor the supply signal voltage waveform from the LM12-based amplifier
Signal Recovery 7265 DSP Lock-in Amplifier	To monitor voltage output signal from Laser Vibrometer (also measures TTL reference frequency from Feedback FG600 Signal Generator)
Polytec OFV-303 Single Point Laser Vibrometer head and associated 3001 Controller System (5 μ m/V sensitivity, displacement mode)	To measure vibration of the strip caused by magnetostriction
In-house drive solenoid	187 turns (two layers). 100mm long, OD: 24mm, ID 19mm

Table 7-1 Equipment used in the single-strip dynamic strain experiments

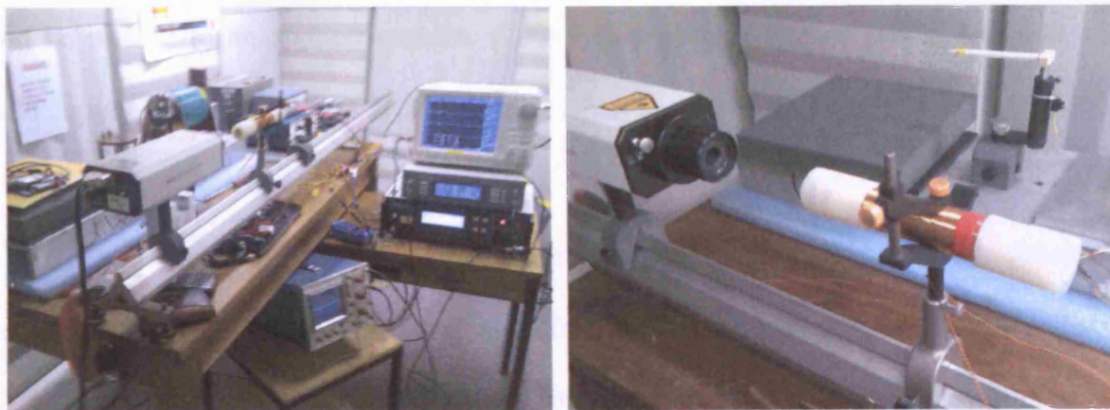


Figure 7-1 Experimental set-up used during the single-strip dynamic strain measurements highlighting the laser head and drive coil

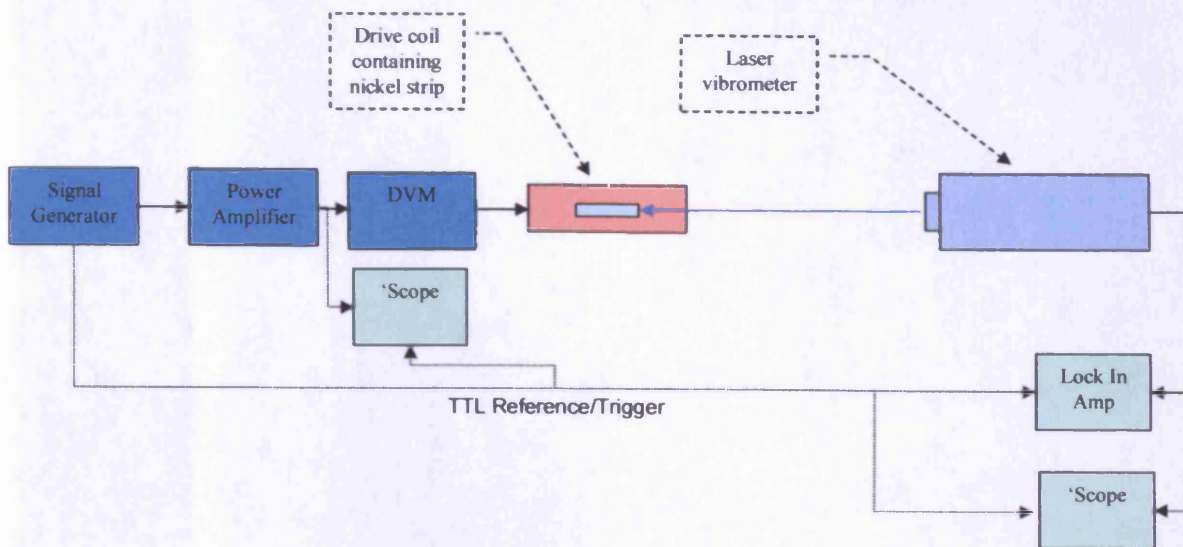


Figure 7-2 Experimental Set-up for dynamic measurements

The drive coil used in these experiments was calibrated [7.2] so that the H-field produced could be related to an applied current. This calibration identified that a 1A peak current would supply a peak H-field of 2674 A/m (± 1 A/m) at the centre of the coil.

In the subsequent measurements, the current applied to the drive coil was maintained at a fixed value (1A peak) so that the applied H-field could be held constant at 2674 A/m peak. This ensured that the increase in impedance of the drive coil with frequency would not result in a reduction of the H-field as the magnetising frequency was increased. However, this resulted in a limit to the maximum H-field that could be applied at the highest measurement frequency (as a result of the inherent limitations of the power amplifier). Consequently, the maximum field that could be achieved at the highest measurement frequency was maintained (by reducing the drive current) as the applied frequency was reduced.

The pre-processor facility of the finite-element modelling package Opera 3d (by Vector Fields) was utilised to create a simple model of the drive coil to further investigate the nature

of the field distribution along its main access (See figure 7-3). To produce this model, the pre-processor automated solenoid generation facility was utilised whereby the dimensional parameters (table 7-1) of the coil are specified and the required applied current was achieved by defining a current density (J) of $7.36 \times 10^5 \text{ A/m}^2$ for the modelled coil. As can be seen in the graph shown in figure 7-2, it displays a maximum predicted RMS H-field for the 187 turn coil of $\sim 1800 \text{ A/m}$. If the peak value is calculated (1.414 times the RMS value) then it is predicted to be 2545 A/m . This compares with the 2674 A/m measured during the calibration process for the real (rather than idealised, modelled) solenoid. In addition, figure 7-1 indicates that the 50 mm long strip sample was located in the most linear portion of the coil's field ($\pm 25 \text{ mm}$ around the centre of the modelled solenoid).

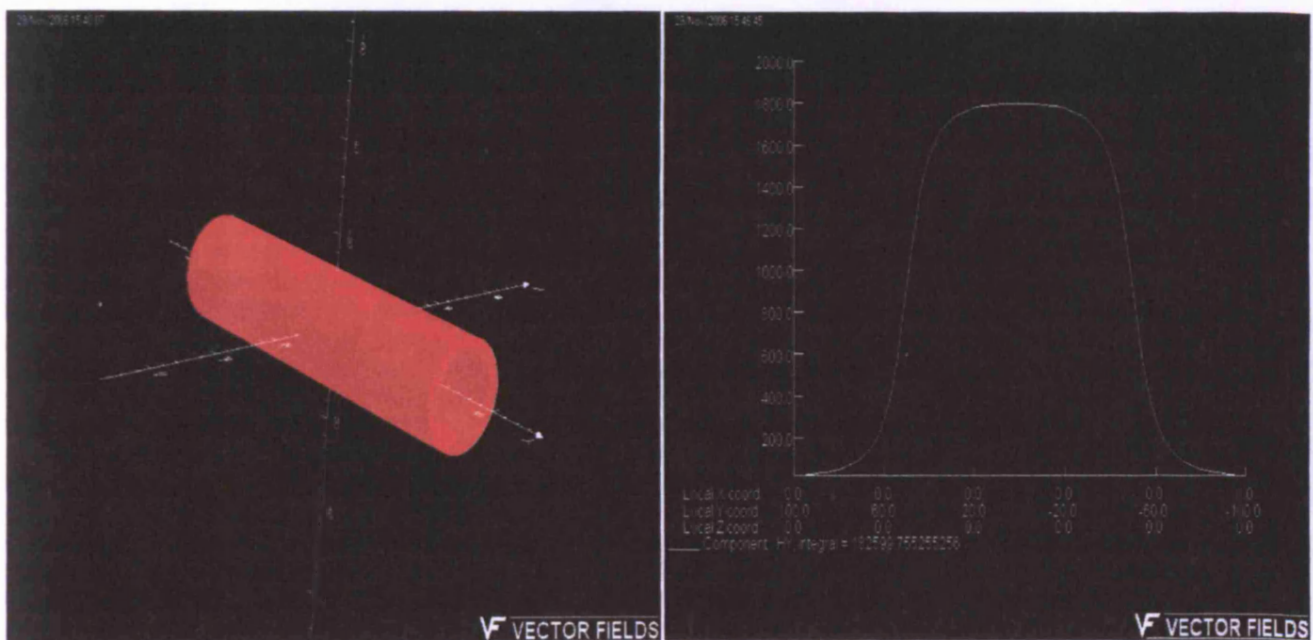


Figure 7-3 Vector Fields Opera 3d model of the 187 turn drive coil and H-field vs Position relative to the centre of the solenoid. X-axis of graph is the distance from coil centre (mm), y-axis is the RMS H-field along the central axis of the coil (A/m).

Single magnetostrictive strip samples were mounted on a semi-circular stage (see figure 7-4). This stage's diameter was only slightly narrower than the 15 mm inner diameter of the drive coil's former so that it was a 'push fit'. It was then possible to locate the centre of the 50 mm sample strip at the centre of the drive coil.

A small reflective target was mounted (with a dab of Araldite) on the end of the strip that would be located closest to the vibrometer so that its laser beam would be incident on it. The other end of the strip was fixed to the sample stage with a ~5 mm x 5 mm drop of Araldite. The sample had a card strap fixed over it so that it was located parallel to the sample stage (see figure 7-4) so that the centre of the sample was coincident with the centre of the drive coil.

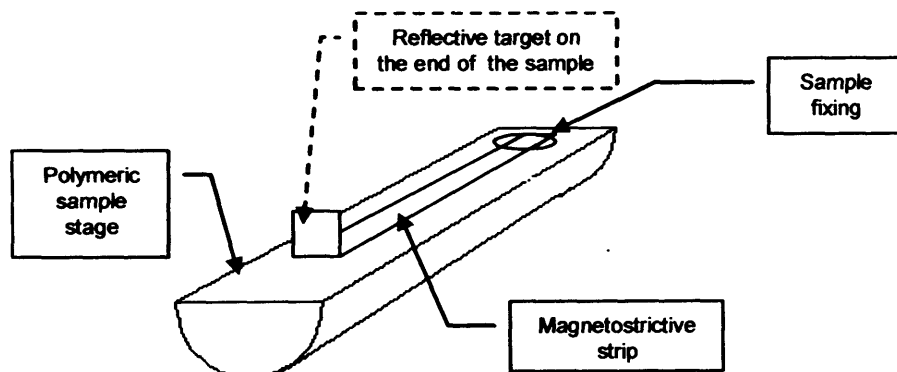


Figure 7-4 Single strip sample stage assembly

The laser vibrometer and drive coil (with the sample stage) were placed on an optical mounting (see figure 7-1) so that it was possible to ensure the components were co-axially located with each other.

By undertaking these experiments, it was possible to compare the dynamic strain outputs of the sample materials.

7.3 Results

The graphs shown in figures 7-5 and 7-6 show the 1st and 2nd harmonic⁴ RMS displacement outputs as measured via the laser vibrometer when a 298 A/m RMS H-field was applied to the strip samples in the range 10 kHz to 30 kHz.

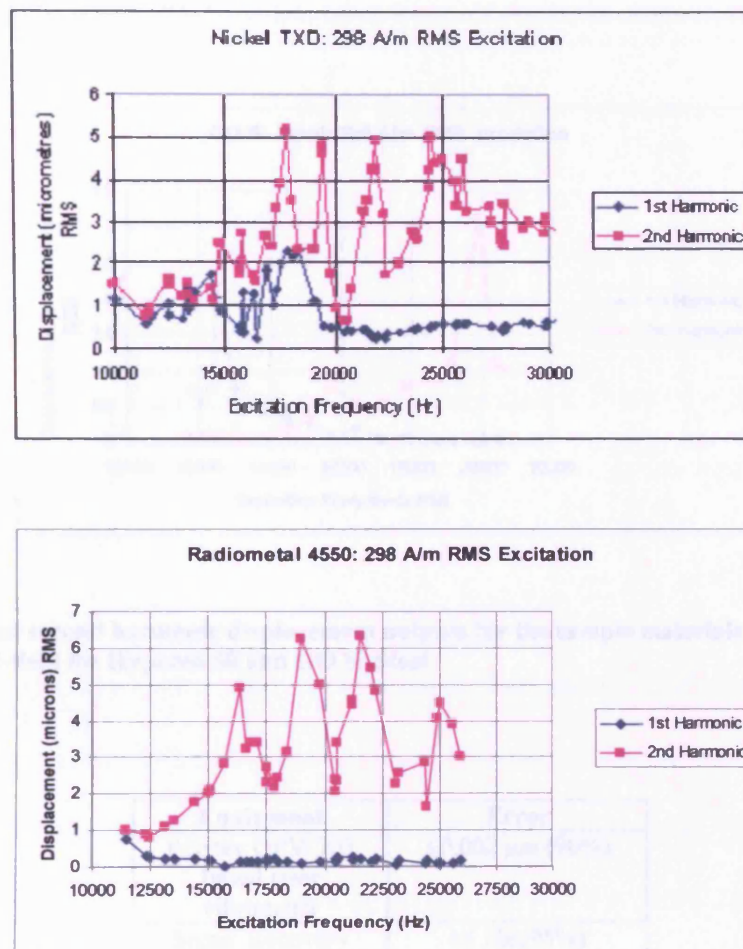


Figure 7-5 First and second harmonic displacement outputs for the sample materials upon application of a 298 A/m RMS H-field for Nickel and Radiometal 4550

⁴ Where the 1st harmonic is the fundamental frequency

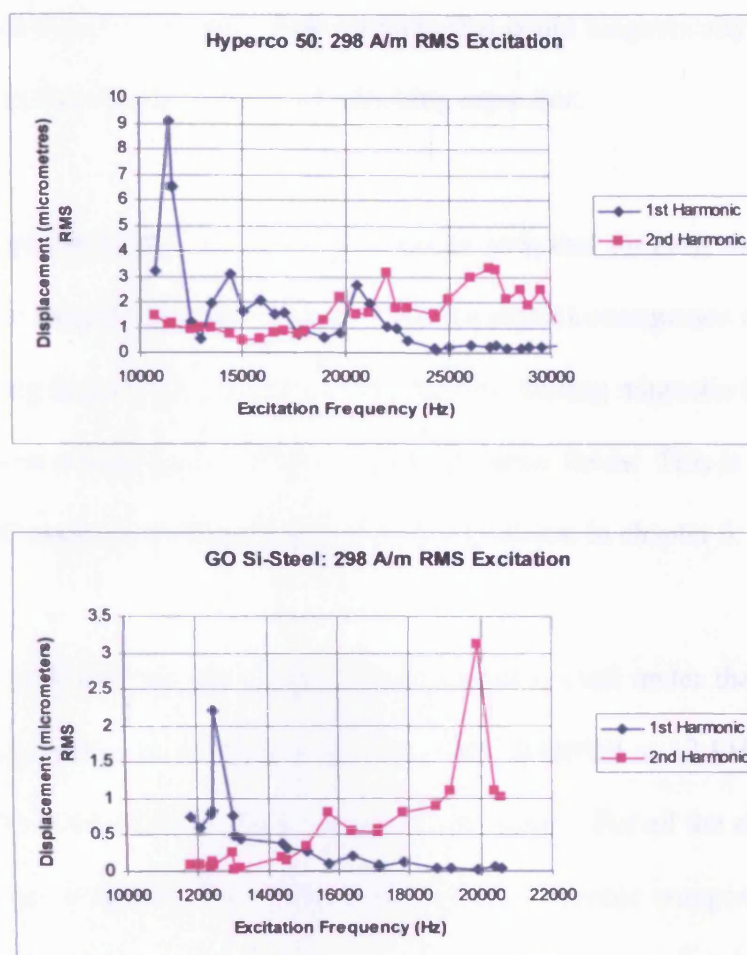


Figure 7-6 First and second harmonic displacement outputs for the sample materials upon application of a 298 A/m RMS H-field for Hyperco 50 and GO Si-Steel

Equipment	Error
Polytec OFV-303 based laser vibrometer	$\pm 0.002 \mu\text{m}$ (90%)
Signal Recovery 7265 DSP Lock-in Amplifier	$\pm 1 \text{ Hz}$ (95%)
Keithley 2001 Multimeter	$\pm 1 \text{ mA}$ (90%) (10 kHz – 50 kHz)

Table 7-2 Errors associated with the measurements taken and displayed in Figure 7-5 (see Appendix A).

The H-field magnitude that was supplied to the sample of 298 A/m RMS was the greatest that could be achieved with this amplifier and for these materials. In some of the materials, the increase in the impedance of the drive coil system limited the maximum frequency that

could be achieved with the sample. Any currents that could magnetically bias the materials were eliminated in these cases with a 1 μ F blocking capacitor.

From the graphs in figures 7-5 and 7-6 it can be seen that for each strip, the majority of the strain is in the second harmonic output. This is a direct consequence of magnetostrictive frequency doubling in a sample that is not exposed to a biasing magnetic field. The GO steel produces the lowest overall strain outputs at these dynamic fields. This is consistent with the low measured DC magnetostrictive strains in this strip shown in chapter 6.

Hyperco 50 produced the next lowest strain output overall under these dynamic fields. However, a 1st harmonic resonant peak of 9 μ m was identified at 12 kHz. The nickel and Radiometal 4550 produced the highest overall strain outputs. For all the strips the magnitude of the 1st harmonic outputs is low relative to the 2nd harmonic components except where possible resonances occur.

It can be noted from these figures that both Radiometal 4550 and nickel from the commercial dental scaler units produced broadly equivalent dynamic strain outputs over the frequency range investigated. The Hyperco 50 and GO steel samples offer lesser dynamic strains. However, for the Hyperco 50, this may be due to the large field requirements to achieve maximum strain (see figure 6-9) compared to nickel or Radiometal 4550 (see figures 6-8 and 6-10). It has been noted [7.3] that the absence of a biasing field can enable the dominance of the second (frequency doubled) strain output component over the first harmonic output. It has also be seen that the strips exhibit a number of displacement peaks when frequency sweeps at a constant drive field were undertaken in the frequency range for

the materials. In addition, the different strips when acting as the core of a solenoid resulted in different impedances in the frequency range.

The influence of eddy current losses is also influencing the performance of these materials with a reduction of 1st harmonic strain with increasing frequency. Using table 7-3, which shows data on typical relative permeabilities and resistivities associated with the candidate materials, it is possible to calculate expected skin depths in the experimental frequency range (see figure 7-6).

Material	Relative Permeability μ_r	Resistivity Ωm
Nickel	600	9.0×10^{-8}
Radiometal 4550	40,000	4.5×10^{-7}
Hyperco 50	3000	4.0×10^{-7}
3% GO Steel	90,000	4.8×10^{-7}

Table 7-3 Relative permeabilities and resistivities for the candidate materials [7.4, 7.5, 7.6, 7.7, 7.8, 7.9]

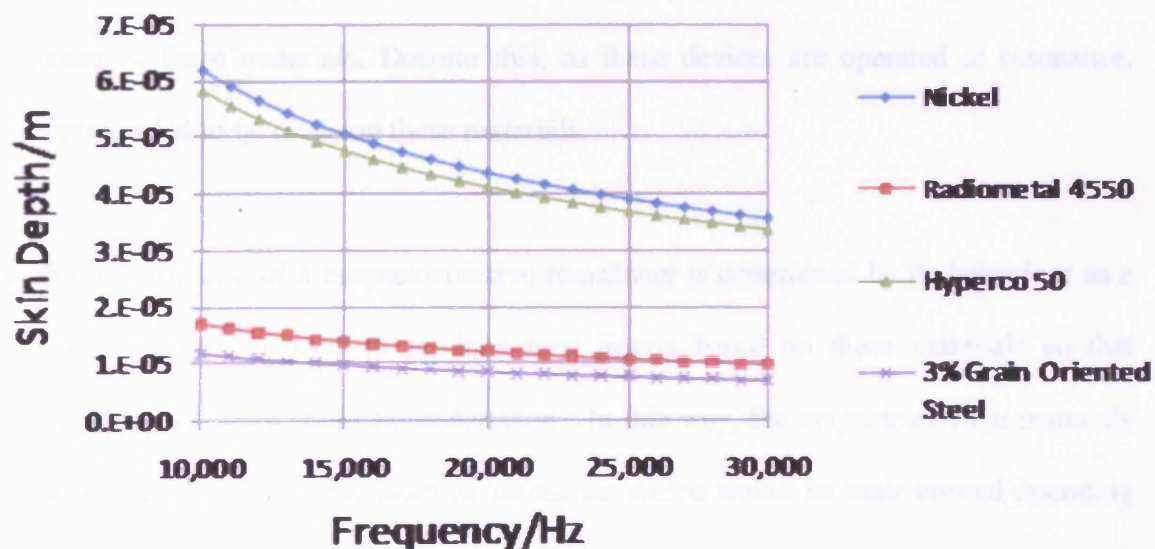


Figure 7-7 Skin depth vs. frequency for the candidate materials based on the data in table 7-3

From figure 7-6, it would seem that although all of the materials have a skin depth that decreases with frequency, nickel and Hyperco 50 start and end with higher values than either Radiometal or the GO steel. However, the drop in skin depth is greater for the former pair than the latter pair. It is possible this is what is being observed in figures 7-5 and 7-6 for the first harmonic displacement outputs. In the cases of nickel and Hyperco 50, the measured displacements seem to reduce less quickly than for those of Radiometal 4550 and the GO steel. It is likely that the reduction of the skin depth with frequency is reducing the internal magnetisation of the strips. Consequently; this is influencing the magnitude of the strain that is produced via magnetostriction across the frequency range.

In conclusion, Hyperco 50 and GO steel may not offer advantages over nickel for dental scalers as they produce lower dynamic strains for the applied drive field in the frequency range. However, Radiometal 4550 may be able to compete with it as a magnetostrictive material replacement, as the strains produced in this analysis were similar to nickel for the applied dynamic fields that were applied but the influence of eddy current effects might restrict the performance of these materials. Despite this, as these devices are operated at resonance, further tests needed to be made on these materials.

As the performance of a magnetostrictive transducer is determined by its behaviour as a whole device, it was decided to produce new inserts based on these materials so that 'transducer oriented' tests could be undertaken. In this way, the magnetostrictive materials would be driving their expected loads at resonance which would be their normal operating conditions.

References for chapter 7

- [7.1] Polytec, Laser Doppler Vibrometer OFV-3001/OFV-3003 User Manual, UK.
- [7.2] Williams P.I., "Solenoid calibration data", private communication, Dec 06.
- [7.3] Bartlett. P.A., "Properties and applications of magnetostrictive materials", MSc Thesis, University of Hull, 1997.
- [7.4] <http://info.ee.surrey.ac.uk/Workshop/advice/coils/mu/>
- [7.5] http://www.kayelaby.npl.co.uk/general_physics/2_6/2_6_6.html
- [7.6] http://www.tpub.com/content/NAVFAC/hdbk419a_vol2/hdbk419a_vol20181.htm
- [7.7] Carpenter Technology Ltd, "Nickel iron alloys" booklet 1999.
- [7.8] Carpenter Technology Ltd, "Cobalt iron alloys" booklet 1999.
- [7.9] Warne D.F., "Newnes electrical power engineer's handbook", 2nd Ed, Elsevier, 2005, p.32

8 THE MANUFACTURE AND TESTING OF INSERTS BASED ON CANDIDATE REPLACEMENT MAGNETOSTRICTIVE MATERIALS

8.1 Introduction

There are a number of issues associated with the design of the magnetostrictive drive for a dental scaler. These can be summarised as:

- What material should be used?
- How will it be designed to guard against frequency-dependent losses?
- What geometry should be used?
- Is the device to be resonant or non-resonant?
- What frequency will it operate at?
- Will the scaler have an insert that comprises both the magnetostrictive material and the tip?
- Will the scaler have a handle that is in effect a magnetostrictive transducer with interchangeable tips?

For commercial nickel-based inserts to be directly replaced with new inserts (with alternative magnetostrictive materials) then any produced would have to be usable with current dental scaler systems. This would mean that any resonances produced in new inserts would have to trigger a resonance 'lock on' in the dental scaler system as described in chapter 5.

8.2 Stack inserts

The current commercial devices have magnetostrictive inserts comprising a stack of nickel laminations soldered at both ends with silver solder [8.1]. One end of the stack is then soldered to one end of the tip.

As a result of the quasi-static and dynamic analyses (described in chapter 6 and 8) of the potential replacement materials, a method to produce new stacks for attachment to tip assemblies needed to be developed and implemented so that new inserts could be tested in current Cavitron dental scaler systems. Consequently, a programme of stack and insert production was undertaken.

8.3 Production of Stacks

Strips of each candidate material used were cut by guillotine to the same length and width (and annealed) as stated in table 6-1. These strips were used to produce magnetostrictive stacks with equivalent overall dimensions as commercial scaler stacks as specified in

table 8-1.

Material	Stack Dimensions (mm)	Laminae Thickness (mm)	No. Laminae
Ni	50 x 5 x 4.0	0.25	16
3% GO Steel	50 x 5 x 4.0	0.31	13
"Hyperco50"	50 x 5 x 4.0	0.36	10
"Radiometal 4550"	50 x 5 x 3.8	0.35	10

Table 8-1 The dimensions and number of strips of the test stacks (NB: the thickness of the Hyperco 50 and Radiometal 4550 samples were measured before an electrically insulating coat of enamel paint was applied to one side of each strip before stack assembly).

8.4 Stack manufacture: Electrical Insulation

It was noted that the nickel stack strips had a highly insulating coating as a result of measurements with a Draper DMM1A multimeter. To measure this resistance, the probes of the multimeter (set to read resistance) were placed on the surface of the sample with a separation of 2mm. The resistance of the coating was such that it was above the 2000k Ω maximum reading capable with the Draper multimeter. The other magnetostrictive materials used in this study were procured without any insulating coating.

It was likely that the plastic grip and O-ring on the commercial inserts were added after the stacks were soldered to the tip assembly. Tip assemblies were required for the new scaler stacks. Consequently, commercial scaler inserts were cut in such a way to provide these assemblies for new stacks. There was a concern that any soldering process could thermally damage the plastic grip/and or O-ring. As a result, methods were sought that could enable stack to tip assembly attachment at low temperatures.

In addition, all but the nickel and grain oriented steel strips lacked any form of electrical insulating coating. This would be needed to minimise the influence of eddy current losses when assembled into stacks. Contact measurements with the Draper multimeter (in the way described above) confirmed this as the resistance in these cases was effectively zero. An enamel spray paint (Humbrol Barbeque and Stove Spray Paint) was obtained that withstand temperatures up to 649°C intermittently and up to 316°C for long periods. The paint was found to produce an insulating coating (above 2000k Ω using the Draper multimeter for contact resistance measurements) thereby electrically isolating the individual stack laminae from each other. Three sprayed layers of paint were applied to one side of every strip.

Restricting the spraying to one side of the strip reduced overall thickness whilst still enabling layers of insulating paint to be present between each pair of strips in physical contact.

8.5 Stack manufacture: Insert binding and soldering

A low temperature ultrasonic dip-soldering technique developed by Solbraz Ltd. (of Erith, Kent) had been identified where the ends of a stack and tip assembly would be dipped in an ultrasonic bath at a low temperature ($\sim 230^{\circ}\text{C}$) filled with a 95% tin 4.5% silver solder [8.2] and then pushed together with the solder re-heated with an additional soldering iron to cause bonding to take place. It was claimed by Solbraz Ltd that the ultrasonic bath would ensure that the solder would flow over the stack and tip assembly ends without the need for additional flux [8.2].

To identify whether it would be possible to connect tip assemblies to stacks via this method, a series of stacks (one for each candidate material) were produced (as specified in table 8.1) that were bound tightly together with copper wire (see figure 8-1) and were supplied to Solbraz Ltd with an equal number of tip assemblies. As there was a need to solder the stacks at both ends, the outer most strips had 5mm of insulation removed with a hand-held, electric grinding wheel so that bare metal was exposed for solder bonding. This ensured that no dirt or oil was present on these surfaces. However, initial trials by Solbraz Ltd. showed that their ultrasonic soldering techniques would not be suitable for fixing scaler stacks to assemblies as the soldered joints were not strong enough to maintain the bond between the individual components. Despite this, the method of binding stacks with copper wire, prior to attachment to tip assemblies, was adopted for all subsequent insert production techniques.

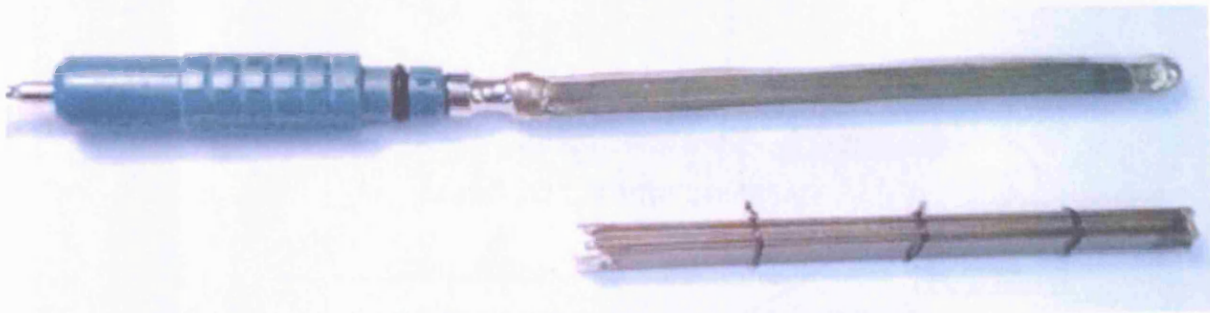


Figure 8-1 Standard commercially produced Dentsply dental scaler insert compared to a stack assembly bound by copper wire prior to soldering to a tip assembly.

As a result of the failure of the Solbraz Ltd soldering technique, a purely mechanical fixing mechanism was devised. This comprised two non-magnetic brass ferrules that were used both to bind one end of a stack together and to enable the attachment of the stack to the tip assembly. Both ferrules were designed to be 'push fit' but Araldite adhesive was also used to aid firm attachment. A rotary grinding wheel was then used to reduce the thickness of the ferrule walls so that the insert could be inserted in a commercial Dentsply drive coil (see figure 8-2). Two inserts were produced with each material stack types using this technique.

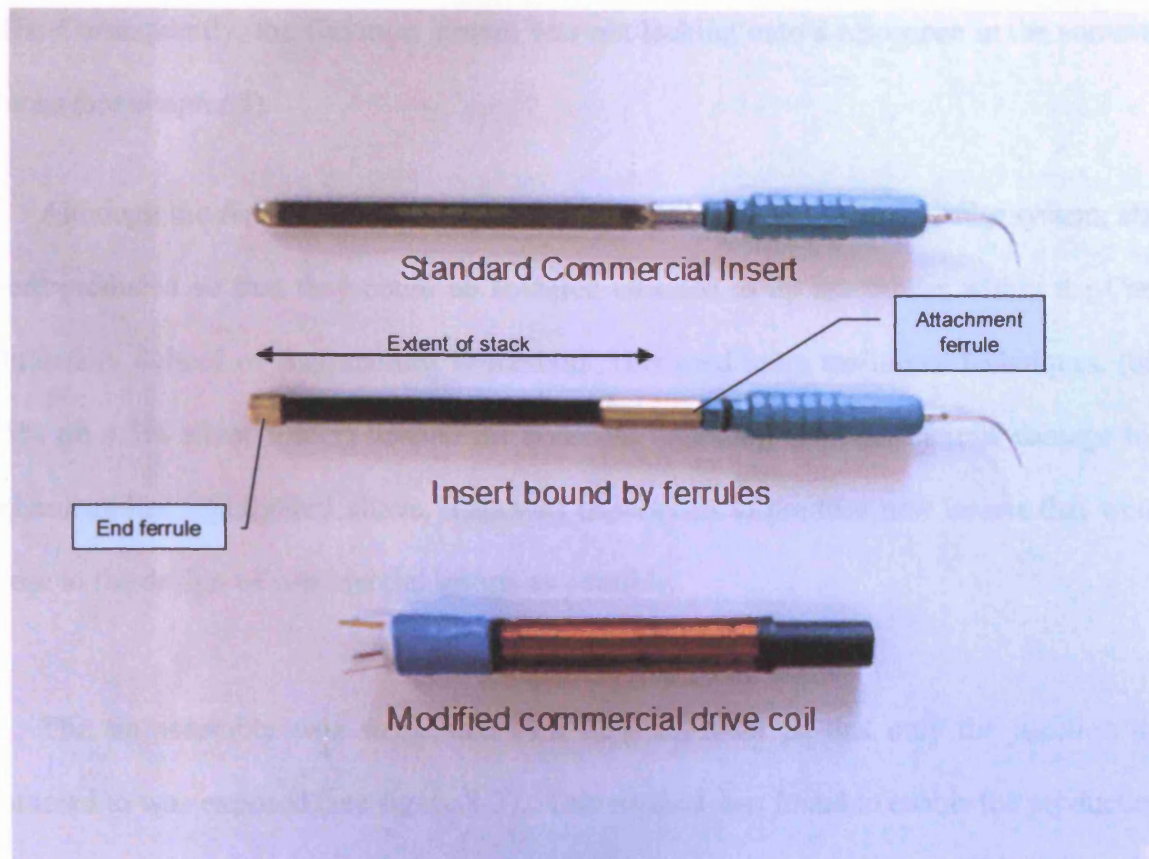


Figure 8-2 Image comparing the standard commercial scaler insert to one using ferrules to both bind the stack together at one end and attach it to the tip assembly.

To confirm that the additional mechanical components did not impede the operation of the dental scaler inserts, a commercial nickel insert had its tip assembly and stack separated and then re-attached using a brass ferrule. It was found in initial tests that when this modified insert was used with a Cavitron power supply system, the insert resonated so that the tip could be used to abrade a surface in the same way as a commercial insert. If the new inserts were to be used to replace current dental scaler inserts, it was clear that they would have to be interchangeable with current commercial inserts. Although the ferrule-modified commercial insert worked in the Cavitron system, the other alternative inserts, made from different magnetostrictive materials, did not produce tip resonances in their stacks. It was noted that the frequency of the current supplied to the drive coil was at 40 kHz rather than settling at 30

kHz. Consequently, the Cavitron system was not locking onto a resonance in the non-nickel stacks (see chapter 5).

Although the ferrule modified nickel inserts worked in the Cavitron scaler system, stacks were produced so that they could be soldered attached to tip assemblies within the Cardiff University School of Engineering Workshop. This used more traditional techniques, (using 95% tin 4.5% silver solder) despite the concerns regarding potential thermal damage to the tip assemblies highlighted above. This was undertaken to produce new inserts that were as close to the design of commercial inserts as possible.

The tip assembly was suspended in a flask of water so that only the junction to be be soldered to was exposed (see figure 8-3). This method was found to enable the production of inserts that had little or no damage to the plastic components of the tip assembly (the O-ring being removed during the procedure).

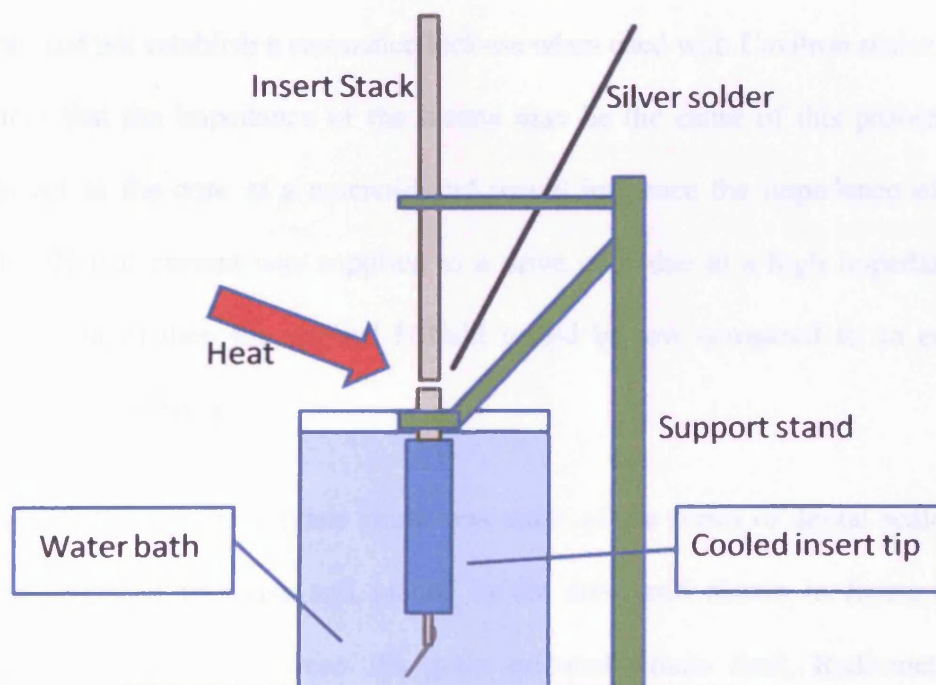


Figure 8-3 Soldering of commercial insert tip assemblies to new insert stacks using a water bath to protect plastic components from thermal damage during heating.

Two inserts were produced for each magnetostrictive material type using this technique. However, as with the ferrule based inserts, only the nickel inserts triggered a resonance lock-on when used in the commercial Cavitron system. As a result, the insert manufacturing method was not considered to be the cause of the lack of Cavitron resonance lock-on when the non-nickel based stack inserts were used with this system.

8.6 Stack manufacture: Impedance measurement and compensation

There was clearly an outstanding issue with the new inserts that would have to be resolved if they were to be used as replacements for current ones. The quasi-static and dynamic magnetostriction measurements indicated that the selected materials should produce equivalent strains to that produced by commercial nickel-based inserts but the newly produced ones did not establish a resonance lock-on when used with Cavitron scaler systems. It was possible that the impedance of the inserts may be the cause of this problem as the stacks would act as the core of a solenoid and would influence the impedance of the coil system. If insufficient current was supplied to a drive coil (due to a high impedance for a given applied voltage) then the applied H-field would be low compared to an equivalent system with a low impedance.

To investigate this, an impedance study was made of the series of dental scaler inserts that had been produced in-house and placed in the drive coil shown in figure 8-3. The materials tested in stack form were 3% grain oriented silicon steel, Radiometal 4550, Hyperco 50. These were compared to a standard nickel-based insert. The geometries of the individual stacks, the lamination thicknesses and number of strips in each stack were shown

in table 8-1. The stacks were attached to tip assemblies using the water-bath soldering method shown in fig.8.2.

The series resistance and reactance of the dental scaler drive coil (see table 5-3 for full details) where the stacks defined in table 8-1 comprised the magnetostrictive cores were obtained using an Agilent 4284A LCR meter over a frequency range of 10 to 50 kHz for each assembly (see fig. 8-4 and 8-5). The measured reactance shown in figure 8-4 was found to be inductive in nature, as would be expected for a solenoid-based transducer system.

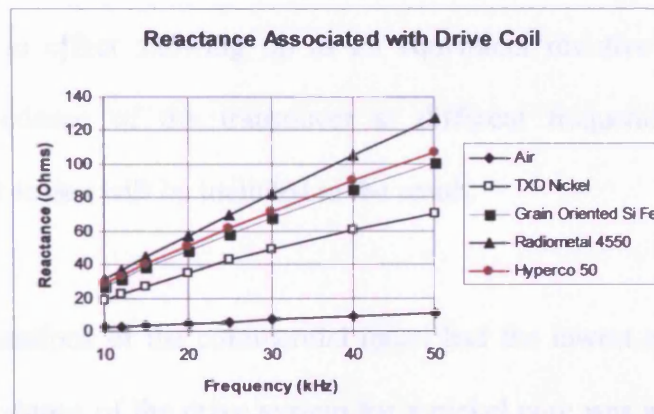


Figure 8-4 The reactance of the Dentsply drive-coil system when fitted with inserts of different magnetostrictive stack materials (and air cored). NB: Txd Nickel = standard Dentsply insert material.

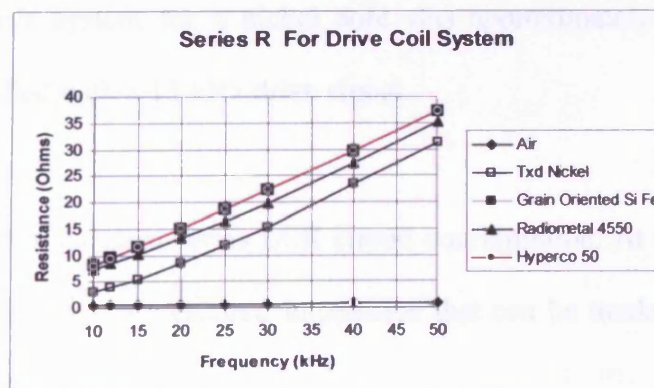


Figure 8-5 The apparent series resistance of the Dentsply drive-coil system when fitted with inserts of different magnetostrictive stack materials (and air cored). NB: Txd Nickel = standard Dentsply insert material.

Equipment	Error
Agilent 4284A LCR Meter	f: $\pm 1\%$ (90%) Reactance/Resistance $\pm 0.1 \Omega$ (90%)

Table 8-2 Errors associated with the measurements taken and displayed in Figures 8-4 and 8-5 (see Appendix A).

The impedance measured in these experiments encapsulates many of the real and imaginary loss mechanisms associated with the transducer under the specific excitation conditions (see Eq. 4.18). However, Eq. 4.18 does not predict an increase in series resistance with frequency. This is due to frequency dependent losses such as eddy currents in the core material and the skin effect showing up as an equivalent resistive loss (Eq. 4.65). By measuring the impedance of the transducer at different frequencies, the influence of frequency dependent losses will be included in the result.

The nickel laminations of the commercial insert had the lowest resistance at any given frequency. The resistance of the drive system for a nickel core was approximately half that of the other materials when supplied with a 15 kHz drive signal. This was repeated in the reactive component of the system impedances for the various core materials. In this case the reactance of the drive system for a nickel core was approximately 3/4 that of the other materials when supplied with a 15 kHz drive signal.

Figure 8-6 shows a standard series LCR circuit configuration. At a given frequency, the transducer system will have a measured impedance that can be modelled by the equivalent circuit components shown [8.6].

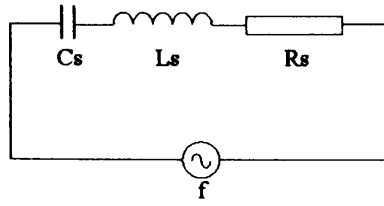


Figure 8-6 Series LCR equivalent circuit of a drive coil and insert assembly.

The standard dental scaler drive-coil/insert assembly has a small series capacitance compared to the inductance of the solenoid. However, if this series capacitance (C_s) is increased to an appropriate value, at the mechanical resonant frequency, then the reactance contribution as a result of the inductor would be compensated for leaving only the purely resistive loss component at this frequency (Eq. 4.65). A Muirhead decade capacitor type B-21-F was used in series with the drive coil to achieve this. Consequently, the reactive ‘imaginary’ component of the impedance is eliminated so that only the ‘real’ resistive impedance contributions remain.

This can be expressed mathematically at the mechanical resonant frequency as;

$$Z = \sqrt{R_s^2 + \left(\omega L_s - \frac{1}{\omega C_s} \right)^2} \quad (8.1)$$

where the total impedance of the transducer system) will equal R_s if

$$\omega L_s = \frac{1}{\omega C_s} \quad (8.2)$$

where R_s is the real component and $j\omega L_s$ is the imaginary component of Eq. 4.65.

In the case of standard dental scalers, this frequency would be ~ 15 kHz or ~ 30 kHz to achieve the desired ~ 30 kHz mechanical resonance. In the former case, this as a result of the magnetostrictive frequency-doubling associated with a stack that does not have any magnetic biasing. In the latter it is due to stimulation of the resonance when a magnetic bias is present.

To obtain the desired value of the additional series capacitance to satisfy Eq. 8.2 at 15kHz, the Muirhead capacitance bank was connected in series with the drive coil with inserts of different magnetostrictive materials acting as the cores. The Agilent 4284A LCR meter was then used to identify when Eq. 8.2 was satisfied at 15kHz with a supply voltage of 2V rms (26 A/m rms). This condition was achieved by changing the capacitance bank value until the measured reactance was a minimum at this drive frequency. This experiment was also conducted with a 30kHz excitation (24 A/m rms). The results are shown in table 8-3 and 8-4 where in each, the initial impedance (before the capacitance bank is connected) can be compared to when the capacitance bank has been set at a value to reduce the measured phase to zero. When the phase measurement of the series circuit is zero, there is only a real impedance component present and the reactive components are equal and opposite in magnitude and phase. Consequently, the impedance of the transducer, at the mechanical resonant frequency is minimised.

Material	Initial Impedance (Ohms)	Initial Phase (degrees)
Nickel	25.97	78.21
Radiometal 4550	40.50	76.10
Hyperco50	38.10	74.10
GO Silicon Steel	36.50	72.90

Material	Lowest Impedance (Ohms)	Capacitance Bank Setting (μF)
Nickel	5.68	0.417
Radiometal 4550	9.74	0.271
Hyperco50	10.48	0.290
GO Silicon Steel	10.93	0.304

Table 8-3 Impedance of the drive-coil with the different core materials with an excitation frequency of 15 kHz. It shows the capacitance bank setting that was required to compensate for the inductive component of the transducer's impedance thereby reducing the impedance from its initial to its lowest value.

Material	Initial Impedance (Ohms)	Initial Phase (degrees)
Nickel	49.80	71.80
Radiometal 4550	75.40	76.00
Hyperco50	69.30	73.20
GO Silicon Steel	66.37	71.85

Material	Lowest Impedance (Ohms)	Capacitance Bank Setting (μF)
Nickel	14.39	0.115
Radiometal 4550	18.38	0.073
Hyperco50	20.30	0.080
GO Silicon Steel	21.40	0.085

Table 8-4 Impedance of the drive-coil with the different core materials with an excitation frequency of 30 kHz. It shows the capacitance bank setting that was required to compensate for the inductive component of the transducer's impedance thereby reducing the impedance from its initial to its lowest value.

Equipment	Error
Agilent 4284A LCR Meter	f: $\pm 1\%$ (90%) Reactance/Resistance $\pm 0.1 \Omega$ (90%) Phase $\pm 0.01^\circ$
Capacitance Bank	$\pm 0.001 \mu\text{F}$

Table 8-5 Errors associated with the measurements taken and displayed in Figures 8-4 to 8-5 (see Appendix A).

Tables 8-3 and 8-4 show that the material used in a magnetostrictive dental scaler stack can have an influence on the dental scaler system's impedance but this can be compensated for. It can be seen that the current nickel-based stacks offer lower impedance than the other materials used in the study. In addition, the operating frequency of the dental scaler will also influence the impedance of the dental scaler with higher impedances at higher frequencies (as would be expected due to such factors as eddy current losses). The use of an air core in these experiments shows the contribution of increasing losses in the coil system itself as a result of increasing excitation frequency. However, tables 8-4 and 8-5 show that it is possible to significantly reduce the impedance of the system by introducing a capacitor whose value creates resonant LCR electrical circuit at the required excitation frequency. This would be a design feature of the next generation of dental scaler systems if a series capacitance is included to compensate for reactive losses (due to both the electrical and mechanical components of the transducer). The impedances achieved via this compensated method for all the materials are also below that which is found for the uncompensated nickel-based scaler system when excited by a 15 kHz or 30 kHz drive signal.

In conclusion, this study has shown the potential advantages and disadvantages of using alternative magnetostrictive stack materials than standard nickel in traditional dental scaler insert designs. At the expected drive frequencies (of 15 or 30 kHz), nickel offers the lowest impedance stacks at the expected repetition of this term drive frequencies, when compared to the other materials measured in the study. However, the work also demonstrated that it is possible to minimise impedance losses by creating a tuned electrical circuit that enables reactive loss compensation at the transducer system's resonant frequency.

Consequently, the use of capacitance compensation can greatly decrease the losses associated with a resonant magnetostrictive dental scaler transducer. This means that such devices can be caused to resonate with lower input power requirements. This is a considerable step forward in dental scaler system design.

Also it suggested that part of the reason that the new dental scaler inserts did not seem to produce expected vibrations at their resonant frequencies, during initial testing, was because of the large impedances of the non-nickel dental scaler stacks in the frequency range from ~15 kHz to ~30 kHz. However, with capacitive compensation, all of the transducers (with different magnetostrictive inserts acting as cores) can be tuned to have an impedance that is lower than that possessed by the original nickel-based dental scaler system.

With the series capacitance compensation for the reactive components of the dental scaler system in place, Eq. 4.65 becomes;

$$Z_{ee} = R_{DC} + \omega \left(\frac{N^2 \mu^T A \chi_L}{l_s} - \frac{N^2 d_{33}^2 A \chi_L}{l_s s_H} + \frac{N^2 d_{33}^2 A k_m^H \chi_R}{2\xi(k_L + k_m^H) l_s s_H} \right) \quad (8.1)$$

The experimental method in this section has identified the minimum impedances that can be achieved with this range of dental inserts and offers a means by which C_s (the compensation capacitance) can be identified for any resonant magnetostrictive transducer. It is clear that the frequency dependent components the second term of Eq. 8.1 will be influenced by mechanical, magnetic and magnetostrictive variables for a particular transducer with a specific magnetostrictive material. Also, if required, the values for such as μ^T , χ and d_{33} will need to be obtained for the specific transducer concerned (and at the frequency of

operation) if the individual contributions of the components of the second term are to be determined [8.7, 8.8, 8.9] assuming that the purely mechanical variable components are constant with frequency.

References for Chapter 8

- [8.1] Griffiths. A., Cardiff University Engineering Dept. Workshop, Private Communication, 2007.
- [8.2] Plummer. B. Solbraze Ltd. Erith, Kent, Private Communication, 2007.
- [8.3] Butler. J.L., “Highly active magnetostrictive transducers”, Image Acoustics Ltd, Oct 1986.
- [8.4] Duffin W.J., “Electricity and magnetism”, 3rd Ed, McGraw-Hill, London, 1980, 277-279.
- [8.5] Engdahl. G., “Handbook of giant magnetostrictive materials”, Academic Press, San Diego, 2000.
- [8.6] Duffin W.J., “Electricity and magnetism”, 3rd Ed, McGraw-Hill, London, 1980, 243-245.
- [8.7] Sarawate N.N. and Dapino M.J., “A dynamic actuation model for magnetostrictive materials”, Smart Mater. Struct. 17 (2008) 065013 (4pp)
- [8.8] Millership R. and Webster F.V., “High frequency permeability of ferromagnetic materials”, Proc. Phys. Soc. B 63 (1950)783-795.
- [8.9] Calkins F.T. et al., “Effect of prestress on the dynamic performance of a Terfenol-D transducer”, Proc. SPIE Vol. 3041, p. 293-304, Smart Structures and Materials 1997: Smart Structures and Integrated Systems, Marc E. Regelbrugge; Ed.

9 THE MODELLING OF MAGNETOSTRICTIVE INSERTS TO IDENTIFY THEIR RESONANCES AND VIBRATION MODES

9.1 *Introduction*

Finite element models can be used to simulate behaviours of complex systems. These systems are subdivided into interconnected elements that represent sections of the material. For example; as mechanical stress is applied to a material, sections within it react in such a way so that they influence the reaction of their adjacent sections. The finite element model simulates this behaviour by solving differential equations for each of the elements that represents a section in the material [9.1].

Triangular and rectangular elements may be selected for 2 dimensional (2D) modelling and tetrahedral elements for 3 dimensional (3D) modelling. The Finite Element Modelling (FEM) system FEMLAB 3.1 by COMSOL Ltd. was used in this project to investigate the mechanical resonances associated with dental scaler inserts in 3D models.

This is beyond the capabilities of simple models of dental scalers based purely on simplistic mathematical representations. In addition, it is possible to investigate the nature of any resonances that are identified so that flexural, torsional or other mode-shapes can be identified.

9.2 FEMLAB 3.1

FEMLAB is an interactive environment for modelling and solving scientific and engineering problems based on partial differential equations (PDEs) [9.2]. By using the built-in physics modules it was possible to build models by defining the material properties, loads and constraints, rather than by defining the underlying equations. FEMLAB internally compiles a set of PDEs representing the entire model. When solving the PDEs, FEMLAB uses finite element analysis together with adaptive meshing and error control using a variety of numerical solvers. By using the Structural Mechanics module, it was possible to define the physics in sub-domains and on boundaries, edges and points along with pre-defined PDEs. A set of application-dependent variables made it possible to visualise and post-process physical quantities (such as the resonant mode shape).

By modelling dental scaler inserts with different stack materials using the Structural Mechanics Module, it was possible to produce models that could be used to identify and analyse specific mechanical resonances and the associated Eigenfrequency vibration modes.

9.3 FEMLAB 3.1 modelling basics

INTRODUCTION

The basic flow of actions when producing and analysing a model is undertaken via a series of toolbar buttons and menus. The following sections correspond to each major step in the modelling process. These roughly correspond to the different modes and menus in FEMLAB 3.1 [9.2].

MODEL NAVIGATOR

The *Model Navigator* enables the user to start a new model by selecting application modes and specifying variable names and other model properties (see figure 9-1).

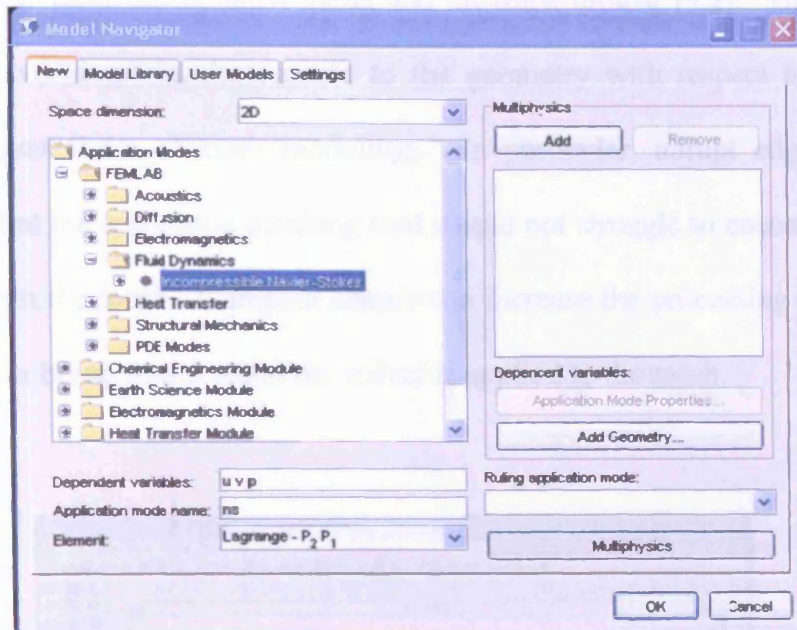


Figure 9-1 FEMLAB Model Navigator window [9.2]

OPTIONS AND SETTINGS

This facility covers basic settings, for example, the axis or grid spacing settings. These were made with commands from the *Options* menu or by double-clicking on the status bar so that the grid size would be of the order of millimetres for the insert model (see figure 9.2). A *Constants* dialog box is used to enter model parameters [9.2].

GEOMETRY MODELING

Using the Geometry Modelling system it was possible to create the model geometry using the CAD tools on the draw menu and the draw toolbar [9.2]. The dental scaler model needed to have simplifications made to the geometry with respect to the 'real' object to enable efficient finite element modelling. In particular, abrupt edges and corners were avoided so that the automatic meshing tool would not struggle to encompass these geometric features within the mesh. Complex shapes can increase the processing time and may prevent solutions from being found when the solver is applied to the mesh.

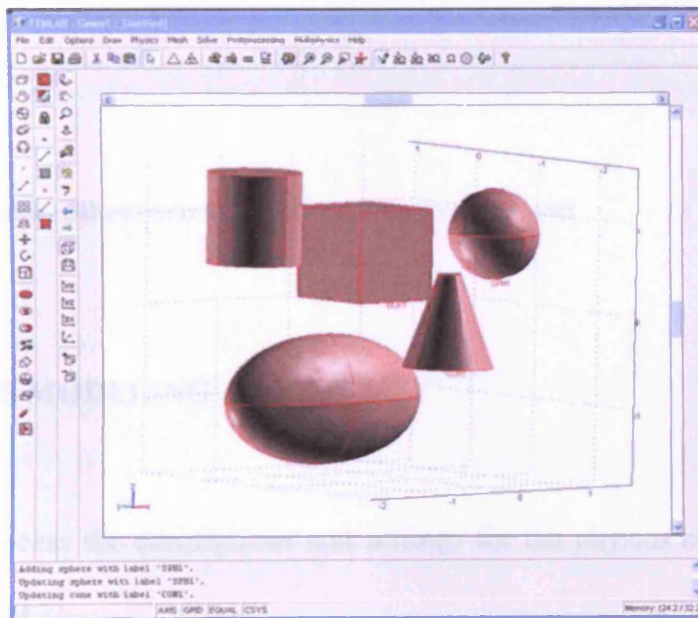


Figure 9-2 FEMLAB Geometry modelling in the FEMLAB main window. All FEMLAB features can be accessed from this window. [9.2]

Once the geometric model has been produced (see figure 9-3), the appropriate physical attributes (such as Young's modulus and density) can be applied to the sub-components of the model.

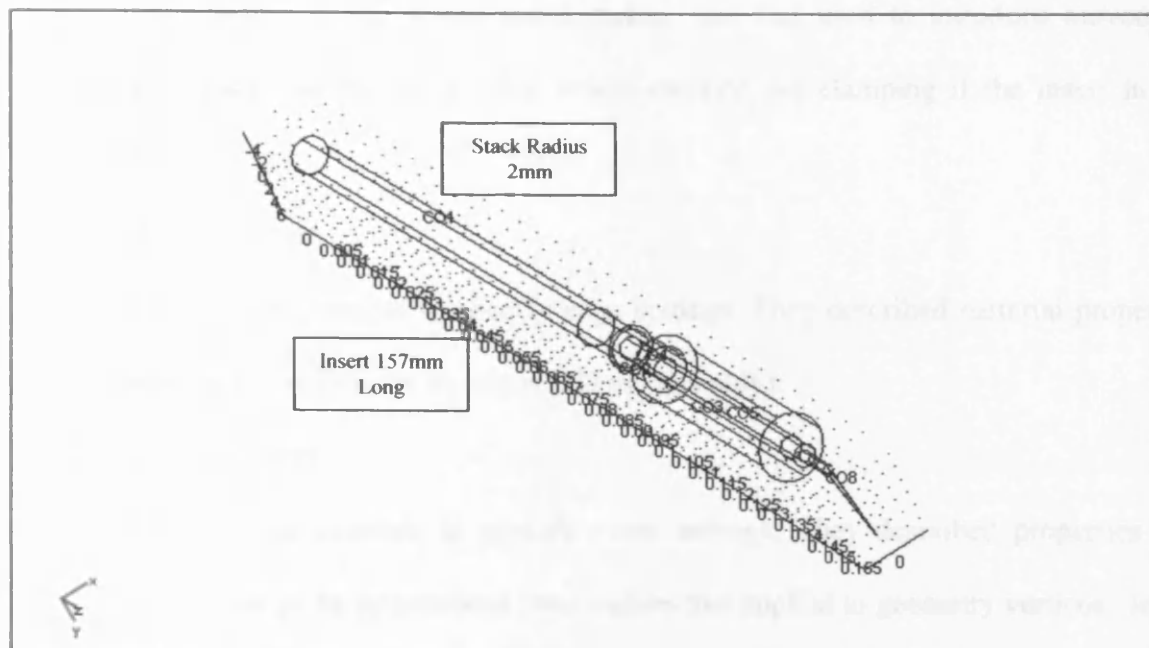


Figure 9-3 Example 3D geometric Model of a dental scaler insert

PHYSICS MODELING

In this process the descriptions and settings for the physics and equations in the model are described [9.2]:

Subdomain Settings

In this section the subdomain settings were set. They described the material properties, sources, and PDE coefficients on the subdomains. On the subdomains it is also possible to specify initial condition and element types:

i. *Boundary Conditions*

Here FEMLAB enabled the specification of any boundary and interface conditions. In the scalar insert model, this was used to introduce movement constraints on the model that would emulate the clamping of the insert in the handle.

ii. *Edge Settings*

Here it was possible to specify edge settings. They described material properties and PDE coefficients on edges (3D models only).

iii. *Point Settings*

Here it was possible to specify point settings. They described properties and values for point sources and other values that applied to geometry vertices. In the scalar mode, this was used to apply a force to the model at a specific point.

MESH GENERATION

Using the mesh generation tool enabled the finite element mesh (see figure 9-4) for the model geometry to be generated. This was achieved by simply clicking the mesh buttons on the main toolbar to create and refine such a mesh [9.2].

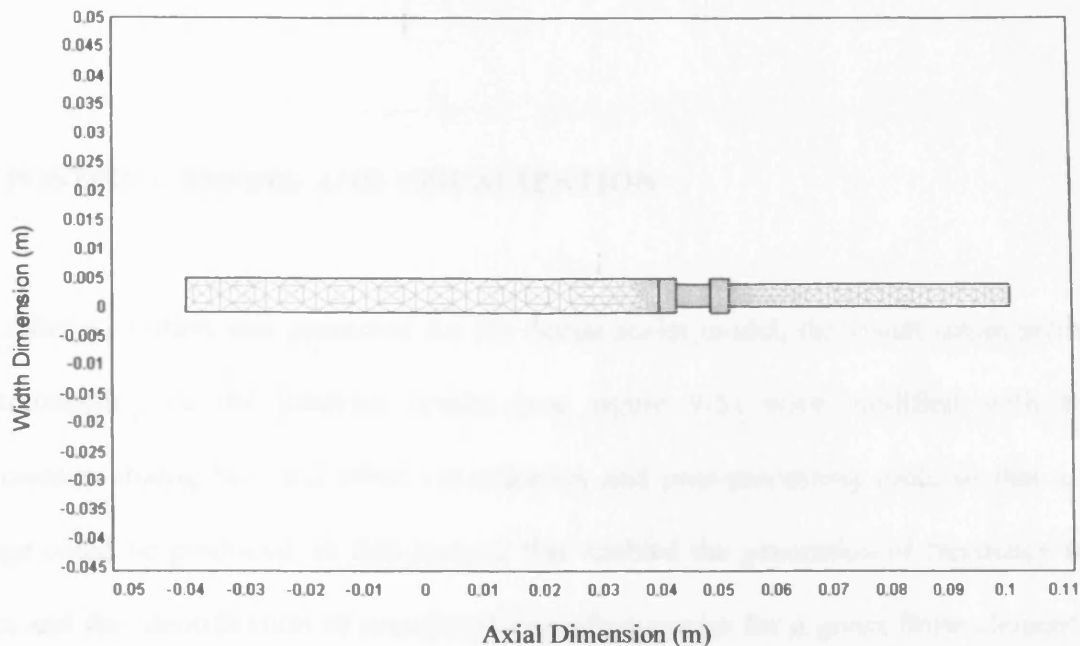


Figure 9-4 Example of a meshed 2d simplified dental scaler insert model to show the mesh produced by the meshing routine. It can be seen that in the region of change from one element to another, the mesh element size is reduced.

COMPUTING THE SOLUTION

In this project the ‘Eigenfrequency’ solver was used to solve for the undamped natural frequencies and vibration modes of a structure and the ‘Frequency Response’ solver (a harmonic analysis tool) was used to solve for the steady-state response from a harmonic excitation. Typically, for the ‘Frequency Response’ analysis a frequency sweep was performed, solving for many excitation frequencies sequentially. These were utilised within the Structural Mechanics modules to investigate the performance of dental scaler related finite element models.

POSTPROCESSING AND VISUALIZATION

After a solution was generated for the dental scaler model, the visualization settings and postprocessing of the analysis results (see figure 9-5) were modified with the *Plot Parameters* dialog box and other visualization and post-processing tools so that a desired image could be produced. In this project, this enabled the generation of frequency response plots and the identification of associated Eigenfrequencies for a given finite element model. In these particular models, *only* the mode shapes and Eigenfrequency values are identified.

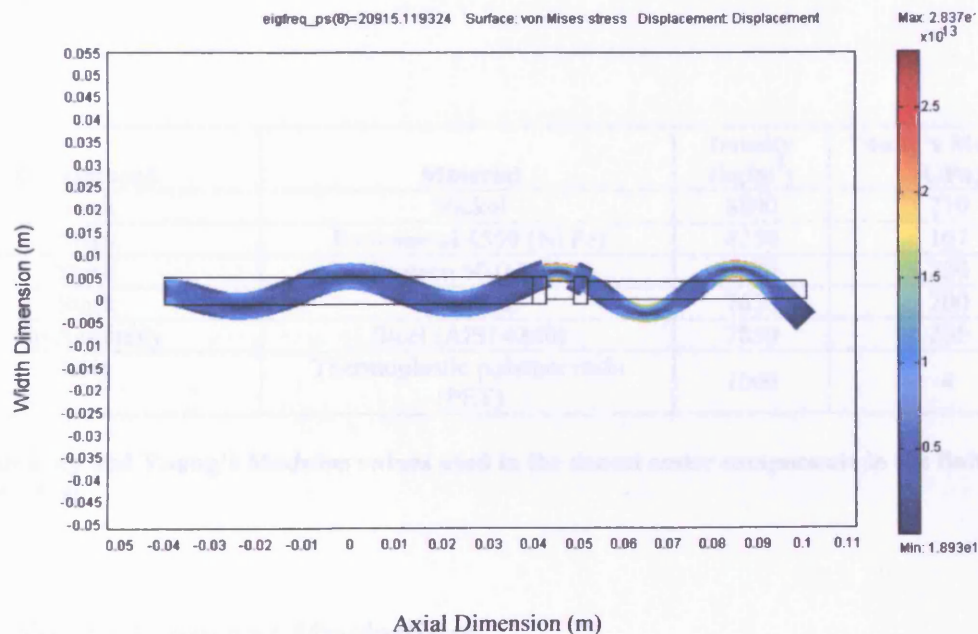


Figure 9-5 Example of a 2d simplified dental scaler insert model showing a specific visualised mechanical Eigenfrequency after the Structural Mechanics finite element model has been solved (20.92 kHz flexural mode Eigenfrequency identified).

9.4 3d Structural Mechanics Module Finite Element Models

As the dental scaler insert possessed a tip that could produce vibrations in more than a plane, 3D models were developed so that the resonances associated with them could be investigated beyond the more simplistic analyses that can be undertaken with basic mathematical relationships for identifying resonant frequencies (such as Eq. 5.1)

To do this, dental scaler insert finite element models were produced that comprised a number of material components. Assumptions were made regarding the materials that were used to make the whole insert (see table 9-1). The properties were selected to enable a comparison of the different dental scaler designs via the FEMLAB finite element modelling system.

Component	Material	Density (kg/m ³)	Young's Modulus (GPa)
Stack	Nickel	8800	210
Stack	Radiometal 4550 (Ni Fe)	8250	167
Stack	Hyperco 50 (Co Fe)	8150	230
Stack	GO Steel	7650	200
Tip Assembly	Steel (AISI 4340)	7850	205
Grip	Thermoplastic polymer resin (PET)	1000	4

Table 9-1 Density and Young's Modulus values used in the dental scaler components in the finite element models [9.4 – 9.9]

9.5 3D Finite Element Modelling

In these models, it was not possible to produce a magnetostrictively developed force and strain as this would have required a more advanced coupled multi-physics model which is not available. Consequently, the analysis undertaken was used purely to identify the Eigenfrequencies that would be produced upon application of an external force. This meant

that the displacements thus produced would not reflect the magnitudes that could be achieved by magnetostrictive action. However, by applying the same force for each model, it would be possible to compare the resonances and associated Eigenfrequencies when the stack material was changed from model to model. By comparing the resonant frequencies and modes of inserts made with different magnetostrictive materials, it would be possible to identify whether they were at the same frequency and have the same mode-shapes.

The Poisson's ratio for each of the materials was set in the model to 0.33 except for the steel (AISI 4340) which was set in the FEMLAB material library at 0.28. The value of 0.33 was considered to be a reasonable approximation of the Poisson's ration for these materials [9.10, 9.11].

To show the resonances in the FEMLAB models, the mass damping factor (see Appendix C) was set to 1×10^{-10} and the stiffness damping factor to 1×10^{-10} based on equivalent models presented in the guidance documentation and through discussion with COMSOL representatives [9.11]. These low values were selected so that the resonant frequencies could be observed and compared without significant damping and were not expected to represent the properties of actual materials. This is acceptable if only the resonant frequencies are to be identified for comparison purposes.

The FEMLAB Solver Settings for the frequency response and Eigenfrequency analyses are shown in table 9-2.

FEMLAB Solver settings (a)	
Analysis type	Freq
Auto select solver	On
Solver	Parametric Linear
Solution Form	Coefficient

FEMLAB Solver settings (b)	
Analysis type	Eigenfrequency
Default element type	Lagrange- Quadratic
Large Deformation	Off
Implementation	Principle of virtual work
Specify Eigenvalues using	Eigenfrequency
Weak Constraints	Off

Table 9-2 FEMLAB Solver settings for Frequency Response (a) and Eigenfrequency (b) analyses

9.6 Simple 3d stack models

Initially a simplified solid of circular cross-section was produced to simulate the dental scaler stack. However, in this initial model, the laminated nature of the stack was not incorporated. This is addressed in section 9.7. The model was produced to see what resonances occurred with the model when a pressure was applied to one side of the stack at frequencies from 15 kHz to 35 kHz with 100 Hz steps. A 60×10^4 Pa pressure was applied to one face of the unconstrained stacks in the x-direction as shown in figure 9-6. The pressure was applied purely to identify the Eigenfrequencies in the system. The mesh parameters for the simplified stack models are shown in table 9-3.

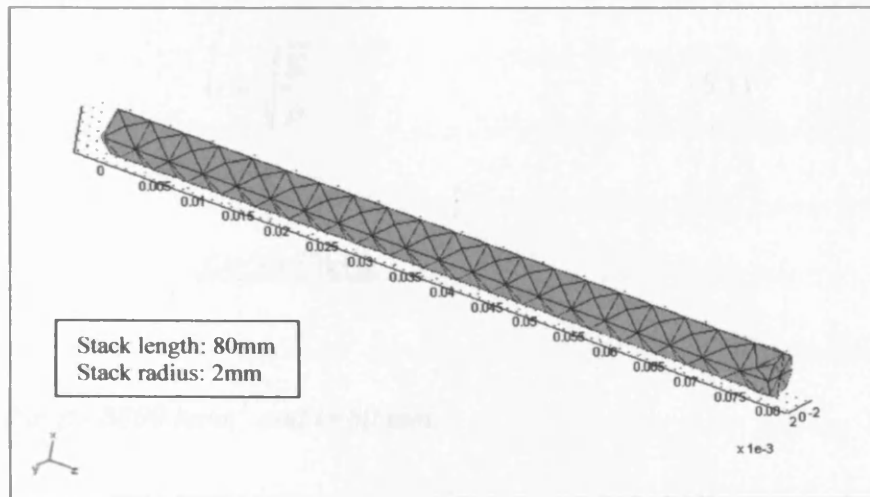


Figure 9-6 Meshed simplified model of a dental scaler stack.

Extended mesh

Number of degrees of freedom	3582
------------------------------	------

Base mesh

Number of edge elements	92
Number of boundary elements	336
Number of elements	613
Minimum element quality	0.3945

Table 9-3 Mesh parameters for the simplified model of a dental scaler stack

Using Eq. (5.2) rather than FEM, it is possible to calculate the fundamental frequency of the nickel rod based on the material parameters shown in table 5-10. The fundamental resonance is:

$$f_r = \frac{v}{2l} \quad (5.2)$$

where

$$v = \sqrt{\frac{E}{\rho}} \quad (5.1)$$

hence

$$f_r = \underline{30.53 \text{ kHz}}$$

If $E = 2.1 \times 10^{11} \text{ Pa}$, $\rho = 8800 \text{ kg/m}^3$ and $l = 80 \text{ mm}$.

However, if this longitudinal resonance is to produce a flexural resonance in an attached scaler tip, other vibrational modes must be considered apart from the longitudinal alone.

As the dental scaler insert is a mechanically coupled system with two main components (the tip assembly and the stack assembly), if the tip displays a flexural mode then the whole insert must undergo a flexural mode, if it is to comply with previous observations. [5.3]. If the tip alone was undergoing a stimulated flexural mode, this would necessarily be at a much higher frequency than 30 kHz (the stated operation frequency of the dental scaler). Consequently, identification of the flexural modes exhibited by a vibrating stack needed to be identified. Finite element modelling with FEMLAB offers a relatively quick way to undertake this investigation. In addition, analysis of the modelled stack would enable a comparison with full inserts which comprise the modelled stack and tip assembly.

The following modelled spectrum plots (figures 9-7 to 9-10) show what flexural resonant frequencies could be expected to be observed in a modelled dental scaler stack (from 15 kHz to 35 kHz with 100 Hz steps) for different modelled magnetostrictive materials.

Figure 9-7 shows the predicted resonances associated with a solid, circular nickel stack (without the tip assembly). Here, resonant peaks can be observed at 17.2 kHz and 27.3 kHz. This modelling process was used purely to identify at what frequency resonances would be expected to occur in the modelled stack as a result of the stimulation of resonant modes. As the forces applied to the modelled stack were selected purely to identify resonances (rather than being representative of the forces produced by a magnetostrictive forcing function) the magnitude of the modelled displacements are arbitrary. It must be noted that in this analysis, the nature of the mode-shapes is not identified. Mode shapes are discussed in section 9.8.

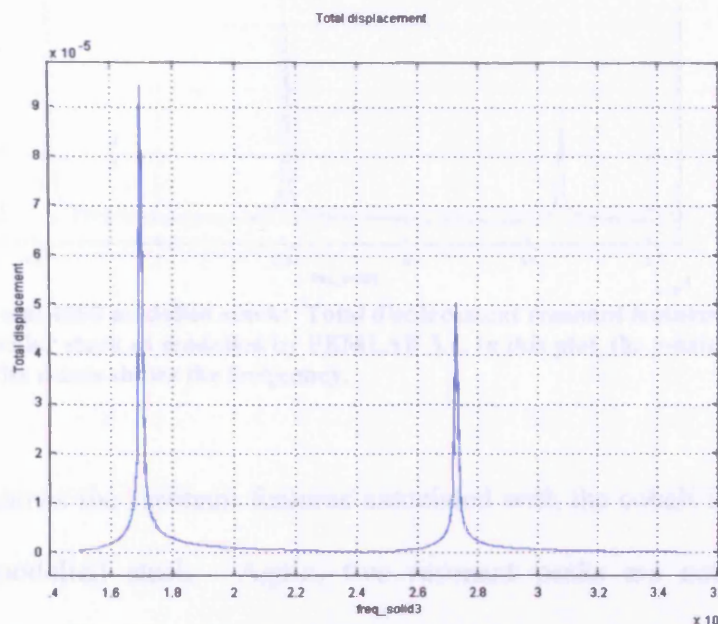


Figure 9-7 Nickel modelled stack: Total displacement resonant features for the simplified model of a dental scaler stack as modelled by FEMLAB 3.1. In this plot, the y-axis shows arbitrary displacement and the x-axis shows the frequency.

Figure 9-8 shows the predicted resonant performance of the Radiometal 4550 modelled scaler stack. Three resonant peaks have been found in the analysed frequency range. It must be noted that the two largest resonant peaks could be compared to the two shown in figure 9-7. In this case, the first peak at 15.9 kHz is found to be at a lower frequency than that of the equivalent 17.2 kHz peak for the modelled nickel stack in figure 9-7. The secondary peak at

25.4 kHz is somewhat lower than that for the modelled nickel stack at 27.3 kHz. The third peak has a frequency (at 36.5 kHz) which can be considered to be too high to be a harmonic of the other resonant features.

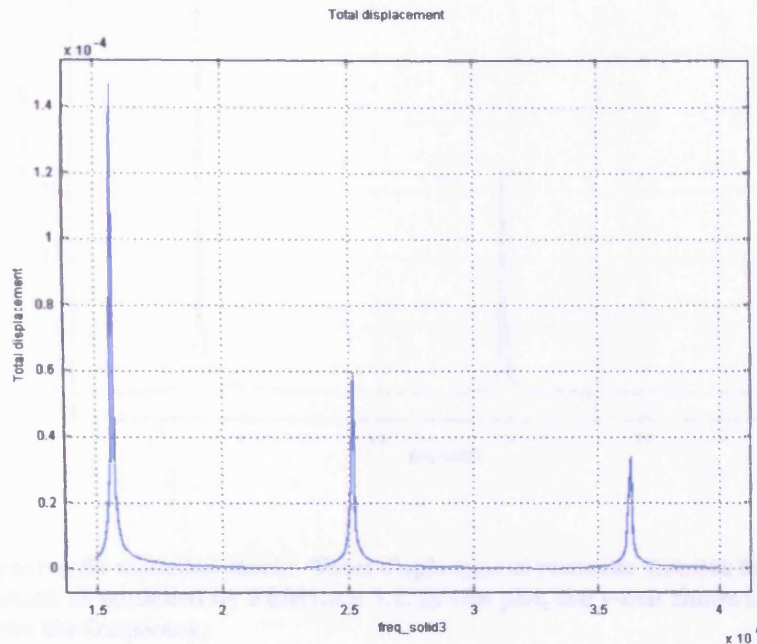


Figure 9-8 Radiometal 4550 modelled stack: Total displacement resonant features for the simplified model of a dental scaler stack as modelled by FEMLAB 3.1. In this plot, the y-axis shows arbitrary displacement and the x-axis shows the frequency.

Figure 9-9 shows the resonant features associated with the cobalt iron change as earlier (Hyperco 50) modelled stack. Again, two resonant peaks are noted in the modelled frequency range with the primary peak at 18.5 kHz and a secondary peak at 29.6 kHz.

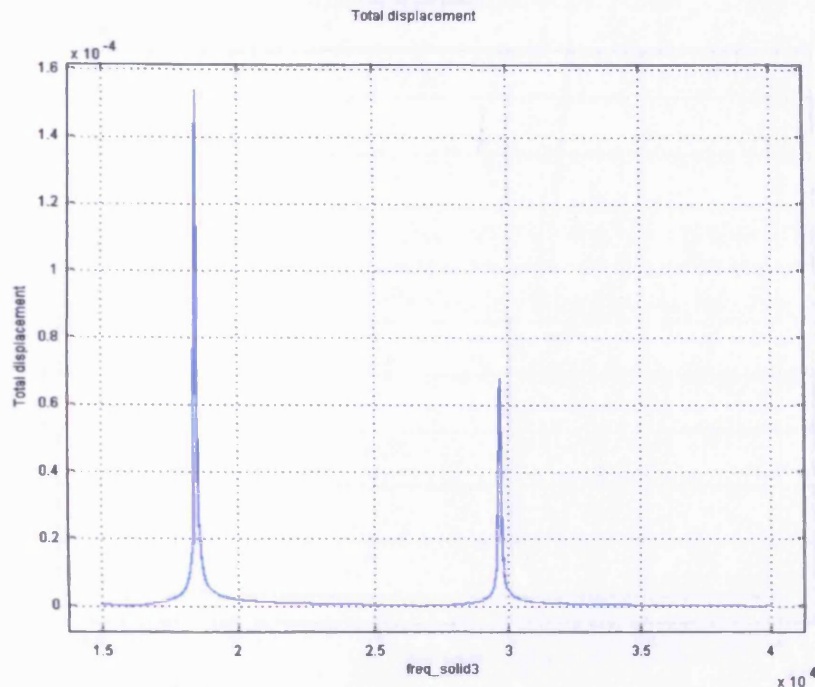


Figure 9-9 Hyperco 50 modelled stack: Total displacement resonant features for the simplified model of a dental scaler stack as modelled by FEMLAB 3.1. In this plot, the y-axis shows arbitrary displacement and the x-axis shows the frequency.

Figure 9-10 shows the resonances for the 3 % grain-oriented steel based modelled scaler stack. In this case, the primary resonance seems to be at 30 kHz with a secondary peak at 18.8 kHz. It is noted that the relative size of the peaks is reversed for the grain-oriented steel model when compared to the other modelled stacks.

The predicted resonances using the simplified stack model are summarised in table 9-4.

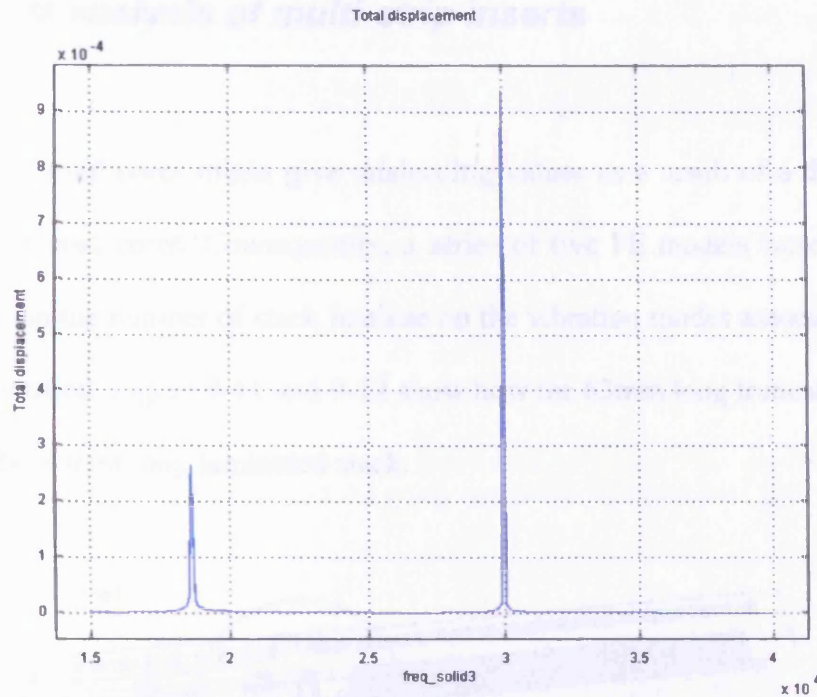


Figure 9-10 Grain Oriented Steel (3%) modelled stack: Total displacement resonant features for the simplified model of a dental scaler stack as modelled by FEMLAB 3.1. In this plot, the y-axis shows arbitrary displacement and the x-axis shows the frequency.

Model Type	Material	Primary Resonance (kHz)	Secondary resonance (kHz)
Isolated Stack	Nickel	17.2	27.3
Isolated Stack	Radiometal 4550 (Ni Fe)	15.9	25.4
Isolated Stack	Hyperco 50 (Co Fe)	18.5	29.6
Isolated Stack	GO Steel	18.8	30.0

Table 9-4 Comparison of the predicted resonances and the associated Young's modulus and density for the stacks of the various materials.

It should be noted that the secondary resonances, identified in the modelling and shown in table 9-4, are not simple multiples of the primary resonance. This indicates that more than one vibrational mode-shape is being stimulated. This is something that Eq. 5.2 does not indicate.

9.7 3d FEM analysis of multi-strip inserts

Modelling solid cores might give misleading values as a result of a difference between solid and laminated cores. Consequently, a series of five FE models were produced so that the influence on the number of stack laminae on the vibration modes associated with an insert could be quantified. Figure 9-11 and 9-12 show how the 63mm long truncated tip assembly is attached to the 80mm long laminated stack.

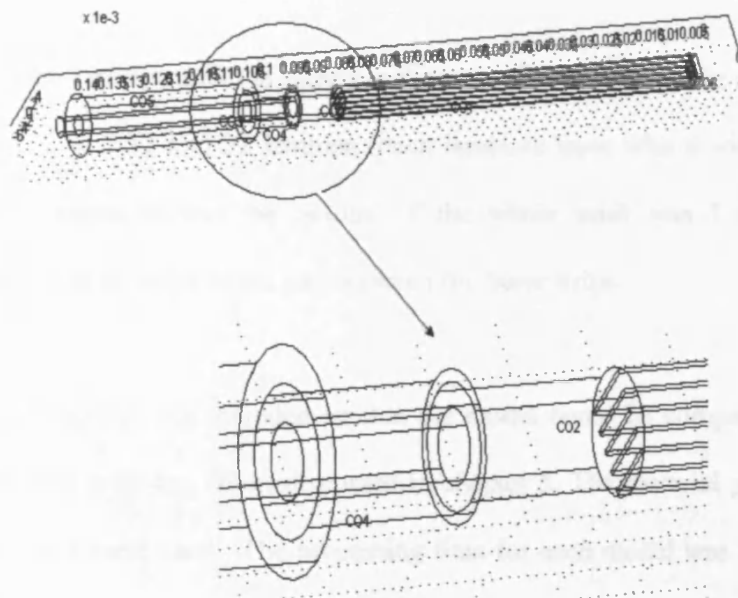


Figure 9-11 Example of a multiple laminae insert models (the layered nature of the stack is highlighted)
In this figure, the laminated stack is on the right and the tip assembly on the left.

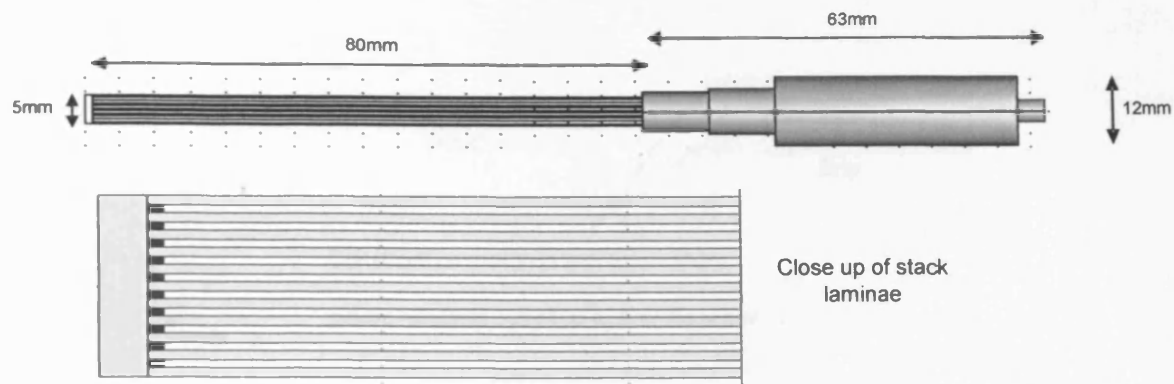


Figure 9-12 Schematic of laminated dental scaler insert with end cap. A close-up of the 11 laminae stack is also shown. The solid disc on the end of the stack emulates the soldered joint that binds the laminae together at one end.

The geometry of the model is shown in figure 9-11 and 9-12 but the stack sub-component comprised of 3, 4, 7 11 and 22 laminae (each laminate layer with a width of 0.3 mm). The strips were arranged so that the 'width' of the whole stack was 5 mm with an evenly distributed number of strips in the gap between the outer strips.

The scaler tip was not included so that the model could be compared to the results of experiments with a tip-less insert discussed in chapter 5. The material parameters for nickel given in table 9.1 were used. The processing time for each model was >14 hrs on a 1 MHz Pentium II PC.

Figure 9-13 shows where movement constraints were applied to the scaler model to simulate the butting of the insert grip to the outer casing of the handle. This was discussed in section 5.4. A rubber O-ring secures the insert in the handle and this limits motion in the z-direction. It was noted that the nickel stack was not restrained when inserted into the scaler handle. This constraint was applied in all subsequent models.

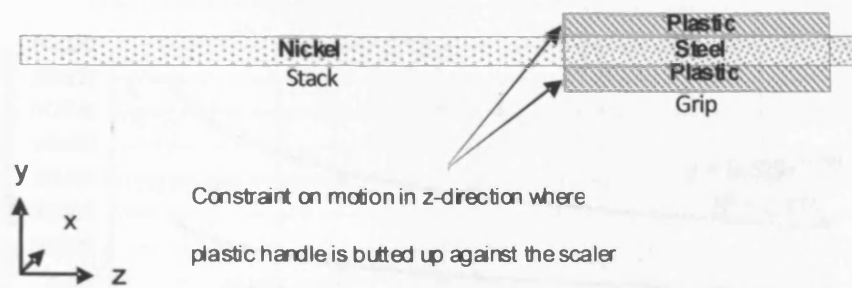


Figure 9-13 Schematic of laminated dental scaler insert showing constraints applied in the model

The model components, shown in figure 9-13, in the FEMLAB model were given the material parameters as specified in table 9.1.

In each model, two flexural modes were identified and their Eigenfrequency values were noted. In these simulated data (see figure 9-14), it was found that that as the number of strips was increased from 3 to 22, the flexural modes' Eigenfrequencies changed tending asymptotically towards a constant value. The frequencies eventually chosen to be tracked were the Eigenfrequencies that were closest to the resonances measured for a tip-less insert (see section 5.7) and tended asymptotically to that of a solid block of nickel as the number of laminae in the modelled stack increased. The stacks that are typically used in dental scalers comprise 16 nickel strips. By interpolation, it can be seen that the Eigenfrequency values of 16 laminae are not significantly different to that expected for a solid stack.

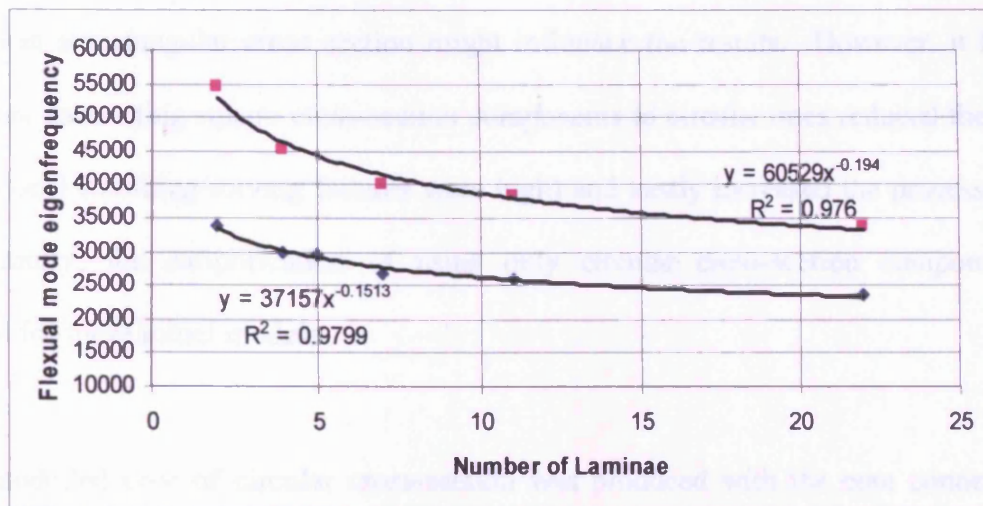


Figure 9-14 Graph showing the change in two equivalent Eigenfrequencies as a result of an increase in the number of stack laminae for a dental scaler model.

Although the Eigenfrequency values for 16 strips and a solid stack are different, the solid core model gives results that are a reasonable approximation and reduces the modelling difficulties and solving times.

9.8 3d Finite element model of Inserts with different solid core materials

Although the analysis in section 9.6 was useful as a means of comparing the predicted resonances for modelled stacks, more representative models (that more closely mirrored the topology of dental scaler inserts) were produced using the same solid cylindrical core magnetostrictive material components connected to tip assemblies. A typical dental scaler was measured with an accuracy of ± 0.5 mm using a steel rule. The angle of the tip compared to the main axis of the insert was measured with a protractor with an accuracy of $\pm 0.5^\circ$. The circular cross-section of the stack was produced with a diameter that was the same as that

measured across the actual scaler stack. It was realised that having a circular cross section rather than a rectangular cross section might influence the results. However, it had been found that connecting square cross-section components to circular ones reduced the stability of the model (meshing/solving failures were high) and vastly increased the processing time. Consequently, the simplification of using only circular cross-section components was accepted for these initial models.

A modelled core of circular cross-section was produced with the core connected to a modelled tip assembly (figure 9-15). The solid stack and tip assembly behave as a single composite component. The resonances subsequently observed are due to the whole insert rather than those for the discrete components.

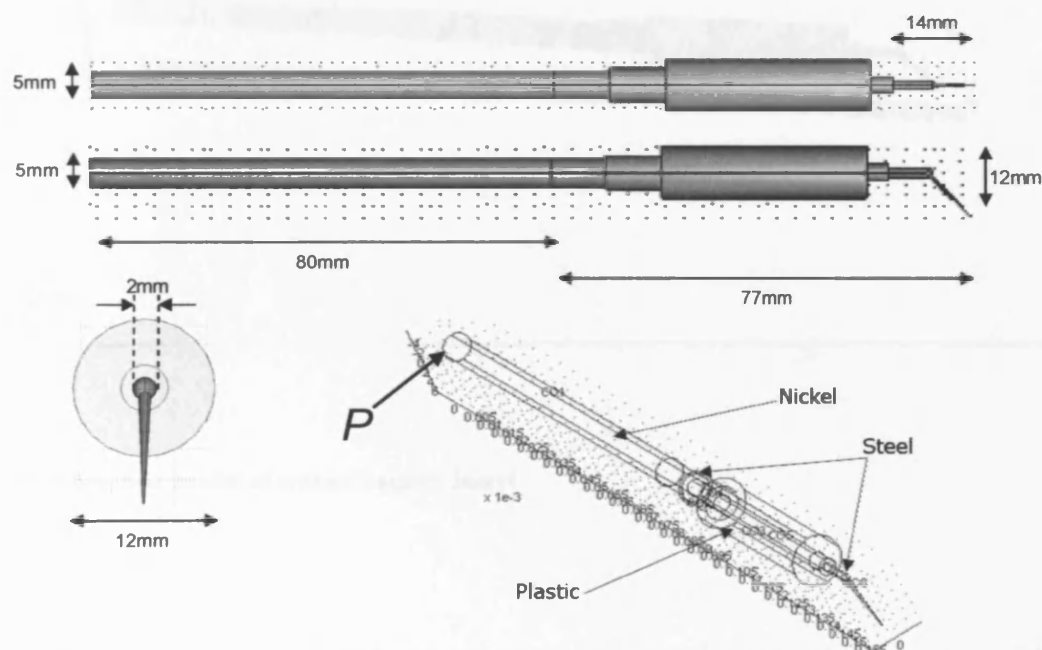


Figure 9-15 Schematic of modelled dental scaler insert showing component materials (in this case, for a nickel solid core)

The model was produced to see what resonances occurred with the insert when a force of 60×10^4 Pa was applied to the core (as in section 9.6) with an applied frequency from 15 kHz to 35 kHz with 100 Hz steps. The pressure P (equivalent to a shear force applied to the area) was applied in the direction orthogonal to the plane of the tip (see figure 9-15) at the opposite end of the insert to the tip assembly. The movement constraints on the model were as in figure 9-13. Figure 9-16 shows the meshed insert used.

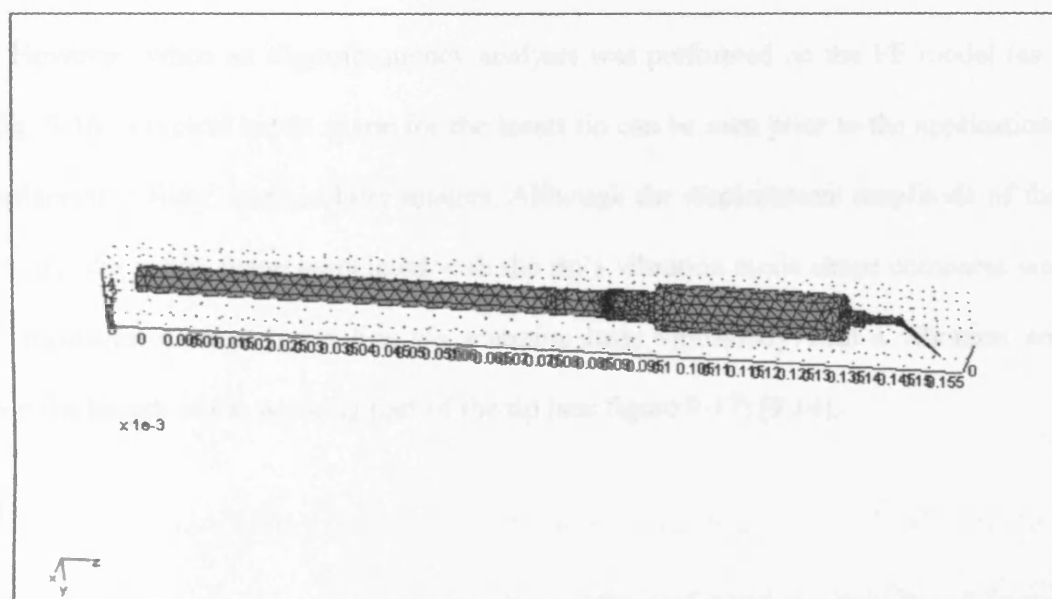


Figure 9-16 Meshed model of a dental scaler insert

In addition to undertaking a simulated 'frequency scan', the mode shapes were identified for the main resonant peaks that were observed in the frequency range of 15 kHz to 35 kHz. These mode shapes were obtained by undertaking an Eigenfrequency analysis that identified the undamped Eigenfrequencies for the simplified insert models. Using the resonant frequency analysis, the main resonant frequencies were identified and then the equivalent

Eigenfrequencies were selected so that a visual display of the mode shape could be produced via the FEMLAB graphical post-processing facility.

As the tip displacements were found to be greater than those of the rest of the insert, the automated scaling system of the Eigenfrequency graphical display system was set so that the overall mode shape could not be seen. This was compensated for by applying a 'filter' that inhibited the display of the large displacements associated with the tips whilst enabling the observation of the overall insert mode shape.

However, when an Eigenfrequency analysis was performed on the FE model (as shown in fig. 9-16) a typical mode shape for the insert tip can be seen prior to the application of the 'displacement filter' used in later images. Although the displacement amplitude of the tip is arbitrary, the mode shape associated with the tip's vibration mode shape compares well with that measured for real insert tips via scanning laser vibrometry with a vibration node $2/3$ down the length of the working part of the tip (see figure 9-17) [9.14].

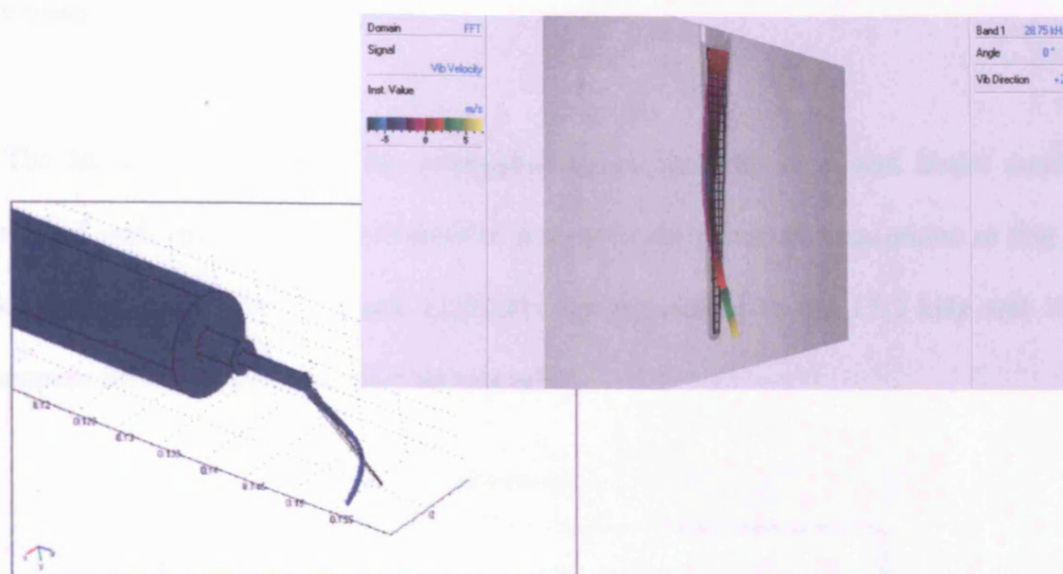


Figure 9-17 Vibration of the modelled insert tip (left) compared to the vibration of a dental scaler insert measured via a scanning laser vibrometer (SLV) (right). In the SLV image, the video image of a real, vibrating insert tip can be seen [9.14].

Yet again, this result is something that could not have been easily achieved through the use of simple single degree of freedom equations.

The modelled spectrum plots shown in figures 9-18, 9-22, 9-25 and 9-28 indicate what resonant frequencies could be expected inserts made with different solid core materials. By identifying the resonances in this way, it was then possible to seek and display the associated vibrational mode-shape using the Eigenfrequency visualisation capability of FEMLAB. Associated with each of the modelled frequency response plots, the mode-shapes for the largest two resonant peaks are displayed.

Figure 9-18 shows the predicted resonances associated with a simplified nickel insert. Here, the two highest resonant peaks occur at 17.9 kHz and 33.4 kHz in the analysed frequency range. This modelled resonant characteristic in the frequency range will be used as

the base line for comparison with the other plots for inserts modelled with different solid-stack materials.

The increased length of the magnetostrictive material core and insert combination (compared with the core alone) results in a drop in the resonant frequencies so that the two peaks identified at 17.9 kHz and 15.0 kHz are equivalent to the 17.2 kHz and 27.3 kHz resonances for the insert without a tip assembly.

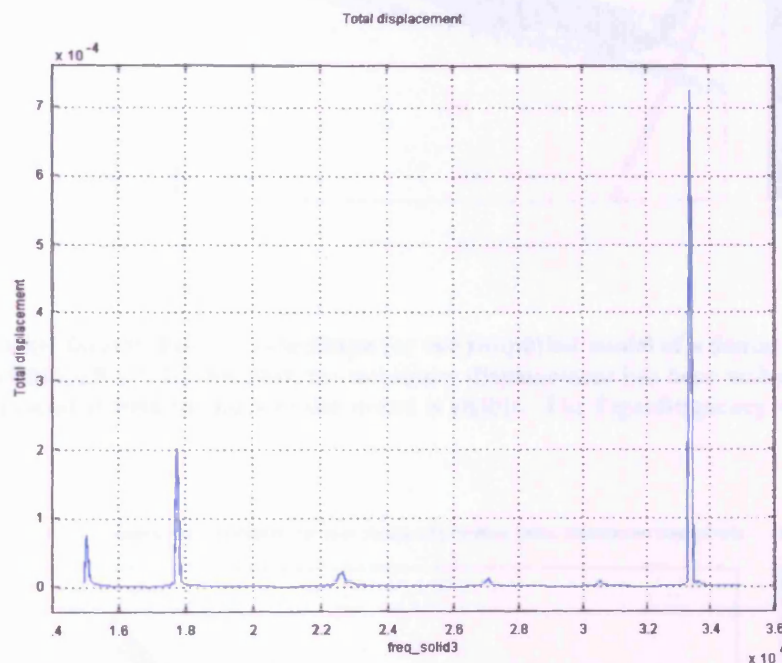


Figure 9-18 Nickel Insert: Total displacement resonant features for the simplified model of an insert as modelled by FEMLAB 3.1. In this plot, the y-axis shows arbitrary displacement and the x-axis shows the frequency.

The mode-shapes associated with the two main resonances can be seen in figures 9-19 and 9-20. They show that a flexural mode is produced in these inserts that results in a significant vibration of the tip itself. As the tip, tip assembly and solid stack are all part of a composite component then any vibrational modes that are produced will be due to the properties of the whole insert. The resonances that have been identified produce mode-shapes

that are unique for that frequency. Away from these resonances, the inserts will not produce significant vibrations.

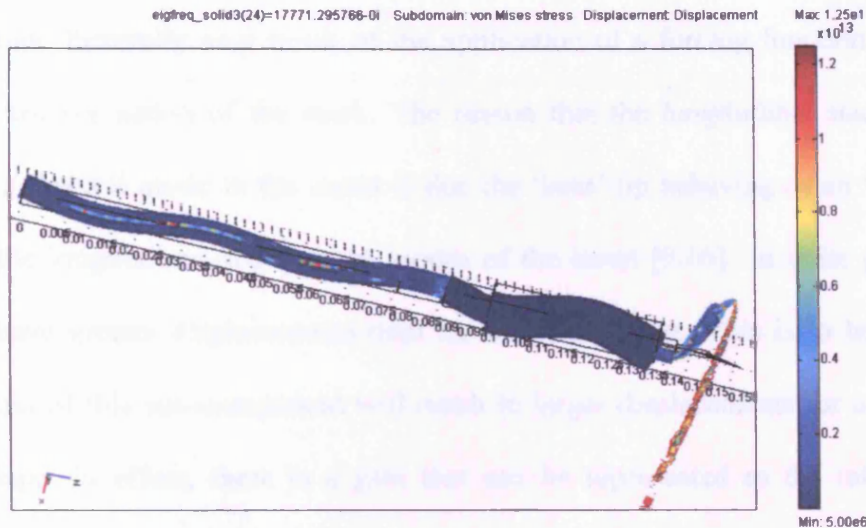


Figure 9-19 Nickel Insert: Insert mode shape for the simplified model of a dental scaler insert as modelled by FEMLAB 3.1. In this plot, the arbitrary displacement has been scaled and filtered so that the mode shape associated with the bulk of the insert is visible. The Eigenfrequency value is given above the image.

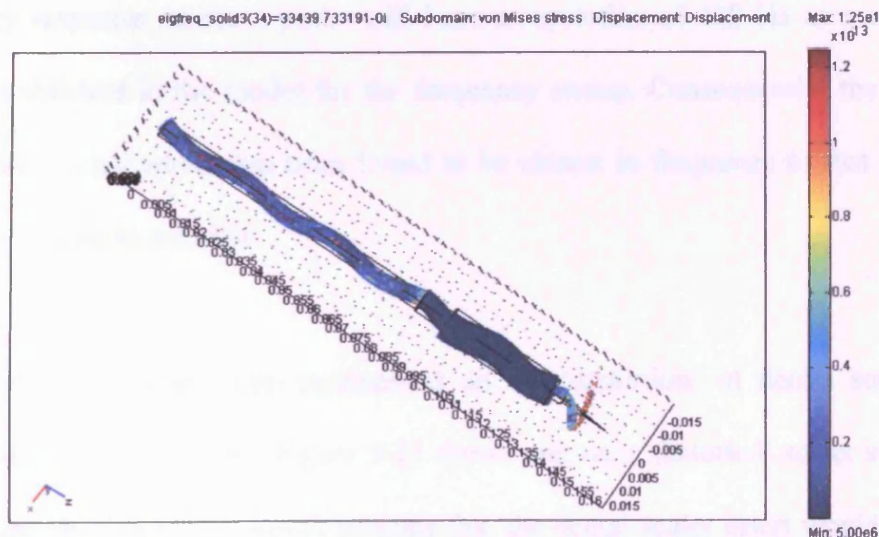


Figure 9-20 Nickel Insert: Insert mode shape for the simplified model of a dental scaler insert as modelled by FEMLAB 3.1. In this plot, the arbitrary displacement has been scaled and filtered so that the mode shape associated with the bulk of the insert is visible. The Eigenfrequency value is given above the image.

This finding was significant as it was initially thought [9.15] that a longitudinal resonance was causing the tip to vibrate alone. The modelling indicated that the whole insert can resonate flexurally as a result of the application of a forcing function supplied via the magnetostrictive action of the stack. The reason that the longitudinal stack resonance can produce a flexural mode in the insert is due the 'bent' tip behaving as an 'offset mass' that couples the longitudinal and flexural modes of the insert [9.16] In these plots, the tips are seen to have greater displacements than the stack possesses. This is to be expected as the lower mass of this sub-component will result in larger displacements for a given stimulated mode shape. In effect, there is a gain that can be represented as the ratio of the tip-end velocity (or displacement) of the insert to the stack end velocity (or displacement) of the insert for the flexural vibration [9.17].

It must be noted that the Eigenfrequencies are calculated with exact values whereas the frequency response resonant peaks will have a resolution of 100 Hz as a result of the step values established in the model for the frequency sweep. Consequently, the Eigenfrequency plot shown is that which has been found to be closest in frequency to that indicated by the frequency response analysis.

Dental scaler users have commented on the 'distortion' of dental scaler stacks after prolonged use [9.18] [9.19]. Figure 9-21 shows one such 'distorted' scaler stack [9.19]. The mode shape in figure 9-20 would indicate that the dental scaler insert would have nodes and anti-modes that are distributed along its length. The distorted insert (shown in figure 9-21) seems to exhibit a distortion that resembles the flexural modes observed in the modelling.

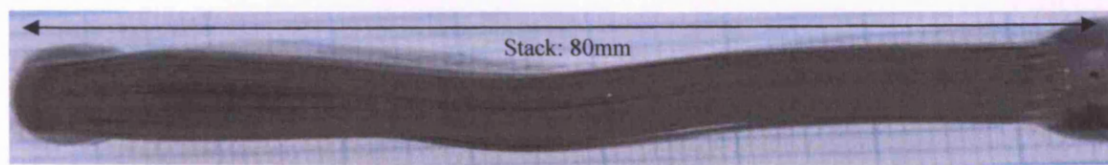


Figure 9-21 Distorted stack of a non-functional scaler insert (laminae planes into paper)[9.19]

The flexural modes shown are such that the maxima and minima are orthogonal to the plane of the tip main axis. By establishing such a flexural mode, maximum displacements can be established in the tip in the plane orthogonal to the tip axis. This would be favourable for dental scaler action if tip impact with the calculus surface results in its removal.

9.9 3d scaler inserts modelled with different solid-stack materials

Figure 9-22 shows the predicted resonances associated with a simplified nickel iron (Radiometal 4550) insert when isolated from the tip assembly. Here, the two largest resonant peaks occur at 16.1 kHz and 20.9 kHz in the analysed frequency range.

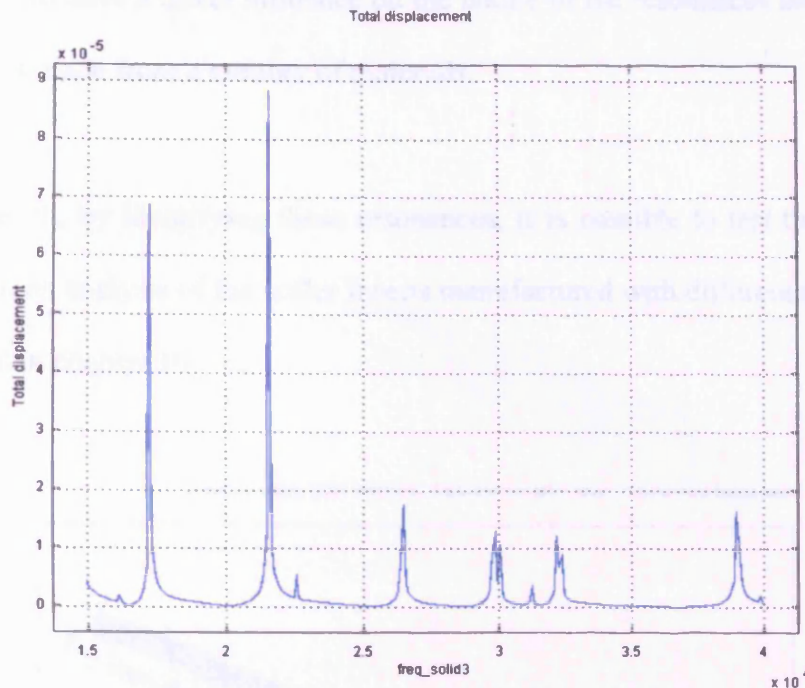


Figure 9-22 Nickel Iron (Radiometal 4550) Insert: Total displacement resonant features for the simplified model of a dental scaler insert as modelled by FEMLAB 3.1. In this plot, the y-axis shows arbitrary displacement and the x-axis shows the frequency.

As was conducted for the nickel stack-insert components, a comparison of the nickel-iron insert's resonant features (when compared to the solid-stack in isolation) shows peaks at 16.1 kHz, 20.9 kHz, 27.6 kHz and 29.9 kHz. Again, as with the nickel insert model, additional resonances can be observed in the analysed frequency range.

Figures 9-23 and 9-24 indicate that the largest two modelled resonances, like the nickel based insert model, have flexural mode-shapes that encourage tip vibrations orthogonal to the plane of the tip main axis.

By comparing the nickel-based and Radiometal 4550 (Nickel Iron) based spectral plots as modelled using FEMLAB, it seems that the main resonances can be expected to lie at different frequencies. Consequently, as the only parameters that have been changed in these models are the Young's modulus and density, it would seem that (as would be expected) these

parameters can have a direct influence on the nature of the resonances associated with dental scaler inserts made from a number of materials.

As a result, by identifying these resonances, it is possible to test the predictions of the models with an analysis of the scaler inserts manufactured with different stack materials. This is discussed in chapter 10.

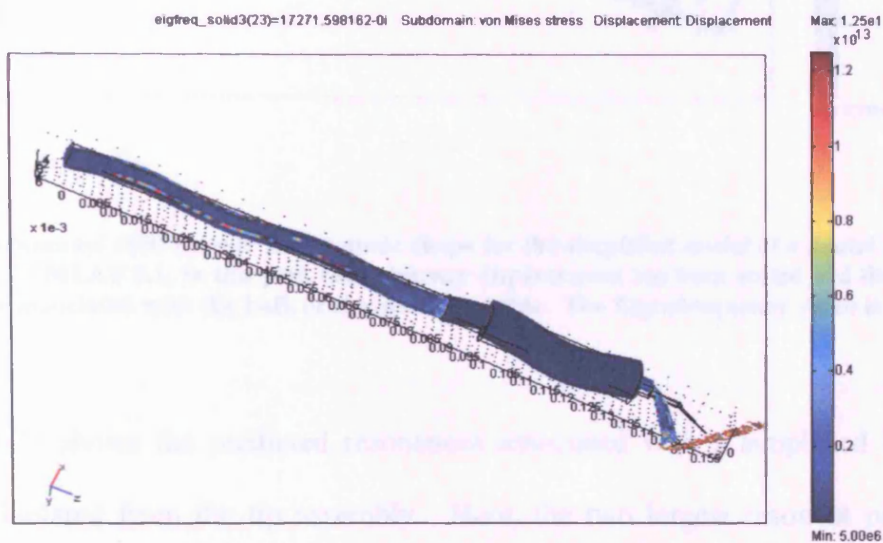


Figure 9-23 Radiometal 4550 Insert: Insert mode shape for the simplified model of a dental scaler insert as modelled by FEMLAB 3.1. In this plot, the arbitrary displacement has been scaled and filtered so that the mode shape associated with the bulk of the insert is visible. The Eigenfrequency value is given above the image.

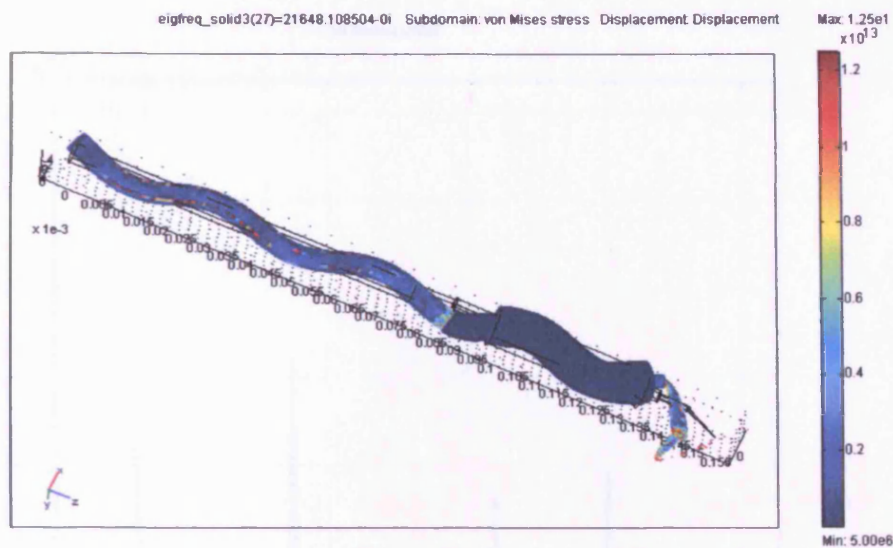


Figure 9-24 Radiometal 4550 Insert: Insert mode shape for the simplified model of a dental scaler insert as modelled by FEMLAB 3.1. In this plot, the arbitrary displacement has been scaled and filtered so that the mode shape associated with the bulk of the insert is visible. The Eigenfrequency value is given above the image.

Figure 9-25 shows the predicted resonances associated with a simplified Hyperco 50 insert when isolated from the tip assembly. Here, the two largest resonant peaks can be observed at 15.2 kHz and 24.0 kHz in the analysed frequency range.

Figures 9-26 and 9-27 indicate that the largest two modelled resonances, like the nickel based insert model, also have flexural mode-shapes that encourage tip vibrations orthogonal to the plane of the tip main axis.

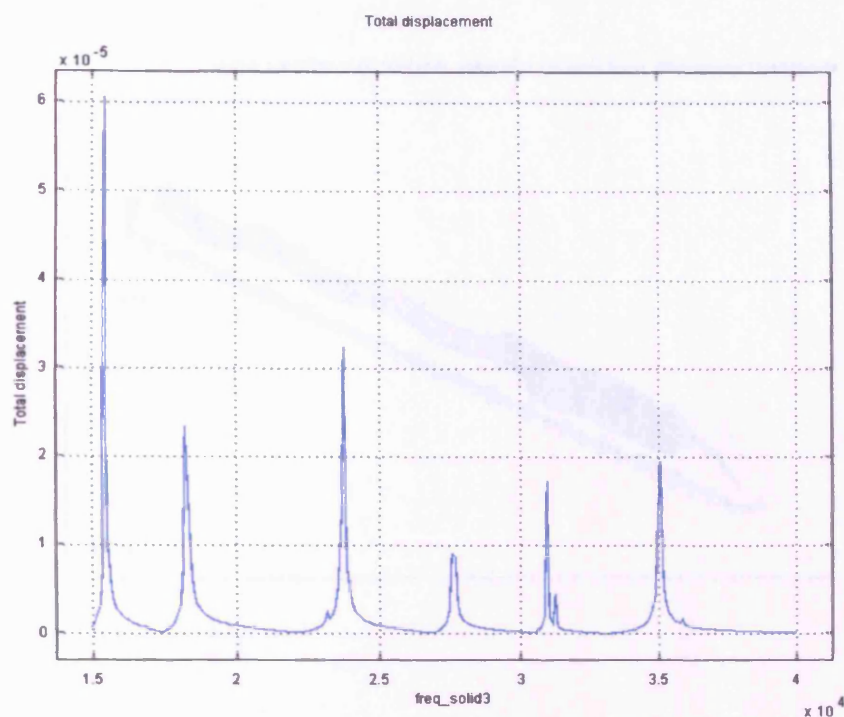


Figure 9-25 Hyperco 50 Insert: Total displacement resonant features for the simplified model of a dental scaler insert as modelled by FEMLAB 3.1. In this plot, the y-axis shows arbitrary displacement and the x-axis shows the frequency.

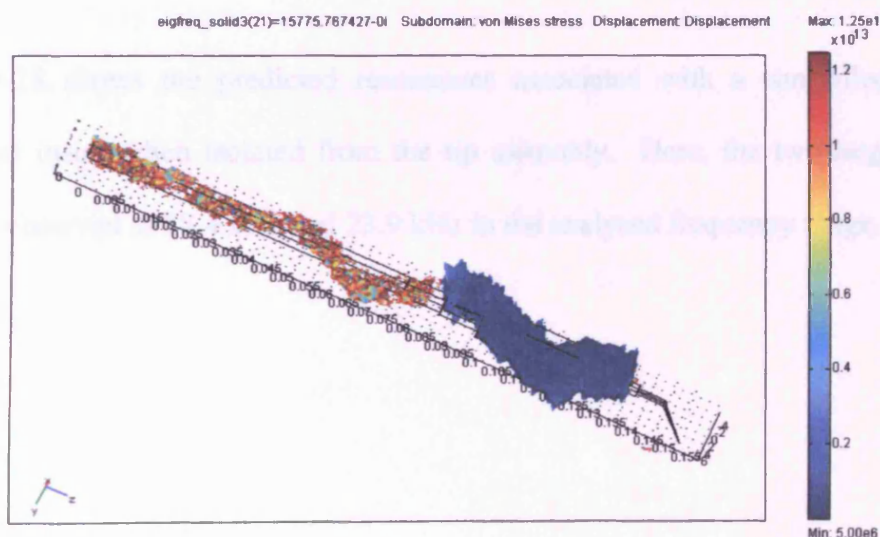


Figure 9-26 Hyperco 50 Insert: Insert mode shape for the simplified model of a dental scaler insert as modelled by FEMLAB 3.1. In this plot, the arbitrary displacement has been scaled and filtered so that the mode shape associated with the bulk of the insert is visible. The Eigenfrequency value is given above the image.

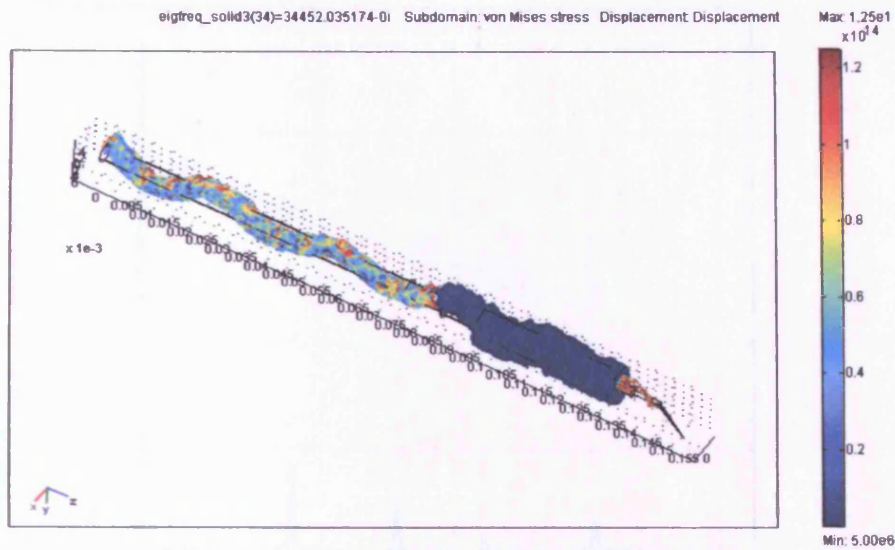


Figure 9-27 Hyperco 50 Insert: Insert modeshape for the simplified model of a dental scaler insert as modelled by FEMLAB 3.1. In this plot, the arbitrary displacement has been scaled and filtered so that the mode shape associated with the bulk of the insert is visible. The Eigenfrequency value is given above the image.

Figure 9-28 shows the predicted resonances associated with a simplified 3% Grain Oriented Steel insert when isolated from the tip assembly. Here, the two largest resonant peaks can be observed at 18.4 kHz and 23.9 kHz in the analysed frequency range.

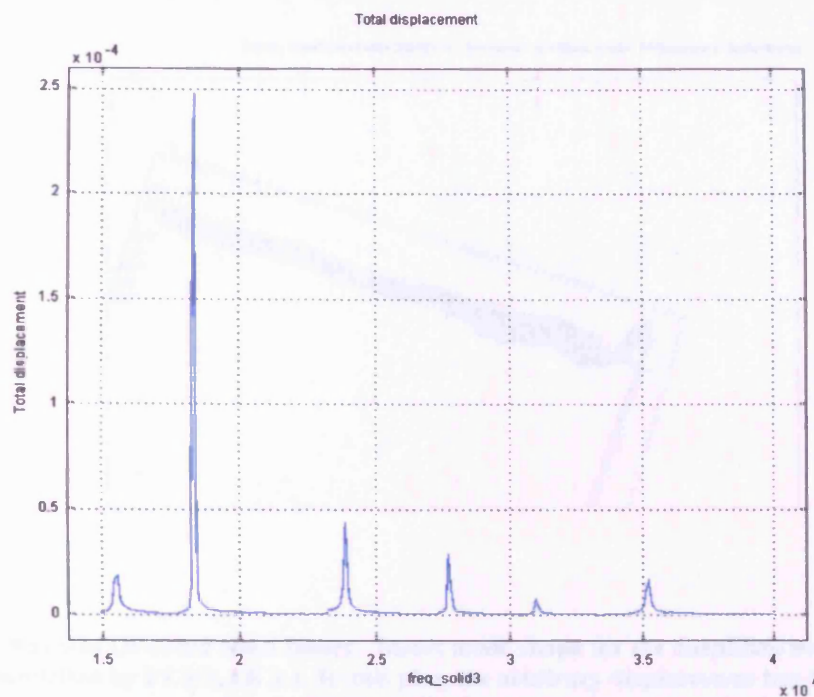


Figure 9-28 Grain Oriented Steel (3%) Insert: Total displacement resonant features for the simplified model of a dental scaler insert as modelled by FEMLAB 3.1. In this plot, the y-axis shows arbitrary displacement and the x-axis shows the frequency.

Figures 9-29 shows that the main resonance at 18.4 kHz is a flexural mode. However, the one at 23.3 kHz (figure 9-30) is a torsional mode. The next peak at (figure 9-31) 27.6 kHz is also a flexural mode

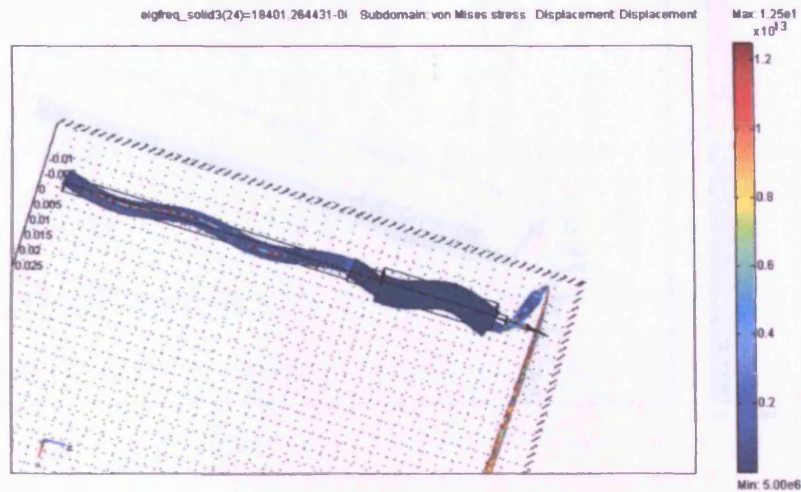


Figure 9-29 Grain Oriented Steel Insert: Insert mode shape for the simplified model of a dental scaler insert as modelled by FEMLAB 3.1. In this plot, the arbitrary displacement has been scaled and filtered so that the mode shape associated with the bulk of the insert is visible. The Eigenfrequency value is given above the image.

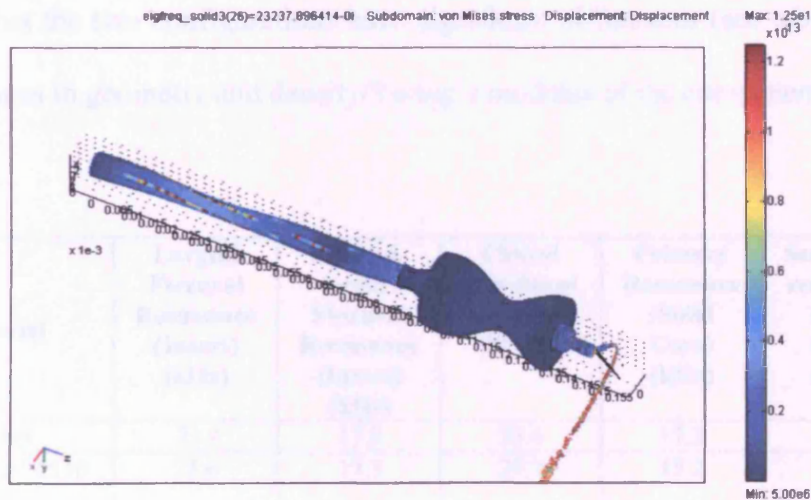


Figure 9-30 Grain Oriented Steel Insert: Insert mode shape for the simplified model of a dental scaler insert as modelled by FEMLAB 3.1. In this plot, the arbitrary displacement has been scaled and filtered so that the modeshape associated with the bulk of the insert is visible. The Eigenfrequency value is given above the image.

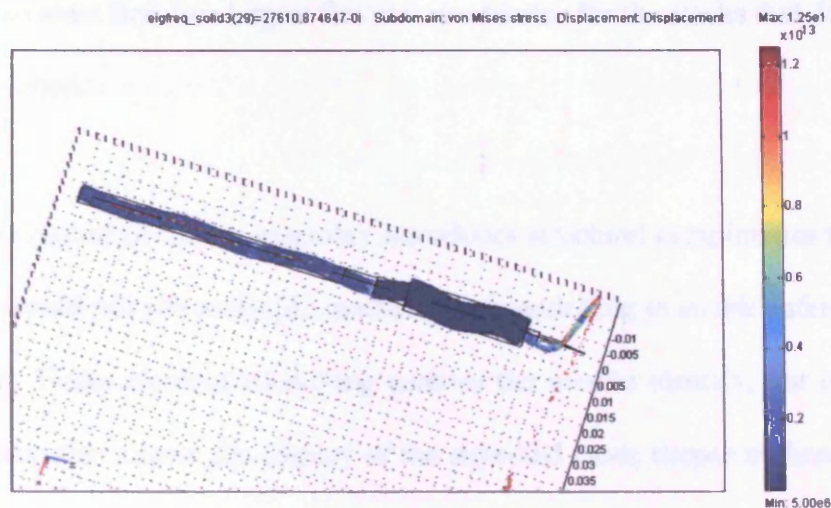


Figure 9-31 Grain Oriented Steel Insert: Insert mode shape for the simplified model of a dental scaler insert as modelled by FEMLAB 3.1. In this plot, the arbitrary displacement has been scaled and filtered so that the mode shape associated with the bulk of the insert is visible. The Eigenfrequency value is given above the image.

Comparing the modelled resonances associated with the solid cores and whole inserts demonstrates that the two configurations have significant differences (see table 9.5). These reflect the changes in geometry and density/Young's modulus of the components.

Material	Largest Flexural Resonance (Insert) (kHz)	Second largest Flexural Resonance (Insert) (kHz)	Closest significant peak to 30 kHz	Primary Resonance (Solid Core) (kHz)	Secondary resonance (Solid Core) (kHz)
Nickel	33.4	17.9	33.4	17.2	27.3
Radiometal 4550 (Ni Fe)	21.6	17.3	29.9	15.2	25.4
Hyperco 50 (Co Fe)	15.8	24.0	34.4	18.5	29.6
GO Steel	18.4	23.9	27.6	18.8	30.0

Table 9-5 Comparison between the main flexural resonances of the solid-stack and insert models

In table 9-5 the first two columns show the first two largest flexural resonances that were observed as a result of the modelling for the material concerned. The middle column shows the closest resonance observed to 30 kHz (regardless of its magnitude). The last two columns

show the equivalent first two largest flexural resonances for the stacks that do not have the tip assembly attached.

The introduction of the tip assembly introduces structural complexities to the component models that would not allow simple mathematical modelling to enable inferences to be made on behaviour. Finite element modelling enables the user to identify, not only the expected resonances, but also allows the display of the expected mode shapes at these frequencies. It is clear that there are differences between the modelled resonance frequency values and those obtained via experimentation with actual devices. However, with further study, the mechanical models could be fine-tuned to more closely represent real dental scalers geometrically. The use of faster computer systems would obviously facilitate such a change if the complexity of the model increases.

9.10 Suggested Future Coupled Models

The next step in modelling is considered to be further refinement of the 3D models and the development of a coupled model via the next version of the COMSOL FEM modelling multiphysics packages. With extended multiphysics models and for certain applications, it is possible to assign coupling variables that connect variables and expressions in various domains. At the time this work was being undertaken (2007) a newer version of FEMLAB (now called COMSOL 3.4: the replacement for FEMLAB 3.1) [9.20] was being produced. It has been stated in the literature that in COMSOL 3.4 it would be possible to achieve a fully coupled mechanical/magnetic/electrical model that will produce results in the time domain that FEMLAB 3.1 could not achieve. However, to achieve such a fully coupled model would be a significant undertaking [9.21].

The multi-physics modelling of magnetostrictive dental scalers will be an important step forward and one that could be utilised in the design de-risking and production of new devices. In the current models, it is not possible to apply a modelled dynamic magnetic field to a model that results in a coupled dynamic magnetostrictive strain based on the overall ‘transfer function’ of the insert. Production of such a model, with appropriate experimental data, would enable the designer to investigate new insert topologies prior to attempting to manufacture them. In particular, it will be possible for designers to ensure that the design of the insert is such that the longitudinal resonance can stimulate a flexural mode in the whole insert. This will be discussed further in chapter 10.

References for chapter 9

- [9.1] <http://www.cas.gsu.edu/acres/sum2000/Fluid/page14.html>
- [9.2] Femlab 3 Quickstart and Quick Reference Guide, COMSOL Ltd, 2004.
- [9.3] Femlab 3 Modelling Guide, COMSOL Ltd, 2004.
- [9.4] http://www.simetric.co.uk/si_metals.htm
- [9.5] Carpenter Technology Ltd, “Cobalt iron alloys” booklet 1999.
- [9.6] Carpenter Technology Ltd, “Nickel iron alloys” booklet 1999.
- [9.7] Williams. P.I., Cardiff University, Private Communication, 2007.
- [9.8] FEMLAB 3.1 Standard Material Library
- [9.9] Ashby, M.F. and Cebon, D. “Case studies in materials selection”, Cambridge Engineering Selector, Granta Design Limited, (1996).
- [9.10] http://www.kayelaby.npl.co.uk/general_physics/2_2/2_2.html
- [9.11] COMSOL Ltd Support Services, Private Communication, 2007.
- [9.12] Femlab 3 Structural Mechanics Module User Guide, COMSOL Ltd, 2004, p.81.
- [9.13] Femlab 3 Structural Mechanics Module User Guide, COMSOL Ltd, 2004, p.89.
- [9.14] <http://www.dentistry.bham.ac.uk/dentalultrasonics/slv.asp>
- [9.15] Lea S. Lea. S.C., The School of Dentistry, The University of Birmingham, (Private Communication), 2005.
- [9.16] Balamuth. L., “A new ultrasonic rotary device”, IEEE Transactions on Ultrasonics Engineering, Vol 10, Issue 2, Sep 1963, pp96-101.
- [9.17] Zhou G., “The performance and design of ultrasonic vibration system for flexural mode”, Ultrasonics Vol. 38, 2000, pp.979-984.
- [9.18] Pinder. J., British Society of Dental Health and Hygiene (Private Communication), 2005.
- [9.19] Lea. S.C., The School of Dentistry, The University of Birmingham, (Private Communication), 2006.
- [9.20] <http://www.comsol.com/products/>
- [9.21] Benatar. J.G., “FEM Implementations of magnetostrictive-based applications”, MS Thesis, Dept. of Aerospace Engineering, The University of Maryland, 2005.

10 RESONANCE MEASUREMENTS OF NEW AND COMMERCIAL INSERTS

10.1 Introduction

The measurements were conducted to identify whether the resonances predicted in chapter 9 would be present in commercial dental scaler inserts discussed in chapter 8. The materials tested in insert form and compared to a standard nickel-based insert were 3% grain oriented silicon steel, Radiometal 4550 and Hyperco 50.

10.2 Use of a new laser vibrometer

A scanning laser vibrometer owned by the School of Dentistry at the University of Birmingham was used to investigate the resonances associated with commercial and experimental inserts. A (PSV-300-F/S High Frequency Scanning Vibrometer System, Polytec GmbH, Germany) was used to identify and compare the resonant frequencies associated with the dental scaler inserts comprising of different magnetostrictive materials. It consisted a scanner head and a controller/workstation, where measured data was decoded and manipulated to identify the main resonances. The optical system of the scanner head (Polytec OFV 056) combined a laser, optics and video camera. The laser is a low power (<1mW), Helium-Neon (He-Ne) beam device with a wavelength of 632.8nm (see fig. 10-1) [10.1].

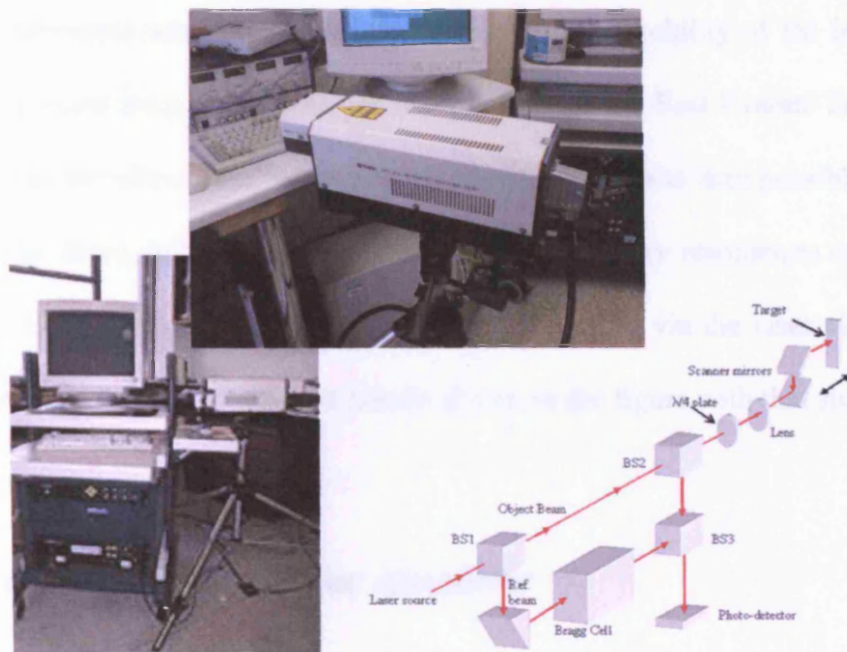


Figure 10-1 Polytec OFV 056 Scanning laser vibrometry system [10.1]

The modified Dentsply drive-coil system (see figure 8-3) was used to apply a dynamic magnetic field to the insert including the magnetostrictive stack. The drive-field was set to a peak value of 500 A/m. The measurement system is shown in figure 10-2.

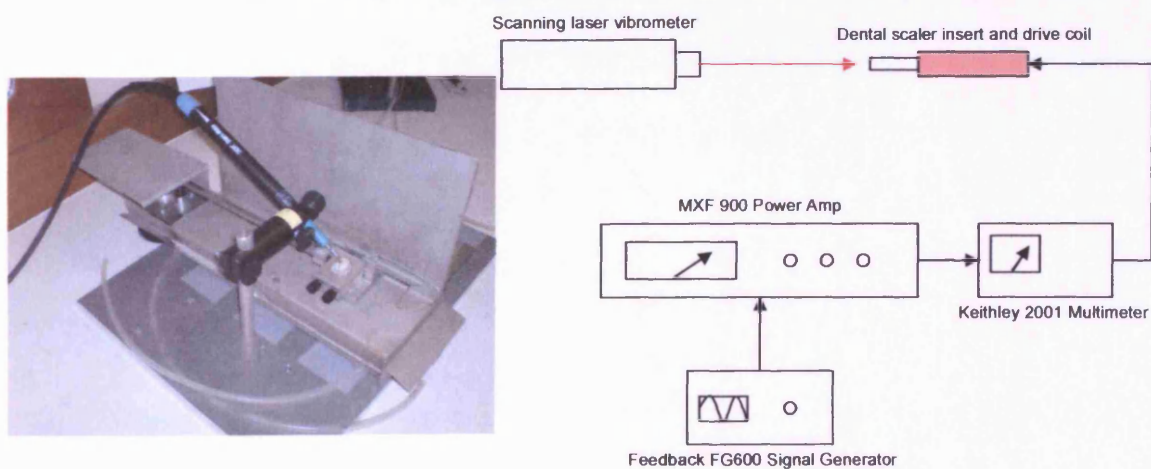


Figure 10-2 Measurement system used for identifying the resonances associated with the dental scaler inserts based on the various magnetostrictive materials.

The measurements were made with the 'single point' capability of the laser vibrometer and the displacement frequency spectrum was displayed via a Fast Fourier Transform (FFT) plotting utility in the vibrometer's data processing system. It was then possible to change the frequency of the drive field and measure the frequency of any resonances appearing in the FFT display. Both ends of the scaler insert were monitored via the laser vibrometer when undergoing resonance by replacing the handle shown in the figure with that shown in fig. 8-3.

10.3 Use of a MXF 900 Power Amplifier

It had been found that although the LM 12 based power amplifier (see fig. 5-12 and 5-13) had successfully enabled the excitation of magnetostrictive material samples, it was limited by being unable to supply high drive-currents at high frequencies. Consequently, the following analyses, a BK Electronics MXF 900 Power Amplifier was obtained as a result of its high power and high bandwidth operational parameters (see table 10.1). The modified commercial drive coil (as in figure 8-2) was connected to the output of the MXF 900 power supply with a variable frequency signal from a Feedback FG600 signal generator.

R.M.S. Watts into 4 Ohms	455 Per Channel
R.M.S. Watts into 8 Ohms	305 Per Channel
3dB Power Bandwidth	1Hz - 50Khz
Damping Factor	>300
Slew Rate	75/uS
Full Power t.h.d.	0.005%
T.h.d. Typical	0.001%
T.i.d	Zero
Input Sensitivity	775mV
Input Impedance	7.5K Ohms
S/N Ratio	110dB
Vu Metering	Visual Display of 11 L.E.D.s zero dBs at rated power
DC loudspeaker Protection	+/- 3V DC
Anti - Thump Loudspeaker	3 Seconds
Connection Delay	
Thermal Protection	90 Deg Centigrade
Fan Cooling	60 Deg Centigrade
Power Requirements - Supply	240V AC 50 - 60Hz
Weight	15Kg
Size - Front Panel	19" (482.6mm) x (3U)
Size - Depth	374.5mm

Table 10-1 BK Electronics Ltd. MXF 900 Power Amplifier Specification

It was possible to measure the resonant frequencies of the inserts when the laser vibrometer was illuminating either the tip or the opposite ends (see tables 10-2 and 10-3) to see if there were any significant differences in the resonant frequencies observed at these points. It was also possible to see if the tip/end resonances would have the same or similar frequencies as a result of the modifications that had been made to the Dentsply drive coil design. This was because the standard handle could be replaced by one that gave the laser access to the non-tip end of the scaler insert (see fig. 8-3).

Material	Laser Analysis of:	1 st Resonant Frequency Fr ₁ (kHz)	2 nd Resonant Frequency Fr ₂ (kHz)
Ni (TXD)	End	18.94	28.77
Radiometal 4550	End	17.88	27.19
Hyperco50	End	17.86	28.75
Grain Oriented Si-Fe	End	18.98	29.27

Bandwidth: 10-50 kHz
 No. FFT lines: 6400
 Frequency Resolution: 7.81 Hz

Table 10-2 Main resonances identified when the laser vibrometer beam was incident on the non-tip end of the scaler insert

Material	Laser Analysis of:	1 st Resonant Frequency Fr ₁ (kHz)	2 nd Resonant Frequency Fr ₂ (kHz)
Ni (TXD)	Tip	19.02	29.15
Radiometal 4550	Tip	18.18	27.32
Hyperco50	Tip	18.21	28.90
Grain Oriented Si-Fe	Tip	18.17	29.27

Bandwidth: 10-50 kHz
 No. FFT lines: 6400
 Frequency Resolution: 7.8 Hz

Table 10-3 Main resonances identified when the laser vibrometer beam was incident on the tip end of the scaler insert

The resonance frequencies obtained from the measurements made at both the tip and stack-ends of the inserts were within 4% in each case. However, the resonance of the insert would be expected to be at the same frequency regardless of the end that it is measured from, and so this difference must be due to measurement errors in the system. As the frequency resolution of the laser system is 7.8 Hz, it is considered that this is the cause of the differences in the identified peak frequencies.

If Eq. 5.1 and 5.2 are used to identify the fundamental longitudinal resonances of the stacks of the different materials (without being connected to the tip assemblies) it is possible

to compare the frequencies that would be expected for such stack when the tip assemblies are not attached, for comparison purposes (see table 10-4) using eq. 5.2 and the material parameters in table 9.1. Clearly, without the tip assemblies attached, the longitudinal resonances for these sub-components would be expected to be higher than for those with tip assemblies attached.

Stack Type	Young's modulus	Density Kg/m ³	Length m	Fundamental Resonance F _r Hz
Nickel	2.10E+11	8800	8.00E-02	30531
Radiometal 4550	1.67E+11	8250	8.00E-02	28120
Hyperco 50	2.30E+11	8150	8.00E-02	33202
GO Steel	2.00E+11	7650	8.00E-02	31957

Table 10-4 Comparison of calculated solid stack resonances for the different materials [10.2, 10.3, 10.4, 10.5]

The similar calculated resonances shown in table 10-4 are a consequence of the similar moduli and densities. This analysis does not predict the lower frequency resonance shown in figure 5-14. The modelling presented in chapter 9 does, however, indicate that other vibrational modes are possible. The modelling of whole inserts in chapter 9 also showed that there were flexural modes that could be stimulated in real inserts. Table 10-5 shows a comparison between the average measured primary and secondary resonances (table 10-2 and 10-3) when compared to the values for resonances as produced by the finite element modelling in chapter 9.

Material	Largest modelled flexural resonance (Insert) (kHz)	Second largest modelled flexural resonance (Insert) (kHz)	Closest significant modelled flexural resonance peak to 30 kHz	Average measured primary resonance (kHz)	Average measured secondary resonance (kHz)
Nickel	33.4	17.9	33.4	18.83	28.96
Radiometal 4550 (Ni Fe)	21.6	17.3	29.9	18.03	27.26
Hyperco 50 (Co Fe)	15.8	24.0	34.4	18.04	28.83
GO Steel	18.4	23.9	27.6	18.58	29.27

Table 10-5 Comparison between the modelled and measured (table 10-2) primary and secondary measured resonances modes and the largest, 2nd largest and 'closest to 30 kHz' modelled peaks (table 9-5)

In table 10-5 the first two columns show the first two largest flexural resonances that were observed as a result of the modelling for a given insert. The middle column shows the closest resonance observed to 30 kHz (regardless of its magnitude). The last two columns show the first two measured resonances obtained from actual dental-scaler inserts. The average value of these resonances was obtained as the mean of those resonant frequencies observed at both ends of the insert using the laser vibrometer system.

Table 10-5 suggests why only the nickel-based dental scaler inserts may produce significant flexural resonances when inserted into the commercial dental scaler system. To produce a coupled flexural-longitudinal resonance, only the nickel-based insert has a measured resonance near to the value of the *largest* modelled flexural mode. This would mean that although resonances have been measured in the real non-nickel inserts, it is likely that only the longitudinal mode is being stimulated rather than the coupled longitudinal-flexural mode [10.6]. If a longitudinal resonant frequency coincides with a flexural mode then there will be maximum transduction into the coupled vibration mode thereby producing the characteristic real dental-scaler tip motion. Those modelled modes that do occur in the

region of the measured peaks for non-nickel stacks (around 30 kHz) are relatively small compared to the largest modelled flexural model. If this statement is correct, it would mean that the reason the non-nickel based scaler stacks do not produce significant flexural mode vibrations is because their *geometry* is not allowing a coupled longitudinal-flexural mode to occur (for an insert possessing a non-nickel stack). This means that the non-nickel inserts will need to be re-designed to produce a geometry that will enable the longitudinal modes stimulated by the magnetostriction of the stack to couple to a flexural mode at the required drive frequency.

10.4 Use of the capacitance compensation system and MXF 900 power supply with non-nickel based inserts

As stated above, although attempts were made to stimulate significant resonances at ~30 kHz with the Dentsply power supply, only the nickel-based inserts functioned as expected when inserted in a standard insert handle assembly.

Supplying higher drive currents to the Dentsply drive coils via the MXF 900 power supply was only partially successful for the nickel-iron stack, as large flexural vibrations were observed but at lower frequencies than those seen with nickel inserts. In initial tests, the stimulation of resonances of ~18 kHz in the Radiometal 4550 insert were achieved that produced tip displacements sufficient to etch marks into plastic (this was not managed with inserts comprising of Hyperco 50 or 3% silicon iron). However, a high current of 1 to 2 A (compared to 0.5A dissipated by the commercial system [10.7]) was necessary to achieve this. For the capacitance compensated load (13.04Ω) this meant that the coil dissipated

between 13 and 52W. Each time these high currents were applied to the drive coil supplying field to the nickel-Iron based insert, and the impedances were compensated for, the plastic drive coil former was destroyed by the high temperatures that were developed in the drive-coil/insert system after ~15 seconds. This made systematic measurement of the performance of the new nickel-iron inserts impossible. However, looking at table 10-4, this suggests that driving the nickel iron insert at 18 kHz enabled the coupling of the lower frequency longitudinal resonance to the flexural mode modelled to be at 17.3 kHz.

10.5 Suggested Future Transducers

Rather than attempting to replace the magnetostrictive materials in present systems, it may be appropriate to produce an 'integrated handle' that contains a fully characterised, bulk material based, magnetostrictive driver (which would not be removed from the device). If it is possible to stimulate the flexural mode of an insert directly, that would remove the need for the coupled flexural-longitudinal mode that is utilised in current scaler inserts.

Hyperco 50, Radiometal 4550 and 3% grain-oriented electrical steel were identified in the initial work as being promising replacement materials for nickel in stack elements. However, this was based on the extant dental scaler system topology. Moving from such a topology will enable the use of giant magnetostrictive materials such as Terfenol-D.

10.6 Conclusions

Based on the analysis in this chapter and chapter 9 (coupled to the results of the rest of this thesis), it seems that the design of new dental scaler inserts cannot be based purely on knowledge of the non-resonant magnetostriction of the stack material and the longitudinal resonant frequency alone. The whole system must be considered from the drive electronics; the dynamic magnetic and magnetostrictive properties and also the material and geometry based characteristics before a successful insert can be designed. Indeed, there is a clear need to have a flexural resonant mode generated via a coupled longitudinal resonant mode to achieve vibrations that are significantly larger than the magnetostrictive strain produced by a non-resonant device.

This chapter has shown that the finite element modelling has given an insight into why these new inserts did not function as initially expected. In addition, an improved finite element model, that more closely resembles particular inserts would need to be developed. This would enable the investigation of geometry changes that could result in the production of inserts that have the required topology to ensure that the flexural and longitudinal modes are coupled for a given insert stack material.

References for Chapter 10

- [10.1] <http://www.dentistry.bham.ac.uk/dentalultrasonics/slv.asp>
- [10.2] http://www.simetric.co.uk/si_metals.htm
- [10.3] Carpenter Technology Ltd, “Cobalt iron alloys” booklet 1999.
- [10.4] Carpenter Technology Ltd, “Nickel iron alloys” Booklet 1999.
- [10.5] Williams. P.I., Cardiff University, Private Communication, 2007.
- [10.6] Balamuth. L., “A new ultrasonic rotary device”, IEEE Transactions on Ultrasonics Engineering, Vol 10, Issue 2, Sep 1963, pp96-101.
- [10.7] Dentsply Ltd, “SPS™ ultrasonic scaler with Steri-Mate® handpiece directions for use” Form #80617 Rev. C 1/99.

11 CONCLUSIONS

As a result of the work undertaken during this study, the following conclusions can be made regarding present and future dental scaler systems:

i. Improvements to current dental-scaler drive coil designs

It has been shown that the field uniformity along the length of the drive coil used in commercial dental scaler systems is not constant. As a consequence of this, maximum magnetostriction is not being achieved for a given applied current along the active length of the insert stack. It is recommended that future drive coils have the profile of the drive coil changed so that there are more turns at the end of the coils to improve field uniformity

ii. Frequency doubling used to stimulate dental scaler insert resonances

It is also pointed out that it is possible to reduce the operational impedance of the dental scaler system by using ‘frequency doubling’ to stimulate a 30 kHz insert resonance by applying a 15 kHz drive field.

iii. Impedance equation for a magnetostrictive transducer operating at resonance

An impedance equation for a resonant magnetostrictive transducer is developed. It shows that the real and imaginary components of its impedance comprise of terms that couple the electrical and mechanical components and their frequency dependencies.

iv. Selection of replacement magnetostrictive materials for dental scaler inserts

As a result of a literature survey coupled to quasi-static and dynamic measurements of the strains produced by a selection of magnetostrictive materials, three alternative stack materials are proposed as replacements for nickel in commercial inserts: Radiometal 4550, Hyperco 50 and 3% grain-oriented steel.

v. Capacitance compensation for the inductive components of impedance in a resonant transducer

To minimise the impedance of magnetostrictive dental scalers at resonance, a series capacitance is introduced into the electrical circuit supplying current to the dental scaler system. By doing so, the imaginary components of impedance are effectively eliminated thereby only leaving the real components. This compensation also eliminates the 'equivalent circuit' imaginary impedances caused by the magnetomechanically coupled mechanical components. As a result of this, the power requirements of a given dental scaler system can be reduced.

vi. Finite element modelling of dental scaler inserts

Three dimensional finite element mechanical models of magnetostrictive inserts have been produced. These were utilised to identify the vibration mode-shapes associated with dental scaler inserts. The models showing tip vibrations have been shown to be comparable to those seen in real dental scalers. The vibration of the tips have been shown to be due to the stimulation of a flexural mode of the scaler insert.

vii. The failure of replacement magnetostrictive materials to replace nickel in current dental scaler insert designs

It was found that dental scalers made with the replacement magnetostrictive materials did not behave in the same way as nickel inserts when placed in a commercial scaler system. They did not produce vibrations that could be used for dental scaling. This was despite the replacement materials having promising magnetostrictive properties and similar stack resonant frequencies. Use of the capacitance compensation system did reduce the impedance of all of the systems, with replacement magnetostrictive materials, to a value below that of the original un-compensated nickel-based system. However, this did not enable the production of a flexural mode resulting in significant tip vibration.

A combination of experimentation and finite element modelling results suggests a reason for this. There needs to be a coupled longitudinal-flexural mode generated by the magnetostrictive strain at resonance. This seems to only take place in nickel-based inserts and (to a lesser extent) the Radiometal 4550 based inserts.

It is clear that it is not enough to consider the properties of the magnetostrictive drive material alone when designing such a transducer. It must be undertaken at a 'system' level so that the overall performance can be assessed.

12 FUTURE WORK

As would be expected in a study of this type there are areas of this field that can be explored further. Future work would include:

- i. Investigate the parameters associated with the impedance equation for a resonant transducer

The impedance equation that was developed is dependent on a number of variables that encompass the magnetic, magnetostrictive and electrical properties of the transducer system. These should be investigated further but must be done for the specific transducer in question. This is because the whole device behaves as a coupled series of sub-components that influence each other's performance. Obtaining the impedance characteristics of such a device will enable the identification of the most critical system parameters.

- ii. Upgrade geometry of models

As it has been found that the finite element modelling of simplified dental scalers has given an insight into the expected resonances and mode shapes of inserts based on different stack materials. Improvements to these models (by improving the fidelity of representation of scaler geometries) may increase the accuracy and precision of predicted outcomes. In addition, the use of finite element modelling will help re-design dental

scalers based on non-nickel stacks so that coupled longitudinal-flexural modes can be achieved at the target operating frequency.

iii. Produce fully coupled FEM

A current limitation of the finite element modelling undertaken in the study is that it only covers the mechanical characteristics of dental scalers. However, with the latest versions of packages such as Comsol's Multiphysics v.3.5a, it is possible to produce coupled models that can include dynamic magnetomechanical coupling. Consequently, using such a system will enable the application of a dynamic drive current to a modelled device and subsequently measure the expected output strain. This will be a significant task as the equations linking the electrical and mechanical systems via magnetomechanical coupling will have to be determined and incorporated into the models.

iv. Produce designs that do away with magnetostrictive stacks

As it has been identified that dental scalers use longitudinal resonances to stimulate a coupled flexural mode in the inserts, it is possible to re-design dental scalers so that they do away with composite stack/tip assembly inserts altogether. This would mean that the flexural mode would be stimulated in a non-magnetostrictive stack by a separate magnetostrictive driver. An example would be to stimulate the flexural mode with (say) a Terfenol-D drive that applies excitation directly to the position where an anti-node is known to exist at the required resonant frequency.

v. Produce feedback sensor system

It would be of use to dentists to know the value of the force that is being applied to the tooth during scaling. Consequently, the incorporation of a force sensor (or magnetostrictive self-sensing) system would facilitate this.

Appendix A: Error Analysis

The following section shows the error analysis that was performed on the experimental data.

Error limits may be expressed in the form $Q \pm DQ$ where Q is the measured quantity and DQ is the magnitude of its limit of error [B.1]. This expresses the experimenter's judgment that the "true" value of Q lies between $Q - DQ$ and $Q + DQ$. The entire interval within which the measurement lies is called the range of error. Manufacturer's performance guarantees for laboratory instruments are often expressed this way.

Uncertainties may be expressed as *absolute* measures, giving the size of the quantity's uncertainty in the same units in the quantity itself. Alternatively, uncertainties may be expressed as *relative* measures, giving the ratio of the quantity's uncertainty to the quantity itself. In general [B.2]:

$$\text{relative error} = \frac{\text{absolute error in a measurement}}{\text{size of the measurement}} \quad (\text{B.1})$$

To add a further specification of the uncertainty of a particular measurement, it is possible for the experimenter to specify certain odds for this uncertainty. This additional uncertainty parameter is based on the total laboratory experience of the experimenter and so can be considered to a subjective additional weighting to the stated uncertainty [B.3].

The performance of the measurement system was investigated (based on manufacturer's manuals) in conjunction with the observed performance of the system during use when making an assessment of the overall error. This took into account the perceived influence of noise observed during measurements.

[B.1] Taylor J. R., "An Introduction to error analysis". University Science Books, 1962.

[B.2] <http://www.lhup.edu/~dsimanek/errors.htm>

[B.3] Holman J. P., "Experimental methods for engineers", 3rd Edition, McGraw-Hill, Tokyo, 1978.

Appendix B: Rayleigh damping

In Rayleigh damping the damping is assumed to be proportional to a linear combination of the stiffness and mass. The equation of motion for a system with a single degree of freedom with viscous (Rayleigh) damping can be described as

$$m \frac{d^2 u}{dt^2} + c \frac{du}{dt} + ku = f(t)$$

where u is the displacement, m is the mass, c is the damping and k is the stiffness of the system. The motion is as a result of the applied forcing function $f(t)$.

In the Rayleigh damping model the damping parameter c is considered to be due to components that are proportional to the system mass m and the stiffness k .

$$c = \alpha m + \beta k$$

where αm and βk are the mass and stiffness damping parameters, respectively. This assumption has no physical basis but it is mathematically convenient to approximate low damping in this way when exact damping values are not known.

Appendix C: Publications and presentations

1. “Magnetostrictive Dental Scalers”

Oral presentation given at “Innovations in Materials and Manufacturing of Dental Devices” meeting, 29th March 2007, Cardiff MediCentre, Wales College of Medicine, Cardiff University, Heath Park

2. “Development of a Multi-Directional Dynamic Load measuring Tooth Model”

S.C. Lea, P. Bartlett, T. Meydan, G. Landini, A.J Moses, A.D Walmsley.

Poster presentation given at the Joint Scientific meeting of the British and Scandinavian Divisions of the International Association for Dental Research (BSDR/NOF), 2nd-5th April 2007. BSDR and NOF 2007 (Abs 0200).

3. “Vibration Modes Generated in Magnetostrictive Ultrasonic Dental Scalers”

P. Bartlett, S.C. Lea, T. Meydan, G. Landini, A.J Moses, A.D Walmsley.

Poster presentation given at the Joint Scientific meeting of the British and Scandinavian Divisions of the International Association for Dental Research (BSDR/NOF), Durham, 2nd-5th April 2007. BSDR and NOF 2007 (Abs 0201).

4. “Vibration modes generated in magnetostrictive ultrasonic dental scaler inserts”

P. Bartlett, S.C. Lea, P. I. Williams T. Meydan, G. Landini, A.J Moses, A.D Walmsley.

An oral presentation and paper given at the Institute of Physics Mechanics of Medical Devices conference, London, 23 May 2007.

5. “A Comparison of and the compensation for magnetostrictive core inductances in magnetic transducer systems”

P. Bartlett, T. Meydan, A.J. Moses, P.I. Williams

Journal of Magnetism and Magnetic Materials, Volume 320, Issue 20, p. e1061-e1064.

6. “A hybrid magnetic sensor system for measuring dynamic forces”

P . Bartlett G.S. Katranas GS, Meydan T et al, IEEE Transactions on Magnetics., vol 42 (10), 3288-3290, 2006.

A Hybrid Magnetic Sensor System for Measuring Dynamic Forces

Paul A. Bartlett, George S. Katranas and Turgut Meydan

Abstract—This paper describes experiments that were carried out to demonstrate that a hybrid device, that comprises of both a magnetostrictive rod and an amorphous wire magnetic sensor, could be used for force sensing applications. The amorphous sensor uses a frequency modulation technique to detect changes in the wire's permeability. These permeability changes were a result of stress-induced changes in magnetization in a dynamically compressed magnetostrictive rod that was in close proximity to the amorphous sensor.

Index Terms—Magnetostrictive sensor, amorphous wire, force measurement, frequency modulation.

I. INTRODUCTION

THE MEASUREMENT of applied stress has been shown to be possible through the use of magnetostrictive materials such as Terfenol-D. A change in the applied stress to such materials results in a change in their magnetization; this is known as the Villari Effect[1].

There are a number of ways to measure the change in magnetization in a rod of Terfenol-D [2]. The typical way is to wind a sensing 'pick-up coil' co-axially on the sensor's Terfenol-D rod. However, in this paper a novel amorphous-wire sensor system is described that can detect the changes in magnetization induced by an externally applied stress. These magnetization changes are then related to the force that was applied to the transducer thereby enabling the calibration of the force sensor.

II. EXPERIMENTAL

A. A Hybrid Magnetostrictive Material/Amorphous Wire Sensor System

1) Sensor Design

The main component of the force sensor was a 15 mm diam. x 50 mm rod of Terfenol-D. It was housed in a cylindrical Tufnol former which enabled the alignment of the sensor within the external test-rig whilst also giving support to the amorphous wire sensor. This sensor comprised of a 30 mm

long FeCoSiB amorphous wire that was surrounded by a 350 turn excitation coil. The amorphous wire sensor was bent so that it would follow the circumference of the 1mm thick Tufnol former that surrounded the Terfenol-D rod.

The coil that was wound around the amorphous wire was supplied with a sinusoidal carrier signal of 5 kHz. Stress induced changes in the magnetization state of the Terfenol-D rod produces a field that alters the impedance of the amorphous-material sensor which in turn shifts the frequency of the carrier signal by Δf , hence producing a frequency modulated waveform (FM). By demodulating the FM signal, the amplitude of the peak-to-peak signal could be measured and then related to the equivalent drive signal produced by applying a sinusoidal stress to the hybrid sensor [2].

The hybrid sensor was placed in a solenoid of 1375 turns, with an inner diameter of 55 mm, outer diameter 84 mm and length 100 mm. This solenoid was incorporated so that a 'biasing field' could be applied to the hybrid sensor.

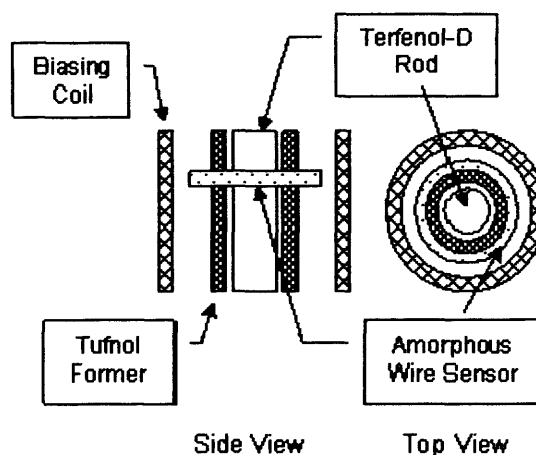


Fig. 1 Schematic of the hybrid sensor.

It is considered that the biasing field moves the operating point of the Terfenol-D rod into a region of the strain vs. induction curve where the $dB/d\lambda$ is greatest, where the value of the magnetic induction B , is a result of an externally applied stress-induced strain λ . Therefore a change in applied stress at a favorable operating point will result in a greater change in magnetization than that produced in a region of lower $dB/d\lambda$. It

must also be noted that the transduction performance of Terfenol-D is also dependent on any applied pre-stress.

The Terfenol-D rod was positioned so that it was in the middle of a biasing solenoid that had a length twice that of the magnetostrictive component. A biasing coil of this length was used in order to improve applied field uniformity in the region of the Terfenol-D rod. At both ends of the Terfenol-D rod, brass 'push rods' enabled the positioning of it in the former whilst also allowing the application of mechanical stress from an external source.

2) Test Rig

The main aim of these experiments was to determine whether it was possible to calibrate the hybrid sensor against a known sensor, so that it could detect a dynamic force that was applied to it. To achieve this, the hybrid sensor was installed in a Schenk RSA 50 Electromechanical Universal Testing Machine. By moving the RSA 50's cross-head it was possible to apply a known dynamic force (and hence a strain) to the Terfenol-D rod in the hybrid sensor (see Fig. 2).

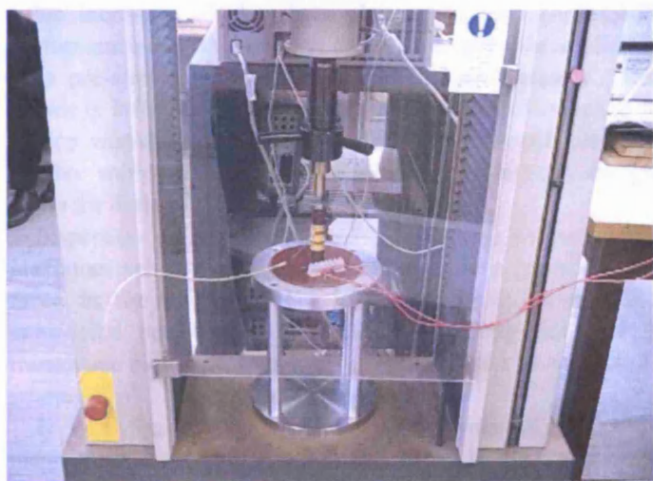


Fig. 2. The hybrid sensor mounted in the RSA 50 test machine. The bias coil is not present in this image.

The force that was applied to the sensor was then directly measured via the RSA 50's integral PM 63k load cell that could measure loads up to 63 kN, via a Schenk M1602 display unit. The output signal from the load cell was processed by the RSA 50's DP 151 control monitor unit before being recorded on an Agilent 54624A oscilloscope where peak-to-peak force values could be identified.

A low-frequency dynamic force (~ 1.7 Hz) was applied to the hybrid sensor with the amplitude of oscillation being controlled via the RSA 50's FP 151, 153 and FG 152 control modules. This was the highest frequency of oscillation that could be produced from the RSA 50. The force was applied so that it ranged from zero to its maximum value without an additionally applied pre-stress.

3) Signal Processing

The FM measurement system consisted of a personal computer (PC) based acquisition arrangement. The detection of the FM signal was conducted through the LabVIEW® package and a National Instruments NI-6120 data acquisition card with a maximum sampling rate of 800 kS/s and 16-bit resolution [3].

Changes in the state of magnetization of the Terfenol-D rod caused co-responding FM to the carrier signal that was applied to the amorphous sensor. By demodulating this signal, the peak to peak amplitude could be calculated by the LabVIEW system and then related to the equivalent drive signal produced by the PM 63k load cell as measured by the Agilent 54624A. This could then be related to the applied force through calibration data that was obtained for the PM 63k's load cell.

B. Low-Frequency Force Measurements

It is understood that the performance of Terfenol-D in a sensor configuration is dependent on the applied stress, applied biasing field and the magnetic history of the active element. As a result, it was certain that the output voltage from the hybrid sensor would be influenced by these factors. Therefore, measurements were made of the voltage output from the sensor system were made for different peak-to-peak amplitudes of the 1.7 Hz applied force (see Fig 3).

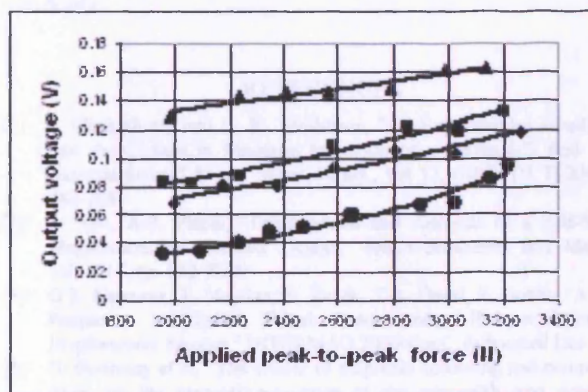


Fig. 3 The measured output voltages from the hybrid sensor system for different applied forces at a frequency of 1.7 Hz with the following bias fields: ▲ = 4.13 kA/m, ■ = 3.50 kA/m, ◆ = 3.34 kA/m, ● = 2.39 kA/m.

For each data point, five sensor output voltage measurements were made and averaged for each force amplitude. In each of the plots shown, different biasing fields were applied to the Terfenol-D rod. As can be seen, changing the bias field offsets the output voltage vs. applied force curve. To investigate this further, the hybrid sensor was subjected to fixed amplitude dynamic forces of 1.46, 1.97 and 2.65 kN and the bias field that was applied to the device was altered between ~ 2 to 8 kA/m (see Fig 4).

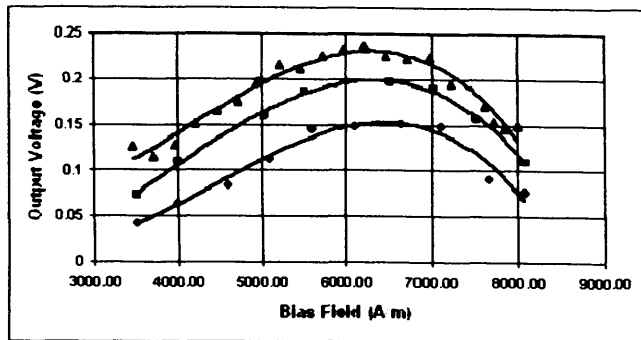


Fig. 4 The influence of a varying bias field on the output voltage from the hybrid sensor at a fixed dynamic stress value. \blacklozenge = 1.46 kN p-to-p, \blacksquare = 1.97 kN p-to-p, \blacktriangle = 2.65 kN p-to-p.

It was noted here that increasing the dynamic force causes an offset of the sensor output curve. This is as to be expected as Fig 3 demonstrates that an increase in the dynamic applied force results in an increase in sensor output. It must be noted that in this system configuration, the 'effective' average force for each dynamic stress increases as the peak-to-peak force value increases. It has been shown [4] that Terfenol-D's performance can be improved through the suitable application of a pre-stress. It is possible that the performance of the sensor is influenced by this factor and an improvement to the device would be the application of an additional pre-stress. Further work will need to be undertaken to identify the pre-stress for optimum hybrid sensor operation.

Inspection of Fig 3 also shows that there seems to be a maximum value of sensor output voltage for a given dynamic force in the region of 6-7 kA/m for each curve. It is considered that this is due to the operating point of the transducer moving away from a region of the B vs. λ curve where $dB/d\lambda$ is at a maximum.

It was found that 'inappropriate' levels of stress and magnetic biasing could result in distortions in the signal output from the sensor. In one case, this seemed to be a result of a 'frequency doubled' output signal component. When the sinusoidal applied stress' amplitude is great enough, it can cause a change in magnetization that results in the detected stress-induced magnetic field changes passing through a minimum value. If this occurs, then a proportion of the signal output will be 'frequency doubled'. This can be mitigated against by supplying sufficient magnetic biasing so that any change in stress-induced magnetization does not occur near the this minimum. It was also noted that for some larger values of dynamic applied stress, the shape of one half of the sensor output signal was 'flattened' somewhat. It is considered that in this case the Terfenol-D's Villari effect is being saturated as a result of the high applied forces. This will need further investigation based on a further characterization of the materials properties of the Terfenol-D rod to confirm this. However, it is possible that selection of an appropriate pre-stress could improve the performance of the sensor and

increase the applied force value at which saturation occurs.

Although the dynamic force-spectrum that was applied to this sensor was limited to 1.7 Hz, it is not considered that there would be any difficulty in significantly increasing the operation frequency of the sensing system. Indeed, it has been shown in [1] that such devices can operate at least to 3 kHz.

III. CONCLUSION

In this paper, a hybrid magnetostrictive force sensor has been described. Experiments have been carried out to prove the principle that it is possible to use an amorphous wire sensor system to detect the change in magnetization in dynamically stressed Terfenol-D rods as part of a hybrid force transducer. This has been successfully achieved for a 1.7 Hz applied force of up to 2.65 kN peak-to-peak. It has been noted that the magnetic history, biasing magnetic field and pre-stress can influence the performance of the hybrid sensor system. This LabVIEW® based hybrid transducer offers considerable potential as a dynamic force sensor. It is considered that this system will lend itself to a number of dynamic force measurement applications.

ACKNOWLEDGMENT

The Authors wish to thank Mr. S.J. Eaton of QinetiQ Ltd for supplying the Rare Earth Products Ltd Terfenol-D rods used in this study.

REFERENCES

- [1] S. Chakraborty and G. R. Tomlinson, "An Experimental Investigation into the Change in Magnetic Induction of a Terfenol-D Rod due to External Stress," *Smart. Mater. Struct.*, vol 12, (MONTH ?) 2003, pp. 763-768.
- [2] J. Pratt, A.B. Flatau, "Development and Analysis of a Self-Sensing Magnetostrictive Actuator Design," *Smart Structures and Materials*, vol. 1917, pp. 952-XXX
- [3] G.S. Katranas, T. Meydan, S. Zurek, T.A. Ovari, F. Borza, "A Novel Frequency Modulation Based System using Bi-layer Thin Film Displacement Sensors," *INTERMAG 2006 Conf.*, Submitted Dec 2005.
- [4] N. Galloway et al, "The effects of magnetic annealing and compressive stress on the magnetic-properties of the rare-earth iron compound Terfenol-D," *J. Magn. Magn. Mater.*, vol. 119, Feb 1993, pp. 107-114.

A comparison of and the compensation for magnetostrictive core inductances in magnetic transducer systems

P.A. Bartlett^{a,*}, T. Meydan^a, S.C. Lea^b, A. J. Moses^a, P. I. Williams^a,
G. Landini^b, A. D. Walmsley^b

^a*Wolfson Centre for Magnetism, School of Engineering, Queen's Buildings, Cardiff University, Cardiff, Wales, CF24 3AA, United Kingdom*

^b*The School of Dentistry, The University of Birmingham, Birmingham, B4 6NN, United Kingdom*

Elsevier use only: Received date here; revised date here; accepted date here

Abstract

Magnetostrictive materials have been utilized for the production of ultrasonic frequency vibrations for a number of years. This has particularly been the case in laminated Nickel-based ultrasonic dental scaler cleaning systems.

In this study, a comparison has been made between the impedances of a number of magnetostrictive stacks of 50mm x 4mm x ~0.3mm strips at frequencies in the range of 10 to 50 kHz in a coil used for the excitation of a stack in a dental-scaler system. The magnetostrictive stacks tested comprised of potential replacement materials for standard nickel ones.

The study showed that it was possible to compensate for the inductive 'imaginary' components of the impedance through the use of a tuned, series capacitance so that only the 'real' resistive component of the impedance remained. This reduced the electrical losses associated with the excitation of the magnetostrictive stacks as a result of the frequency-dependent inductance of the coil system. Consequently, the maximum power transfer from an amplifier to the transducer was increased. Also, the investigation showed how the 'real' component of impedance of the different stacks varied with frequency. In a tuned resonant electrical circuit, the resistive component of the impedance, if considered as a loss, would be the lowest that could be achieved with such a magnetic circuit. Consequently, the losses associated with resonant magnetostrictive devices, like dental scalers, can be reduced.

© 2009 Elsevier B.V. All rights reserved

PACS: 75.20.En; 75.50.Bb; 75.50.Cc; 75.80.+q

*Keywords: Inductance; magnetostrictive; transducer; impedance"

1. Introduction

When plaque forms on tooth surfaces, it may be removed through brushing. However, if plaque is not removed (through inadequate brushing or because of

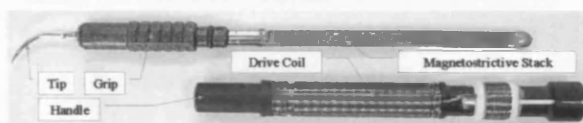
its location in tooth furcations that are inaccessible to brushing) it may become mineralised. Mineralised plaque, also known as calculus, is a hard, tenacious deposit that requires intervention by a dentist to remove it. If it is not removed, periodontal disease may ensue, with inflammation of the gingiva (gums) with eventual bone resorption and, finally, tooth loss.

* Corresponding author. Tel.: +44 (0)29 20875934 ; fax: +44 (0)29 208 79538.
E-mail address: bartlettpa1@cardiff.ac.uk.

In dentistry, one of the most important tools available to the clinician for helping his patients maintain their oral health is the ultrasonic scaler. Ultrasonic scalers consist of metal probes, driven to resonate at ultrasonic frequencies. These probes are manoeuvred over the surface of the tooth and physically chip away the calculus deposits.

The ultrasonic probe vibrations are driven by a magnetostrictive stack, attached to the probe tip assembly. The assembled ‘insert’ is then placed within a coil located in the instrument handle. This coil uses an AC signal to create the stack oscillations. A typical Dentsply™ dental scaler insert and associated drive coil system can be seen in Fig. 1.

Fig 1 Typical Dentsply dental scaler insert and drive coil system



In this work, a series of alternative magnetostrictive materials were investigated as potential replacements to the Nickel stacks that are used in commercial units. It was noted that the impedance associated with each new material insert differed from that of a standard Nickel Dentsply™ insert. As the dental scalers can operate with an excitation frequency of 15 or 30 kHz (with a 30 kHz resonant insert vibration in both cases), this could result in significant differences in the power requirements to achieve the required dynamic magnetic fields for optimum scaler tip vibration. This paper addresses the need to minimize the power requirements.

2. Experimental method and results

Initially, an impedance study was made of a series of dental scaler inserts that had been produced in-house and placed in the Dentsply™ drive coil assembly. The materials tested in stack form were 3% grain oriented silicon steel, “Radiometal 4550” (Ni Fe alloy), “Hyperco 50” (Co Fe alloy). This was compared to a standard Dentsply™ insert. An energy dispersive spectroscopy analysis, via the WINEDS® X-Ray microanalysis system, indicated that the magnetostrictive stack of this ‘Slimline’ dental scaler insert used comprised of 16 Nickel strips (99% Ni).

The geometries associated with the individual

stacks are shown in Table 1. The thicknesses of the laminae and number of stack elements.

As a result of the difficulty in obtaining samples of identical thicknesses, stacks were made with the appropriate number of laminae that would result in equivalent dimensions.

In these experiments, the series resistances and reactances were measured for the dental scaler drive coil when the various magnetostrictive materials were acting as the core. These impedances were initially measured via an Agilent 4284A LCR meter that supplied a 2V rms to the circuit at the desired drive frequency for the different core materials (see Figs. 2 and 3).

There are a number of contributions to the measured impedances. Some of these are those that are purely associated with the ‘electrical’ components of the transducer but some are also related to losses in the magnetostrictive material itself. For example; the magnitude of eddy current losses that are established in such a stack will be determined by the geometry of the stack elements, their resistivities and the frequency of operation. From the perspective of the measurement system, these losses will be added to those that also contribute to the overall impedance. Indeed, it must also be considered that mechanical losses associated with the magnetomechanical coupling within the magnetostrictive transducer will also contribute to the measured electrical impedance. Therefore, the impedance measured in these experiments encapsulates all of the losses associated with the transducer under the specific excitation conditions.

Table 1. The dimensions and number of strips of the test stacks (nb: the thickness of the “Hyperco 50” and “Radiometal 4550” samples were measured before an electrically insulating coat of enamel paint was applied to one side of each strip before stack assembly).

Material	Stack Dimensions (mm)	Laminae Thickness (mm)	No. Laminae
Ni	50 x 5 x 4	0.25	16
3% GO Steel	50 x 5 x 4	0.31	13
“Hyperco 50”	50 x 5 x 4	0.356	10
“Radiometal 4550”	50 x 5 x 3.8	0.35	10

Fig 2. The apparent series resistance of the Dentsply drive-coil system when fitted with inserts of different magnetostrictive stack materials (and air cored). Nb: 'Txd Nickel = standard Dentsply insert material.

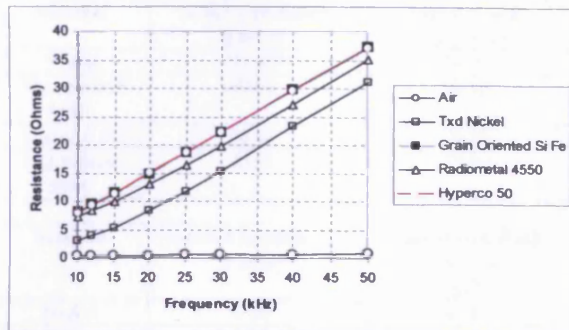
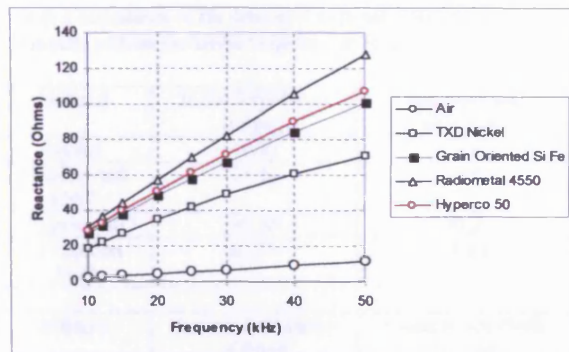


Fig 3. The reactance of the Dentsply drive-coil system when fitted with inserts of different magnetostrictive stack materials (and air cored). Nb: 'Txd Nickel = standard Dentsply insert material.

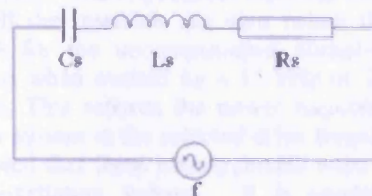


In Fig. 3, the effective resistance seems not to remain constant with frequency. It is likely that this is due to frequency dependent losses such as eddy currents in the core material and the skin effect showing up as an equivalent resistive loss when measured by the LCR meter. It is noted that the Nickel of the commercial insert presented the lowest resistance for a given frequency. The resistance of the drive system for a Nickel core was approximately half that of the other materials when supplied with a 15 kHz drive signal. This was also repeated in the reactive component of the system impedances for the different core materials. In this case the reactance of the drive system for a Nickel core was approximately 3/4 that of the other materials when supplied with a 15kHz drive signal.

As the dental scaler system is operated in such a way so that a mechanical resonance is stimulated, it was thought possible to use these impedance data to minimize the electrical power requirements for such a

system. Figure 4 shows a standard series LCR circuit configuration.

Fig. 4. Series LCR circuit equivalent to the drive coil and insert assembly.



The standard dental scaler drive-coil/insert assemblies have negligible series capacitances. However, if a capacitance of an appropriate value (C_s) is added to the series circuit then the reactance contribution as a result of the inductor is compensated for leaving only the purely resistive loss component [2]. Consequently, the reactive 'imaginary' component of the impedance is eliminated so that only the 'real' resistive impedance contributions remain.

This can be expressed mathematically as;

$$Z = \sqrt{R_s^2 + \left(\omega L_s - \frac{1}{\omega C_s} \right)^2} \quad (1)$$

where the total impedance will equal R_s if

$$\omega L_s = \frac{1}{\omega C_s} \quad (2)$$

This can be achieved if the electrical circuit is tuned to resonate at a particular frequency to achieve maximum power transfer. In the case of standard dental scalers, this frequency would be ~15 kHz or ~30 kHz to achieve ~30 kHz vibration. In the former case, this as a result of the magnetostrictive frequency doubling associated with a stack that does not have any magnetic biasing. In the latter it is due to stimulation of the resonance when a magnetic bias is present [3].

To obtain the desired value of C_s to satisfy (2) at 15kHz, a capacitance bank was inserted in series in the previous drive-coil circuit. Again, the Agilent 4284A LCR meter was used to identify when (2) was satisfied at 15kHz with a supply voltage of 2V rms (26 A/m rms). This was achieved by changing the capacitance bank value until the measured reactance was as close to zero as possible. This experiment was also conducted with a 30kHz excitation for comparison purposes (24 A/m rms). The results are

shown in Table 2 and 3.

Table 1 Impedance of the drive-coil with the different core materials with an excitation frequency of 15 kHz

Material	Initial Impedance (Ohms)	Initial Phase (degrees)
Nickel	25.97	78.21
"Radiometal 4550"	40.50	76.10
"Hyperco 50"	38.10	74.10
GO Silicon Steel	36.50	72.90

Material	Lowest Impedance (Ohms)	Capacitance Bank Setting (μF)
Nickel	5.68	0.417
"Radiometal 4550"	9.74	0.271
"Hyperco 50"	10.48	0.290
GO Silicon Steel	10.93	0.304

Table 2 Impedance of the drive-coil with the different core materials with an excitation frequency of 30 kHz

Material	Initial Impedance (Ohms)	Initial Phase (degrees)
Nickel	49.80	71.8
"Radiometal 4550"	75.40	76.0
"Hyperco 50"	69.30	73.2
GO Silicon Steel	66.37	71.85

Material	Lowest Impedance (Ohms)	Capacitance Bank Setting (μF)
Nickel	14.39	0.115
"Radiometal 4550"	18.38	0.073
"Hyperco 50"	20.30	0.08
GO Silicon Steel	21.40	0.085

3. Discussion

Figs. 2 and 3 show that the material used in a magnetostrictive dental scaler stack can have an influence on the dental scaler system's impedance. It can be seen that the current Nickel-based stacks offer lower impedance than the other materials used in the study. In addition, the operating frequency of the dental scaler will also influence the impedance of the dental scaler with higher impedances at higher frequencies (as would be expected due to such factors as eddy current losses and skin effect [4][5]). The use of an air core in these experiments shows the contribution of increasing losses in the coil system

itself as a result of increasing excitation frequency. However, Tables 2 and 3 shows that it is possible to significantly reduce the impedance of the system by introducing a capacitor whose value creates resonant LCR electrical circuit at the required excitation frequency. The impedances achieved via this method for all the materials are also below that which is found for the uncompensated Nickel-based scaler system when excited by a 15 kHz or 30 kHz drive signal. This reduces the power requirements of the scaler system at the selected drive frequency. It must be noted that these measurements were taken with a low excitation voltage. It is expected that the compensation capacitance value will need to be adjusted for higher power operation due to changes in material permeabilities when higher excitation voltages and frequencies are applied. However, the technique seems to offer advantages for the operation of resonant dental scaler systems. In addition, it reduces the power requirements for alternative stack materials when compared to standard, uncompensated Nickel-based scaler devices.

4. Conclusions

In conclusion, this study has shown the potential advantages and disadvantages of using alternative magnetostrictive stack materials than standard Nickel in traditional dental scaler insert designs. At the expected drive frequencies, Nickel offers the lowest impedance stacks at the expected drive frequencies, when compared to the other materials measured in the study. However, the work also demonstrated that it is possible to minimise impedance losses by creating a tuned electrical circuit that enables reactive loss compensation at the mechanical components resonant frequency. Consequently, the use of capacitance compensation can greatly decrease the losses associated with a resonant magnetostrictive dental scaler transducer. This means that such devices can be caused to resonate with lower input power requirements.

References

- [1] S.C. Lea, G. Landini, A.D. Walmsley. J. Clinical Periodontology, 2003; 30 (6): 505-510.
- [2] W.J. Duffin, Electricity and Magnetism, 3rd Ed, McGraw-Hill, London, 1980, 277-279.
- [3] G. Engdahl, Handbook of Giant Magnetostrictive Materials, Academic Press, San Diego, 2000.
- [4] R.M. Bozorth, Ferromagnetism, IEEE Press, New York, 1993, 769-770.
- [5] W.J. Duffin, Electricity and Magnetism, 3rd Ed, McGraw-Hill, London, 1980, 243-245.

